$B \to V\ell + \ell - -$ in the Standard Model from Light-Cone Sum Rules

Aoife Bharucha, David M. Straub, Roman Zwicky

Published for SISSA by Springer

Received: June 10, 2016
Revised: July 11, 2016
Accepted: July 31, 2016
Published: August 16, 2016

$B \to V\ell^+\ell^-$ in the Standard Model from light-cone sum rules

Aoife Bharucha,[a,b] **David M. Straub**[c] **and Roman Zwicky**[d]

[a] *Physik Department T31, Technische Universität München, James-Franck-Str. 1, 85748 Garching, Germany*
[b] *CNRS, Aix Marseille Université, Université de Toulon, CPT, UMR 7332, F-13288 Marseille, France*
[c] *Excellence Cluster Universe, Technische Universität München, Boltzmannstr. 2, 85748 Garching, Germany*
[d] *Higgs Centre for Theoretical Physics, School of Physics and Astronomy, University of Edinburgh, Edinburgh EH9 3JZ, Scotland, U.K.*

E-mail: aoife.bharucha@cpt.univ-mrs.fr, david.straub@tum.de, roman.zwicky@ed.ac.uk

Abstract: We present $B_q \to \rho$, $B_q \to \omega$, $B_q \to K^*$, $B_s \to K^*$ and $B_s \to \phi$ form factors from light-cone sum rules (LCSR) at $\mathcal{O}(\alpha_s)$ for twist-2 and 3 and $\mathcal{O}(\alpha_s^0)$ for twist-4 with updated hadronic input parameters. Three asymptotic light-cone distribution amplitudes of twist-4 (and 5) are determined, necessary for the form factors to obey the equations of motion. It is argued that the latter constrain the uncertainty of tensor-to-vector form factor ratios thereby improving the prediction of zeros of helicity amplitudes of major importance for $B \to K^*\ell\ell$ angular observables. We provide easy-to-use fits to the LCSR results, including the full error correlation matrix, in all modes at low q^2 as well as combined fits to LCSR and lattice results covering the entire kinematic range for $B_q \to K^*$, $B_s \to K^*$ and $B_s \to \phi$. The error correlation matrix avoids the problem of overestimating the uncertainty in phenomenological applications. Using the new form factors and recent computations of non-factorisable contributions we provide Standard Model predictions for $B \to K^*\gamma$ as well as $B \to K^*\ell^+\ell^-$ and $B_s \to \phi\mu^+\mu^-$ at low dilepton invariant mass. Employing our $B \to (\rho, \omega)$ form factor results we extract the CKM element $|V_{\rm ub}|$ from the semileptonic decays $B \to (\rho, \omega)\ell\nu$ and find good agreement with other exclusive determinations.

Keywords: Heavy Quark Physics, Quark Masses and SM Parameters

ArXiv ePrint: 1503.05534

doi:10.1007/JHEP08(2016)098

JHEP08(2016)098

Contents

JHEP08(2016)098

JHEP08(2016)098

1 Introduction

Exclusive semi-leptonic B decays are important tools to test the Standard Model (SM) and to look for new physics. Among these processes, the decays $B \to K^*(\to K\pi)\mu^+\mu^-$ and $B_s \to \phi(\to K^+K^-)\mu^+\mu^-$ are of particular relevance as their angular distributions give access to a host of observables that are sensitive to new physics (e.g. [1] for arecent review). Predicting these observables, either within the SM or beyond, requires the knowledge of the form factors (FFs) — in the case of $B \to V$ transitions, these are 7 functions of the dilepton invariant mass squared q^2. In the low q^2 region, where the vector meson is energetic, the FFs can be computed using the method of sum rules on the light cone (LCSR) whereas at high q^2 the FFs can be computed using lattice QCD.

In this work we present an update of the FF computation in [2], for the modes $B_q \to \rho$, $B_q \to \omega$, $B_q \to K^*$, $B_s \to K^*$ and $B_s \to \phi$ (with $q = u, d$), using current hadronic input and a concise discussion of the role of *the equation of motion* (EOM) in correlating vector and tensor FFs. The FFs are fitted to the z-expansion parameterisation in the helicity basis, *retaining all correlations* among the expansion coefficients.[1] This information is made publicly available as ancillary files on the arXiv web pages in a form which is easy to use for phenomenology.

Crucially the correlation of the uncertainties avoids overestimating uncertainties in observables. A particularly important example are the angular observables in $B \to K^*\mu^+\mu^-$-type decays since they are sensitive to ratios of FFs and zeros of helicity amplitudes. For the latter two, the uncertainty is considerably reduced when taking correlation into account.

We argue, extending the work in ref. [4], that the use of the EOM enforces the correlation of the non-parametric, sum rule specific, input parameters. This can be seen as an application of the large energy limit (LEL) ideas [5] to the sum rules on the light-cone. It is in giving numerical predictions and not relying on the heavy quark limit that the LCSR computations go beyond the LEL ideas [5] (this includes the case factorisable hard α_s-corrections [6]). The LCSR therefore give corrections to the LEL [5] and soft-collinear effective theory (SCET) [6] relations. Going beyond the SCET framework of two soft FFs and hard α_s-correction in the heavy quark limit involves using the numerical predictions

[1] Similar fits retaining correlations have recently been performed for the $B \to \pi$ FFs [3].

from LCSR, e.g. [7, 8]. Going beyond the SCET framework has become increasingly important since observables designed to minimise the impact of the soft FFs [9] are, of course, sensitive to $1/m_b$-corrections.

We perform *combined fits* of the FFs to the LCSR at low q^2 and a recent lattice computation at high q^2 [10, 11]. This serves to test the consistency of the two complementary methods and provides FF sets valid over the entire kinematical region. We extract the CKM element $|V_{\rm ub}|$ from $B \to (\omega, \rho)\ell\nu$ BaBar- and Belle-data using the $B \to (\omega, \rho)$ FF predictions of this paper. This can either be viewed as an extraction of $|V_{\rm ub}|$ or as a check of the normalisation of the FF when compared to global fits or $B \to \pi\ell\nu$ extractions of $|V_{\rm ub}|$. In addition to the FFs, the calculation of $B \to V\ell^+\ell^-$ observables involves *non-factorisable contributions* from the weak hadronic Hamiltonian. Some of these contributions have been recently computed within LCSR. Including all of these ingredients, we present SM predictions for the branching ratios and angular observables of $B \to K^*\mu^+\mu^-$ and $B_s \to \phi\mu^+\mu^-$. We also compare the prediction for the branching ratio of $B \to K^*\gamma$, that has been measured precisely at the B factories, to the data.

The paper is organised as follows. In section 2 we present and discuss the seven $B \to V$ FFs within the LCSR context, discussing the implication of the EOM, finite width effects, input parameters and the interpolating fits to the lattice data. In section 3 phenomenological aspects of $B \to K^*\mu\mu$, $B \to K^*\gamma$, $B_s \to \phi\mu\mu$, $B \to K^*\mu\mu$ versus $B_s \to \phi\mu\mu$ and the determination of $|V_{\rm ub}|$ from $B \to (\rho, \omega)\ell\nu$ are discussed: see subsections 3.1, 3.2, 3.3, 3.4 and 3.5 respectively. Conclusions figure in section 4. Appendix A assembles aspects of the EOM, explicit tree level results, scheme dependence and remarks on the Borel parameters. The determination of the three light-cone distribution amplitudes $\mathbb{A}_\parallel$ (twist-4) and $\mathbb{G}_\perp^{v,a}$ (twist-5), using an alternative method, is discussed in appendix B. A detailed discussion on the determination of the decay constants from experiment is given in appendix C. Conversion between bases, further plots and fit coefficients are given in appendixes D, E, and F respectively. The effect of the sizeable B_s-lifetime is worked out in appendix G.

2 $B \to V$ form factors from light-cone sum rules

The short distance matrix elements, relevant for the dimension six effective Hamiltonian, are parameterised by seven FFs[2]

$$\begin{aligned}\langle K^*(p,\eta)|\bar{s}\gamma^\mu(1\mp\gamma_5)b|\bar{B}(p_B)\rangle &= P_1^\mu\,\mathcal{V}_1(q^2) \pm P_2^\mu\,\mathcal{V}_2(q^2) \pm P_3^\mu\,\mathcal{V}_3(q^2) \pm P_P^\mu\mathcal{V}_P(q^2)\,,\\ \langle K^*(p,\eta)|\bar{s}iq_\nu\sigma^{\mu\nu}(1\pm\gamma_5)b|\bar{B}(p_B)\rangle &= P_1^\mu T_1(q^2) \pm P_2^\mu T_2(q^2) \pm P_3^\mu T_3(q^2)\,,\end{aligned} \tag{2.1}$$

where the Lorentz structures P_i^μ are defined as in [12]

$$\begin{aligned} P_P^\mu &= i(\eta^*\cdot q)q^\mu, & P_1^\mu &= 2\epsilon^\mu{}_{\alpha\beta\gamma}\eta^{*\alpha}p^\beta q^\gamma, \\ P_2^\mu &= i\{(m_B^2-m_{K^*}^2)\eta^{*\mu}-(\eta^*\cdot q)(p+p_B)^\mu\}\,, & P_3^\mu &= i(\eta^*\cdot q)\left\{q^\mu-\frac{q^2}{m_B^2-m_{K^*}^2}(p+p_B)^\mu\right\}, \end{aligned} \tag{2.2}$$

[2]Due to the composition of the wave functions of the $\rho^0 \sim 1/\sqrt{2}(\bar{u}u-\bar{d}d)$ and $\omega \sim 1/\sqrt{2}(\bar{u}u-\bar{d}d)$, extra factors $c_V^{b\to q}$ have to attached to the matrix elements on the left-hand side, cf. [2]. They read: $c_{\rho^0}^u = -c_{\rho^0}^d = c_\omega^u = c_\omega^d = \sqrt{2}$ and $c_V = 1$ in all other cases.

JHEP08(2016)098

with the $\epsilon_{0123} = +1$ convention for the Levi-Civita tensor. The relation $T_1(0) = T_2(0)$ holds algebraically. The parameterisation (2.1) makes the correspondence between vector and tensor FFs explicit. The correspondence of the $\mathcal{V}_{P,1,2,3}$ to the more traditional FFs $A_{0,1,2,3}$ and V is as follows

$$\mathcal{V}_P(q^2) = \frac{-2m_{K^*}}{q^2} A_0(q^2)\,, \qquad \mathcal{V}_1(q^2) = \frac{-V(q^2)}{m_B + m_{K^*}}\,, \qquad \mathcal{V}_2(q^2) = \frac{-A_1(q^2)}{m_B - m_{K^*}}\,,$$
$$\mathcal{V}_3(q^2) = \left(\frac{m_B + m_{K^*}}{q^2} A_1(q^2) - \frac{m_B - m_{K^*}}{q^2} A_2(q^2)\right) \equiv \frac{2m_{K^*}}{q^2} A_3(q^2)\,. \tag{2.3}$$

The relation $A_3(0) = A_0(0)$ assures finite matrix elements at $q^2 = 0$. The last relation in (2.3) indicates that one FF out of $A_{1,2,3}$ is redundant.[3] The pseudoscalar matrix element is related to A_0 through an axial Ward Identity:

$$\langle K^*(p,\eta)|\bar{s}\gamma_5 b|\bar{B}(p_B)\rangle = \left(\frac{P_P \cdot q}{m_s + m_b}\right)\mathcal{V}_P(q^2) = \left(\frac{2m_{K^*}(\eta^* \cdot q)}{i(m_s + m_b)}\right) A_0(q^2)\,. \tag{2.4}$$

The projection on the helicity basis, using the Jacob-Wick polarisation convention, is given in appendix D. In the next section we briefly discuss the use of the method of LCSR before investigating the implications of the EOM on certain sum rule specific parameters.

2.1 Calculation of the form factors in light-cone sum rules

Light-cone sum rules (similar to QCD sum rules [13, 14]) for the FFs are derived by considering the correlator of the time-ordered product of two quark currents evaluated between the final state on-shell meson (in this case V) and the vacuum [15, 16]. On expanding this correlator about the light-cone, one obtains a series of perturbatively calculable hard scattering kernels convoluted with non-perturbative, universal light-cone distribution amplitudes, ordered by increasing twist (dimension minus spin). Reasonable convergence of the LC-expansion is formally and by experience limited up to $q^2 \simeq \mathcal{O}(m_b \Lambda_{\rm QCD}) \simeq 14\,\text{GeV}^2$. In the hadronic picture the correlator is expressed as the sum over excited states, the dominant state being the B-meson, and this is followed by the continuum. Assuming quark-hadron duality above a certain continuum threshold s_0 [13, 17], an approximation referred to as the semi-global quark-hadron duality assumption, one arrives at an expression for the lowest lying hadronic parameter in terms of an expression of partonic QCD and s_0. A Borel transformation which ameliorates both the hadron and the parton evaluation leads to a numerical improvement of the procedure.

Light-cone sum rules results, with light-meson distribution amplitudes (DAs), have been computed for the $B \to P$ transition up to twist-3 $\mathcal{O}(\alpha_s)$ in [18–20] and for the $B \to V$ transition up to twist-4 at tree level and twist-2 $\mathcal{O}(\alpha_s)$ [21] as well as twist-3 $\mathcal{O}(\alpha_s)$ [2]. In this paper we make use of the results in [2].[4] Alternatively the FFs can be determined using V-meson DA and an interpolating current for the B-meson. This program has been

[3] From the viewpoint of the projections the traditional nomenclature is unfortunate. It would have been better not to have A_2 at all and use the notation $A_1 \to A_2$.

[4] In [2] the size of the twist-3 $\mathcal{O}(\alpha_s)$ corrections were not explicitly given. At $q^2 = 0$ the twist-3 $\mathcal{O}(\alpha_s)$ corrections lead to a raise of around 10% of the FF T_1.

JHEP08(2016)098

pursued in [22] at tree level in QCD and in SCET [23]. In this work we improve on the previous LCSR work [2] by

- computation of the full twist-4 (and partial twist-5) 2-particle DAs contribution to the FF (appendix B — available a downloadable Mathematica notebook),
- determination of the DAs $\mathbb{G}_\perp^{v,a}$ (twist-5), in the asymptotic limit, filling a gap in the literature (appendix B),
- discussing the impact of the EOM on uncertainty correlations (section 2.2), including the aspect of scheme-dependence (appendix A.5),
- explicit verification of the EOM at tree level (appendices A.3, A.4), for the asymptotic 2-particle DAs including $\mathcal{O}(m_s)$-corrections.
- verification of the compatibility of the composite operator renormalisation with the EOM (appendix A.5.1),
- discussion of non-resonant background for vector meson final states (section 2.3),
- determination and usage of updated hadronic parameters (section 2.4), specifically the decay constants (appendix C),
- fits with full error correlation matrix for the z-expansion coefficients (section 2.5), as well as an interpolation to the most recent lattice computation (section 2.6).

2.2 Equation of motion and form factors

In this section we reiterate the use of the EOM [4]. As discussed in [4] this is of importance in reducing the uncertainty between certain FFs. Below we give more details and strengthen the argument. The following EOM

$$i\partial^\nu\big(\bar{s}i\sigma_{\mu\nu}(\gamma_5)b\big) = -(m_s \pm m_b)\bar{s}\gamma_\mu(\gamma_5)b + i\partial_\mu\big(\bar{s}(\gamma_5)b\big) - 2\bar{s}i\overleftarrow{D}_\mu\,(\gamma_5)b\,, \tag{2.5}$$

are valid on physical states. Equations of the form (2.5) are sometimes also referred to as Ward identities. In particular, evaluated on $\langle V|\ldots|B\rangle$, eq. (2.5) yields

$$T_1(q^2) + (m_b + m_s)\mathcal{V}_1(q^2) + \mathcal{D}_1(q^2) = 0\,, \tag{2.6}$$
$$T_2(q^2) + (m_b - m_s)\mathcal{V}_2(q^2) + \mathcal{D}_2(q^2) = 0\,, \tag{2.7}$$
$$T_3(q^2) + (m_b - m_s)\mathcal{V}_3(q^2) + \mathcal{D}_3(q^2) = 0\,, \tag{2.8}$$
$$(m_b - m_s)\mathcal{V}_P(q^2) + \left(\mathcal{D}_P(q^2) - \frac{q^2}{m_b + m_s}\mathcal{V}_P(q^2)\right) = 0\,. \tag{2.9}$$

One of the above four equations corresponds to each of the directions (2.2) [4, 24], where $\mathcal{D}_i$ are defined

$$\langle K^*(p,\eta)|\bar{s}(2i\overleftarrow{D})^\mu(1\pm\gamma_5)b|\bar{B}(p_B)\rangle = P_1^\mu\,\mathcal{D}_1(q^2) \pm P_2^\mu\,\mathcal{D}_2(q^2) \pm P_3^\mu\,\mathcal{D}_3(q^2) \pm P_P^\mu\mathcal{D}_P(q^2)\,, \tag{2.10}$$

JHEP08(2016)098

in complete analogy with (2.1). Note that the $i\partial_\mu\big(\bar{s}(\gamma_5)b\big)$ operator only contributes to $P_P^\mu \sim q^\mu$, since the total derivative is replaced by the momentum transfer q^μ. In eq. (2.9) we have included this contribution into round brackets with the other derivative FF. Before discussing eqs. (2.6)–(2.9) in various limits, we wish to stress that the equations are completely general and have to be obeyed by any FF determination.

The Isgur-Wise relations [25] follow from a clear physical picture. At low recoil the non-relativistic heavy quark effective theory applies and it can be shown that $\mathcal{D}_i$ are suppressed by $(\Lambda_{\rm QCD}/m_b)$ with respect to the vector and tensor FFs [24]. This raises the question of whether there are combinations of $\mathcal{D}_i$'s which are small at large recoil. Eqs. (2.6), (2.7) are direct candidates but eqs. (2.8), (2.9) require some thought because of the common direction q_μ. In fact in eqs. (2.8), (2.9) the poles in q^2 cancel between the FF $\mathcal{V}_3, \mathcal{V}_P$ and $\mathcal{D}_3, \mathcal{D}_P$ which implies that $\mathcal{D}_3, \mathcal{D}_P$ are not individually small. Since the $\langle K^*|\bar{s}\gamma_\mu\gamma_5 b|\bar{B}\rangle$ matrix element is free from singularities, adding eqs. (2.8), (2.9) yields a combination for which the derivative FFs are potentially small. We define the following ratios

$$\begin{aligned}
r_\perp(q^2) &= -\frac{(m_b+m_s)\mathcal{V}_1(q^2)}{T_1(q^2)} = \frac{m_b+m_s}{m_B+m_{K^*}}\frac{V(q^2)}{T_1(q^2)}\,,\\
r_\parallel(q^2) &= -\frac{(m_b-m_s)\mathcal{V}_2(q^2)}{T_2(q^2)} = \frac{m_b-m_s}{m_B-m_{K^*}}\frac{A_1(q^2)}{T_2(q^2)}\,,\\
r_{0+t}(q^2) &= -\frac{(m_b-m_s)\big(\mathcal{V}_2(q^2)-c_{23}(q^2)\big(\mathcal{V}_3(q^2)+\mathcal{V}_P(q^2)\big)\big)}{T_2(q^2)-c_{23}(q^2)T_3(q^2)}\\
&= -\frac{(m_b-m_s)\big(\mathcal{V}_0(q^2)-c_{23}(q^2)\mathcal{V}_P(q^2)\big)}{T_0(q^2)}\\
&= \frac{m_b-m_s}{m_B-m_{K^*}}\frac{A_1(q^2)+c_{23}(q^2)\frac{2m_{K^*}(m_B-m_{K^*})}{q^2}\big(A_3(q^2)-A_0(q^2)\big)}{T_2(q^2)-c_{23}(q^2)T_3(q^2)}\,,
\end{aligned} \tag{2.11}$$

where $X_0 = X_2 - c_{23}X_3$ for $X = T, \mathcal{V}$ with $c_{23}(q^2)$ being a kinematic function defined in (D.3). The deviations of these quantities from one measure the relative size of the derivative FFs with respect to vector and tensor FFs,

$$r_\perp = 1 + \frac{\mathcal{D}_\perp}{T_1}\,, \qquad r_\parallel = 1 + \frac{\mathcal{D}_\parallel}{T_2}\,, \qquad r_{0+t} = 1 + \frac{\mathcal{D}_{0+t}}{T_0}\,, \tag{2.12}$$

where $\mathcal{D}_\perp = \mathcal{D}_1$, $\mathcal{D}_\parallel = \mathcal{D}_2$ and $\mathcal{D}_{0+t} = \mathcal{D}_2 - c_{23}(\mathcal{D}_3 + \mathcal{D}_P)$. In figure 1 we show plots of these ratios from $0 < q^2 < 14\,\text{GeV}^2$. The quantities $r_{\perp,\parallel}$ and, somewhat less, r_{0+t} are found to be very close to unity over this range. The basic idea is that if the $\mathcal{D}_i$ are considered as regular FFs with controlled uncertainty[5] then this implies a high degree of correlation between vector and tensor FFs of a given polarisation. This is partly reflected in the controlled error bands.

The aspect of the correlation between the continuum thresholds is discussed in some more detail in appendix A.2. Here we just summarise the main argument and result.

[5]For the $B \to K^*$ channel at $q^2 = 1\,\text{GeV}^2$ the corrections due to twist-4 and α_s-correction for $\{(T_1, \mathcal{D}_\perp), (T_0, \mathcal{D}_{0+t})\}$ are $\{(4,6),(7,28)\}\%$ and $\{(12,27),(11,31)\}\%$ respectively indicating regularity of $\mathcal{D}_i$ with regard to the twist- and the α_s-expansion.

JHEP08(2016)098

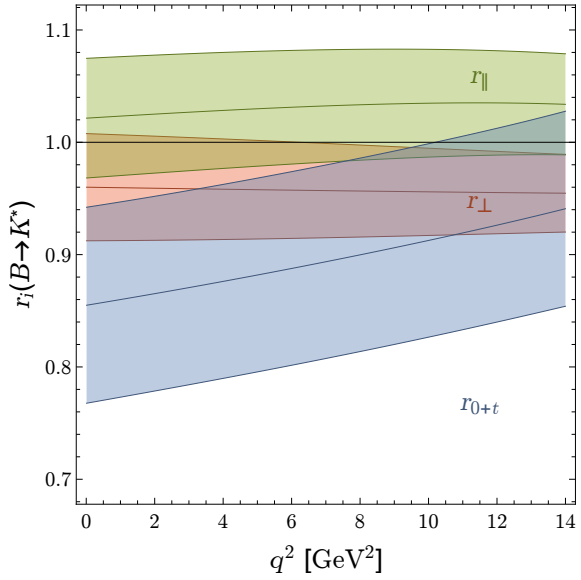

Figure 1. Plots of $r_\perp$, $r_\parallel$ and r_{0+t} eq. (2.11) (for the $B \to K^*$-transition) as a function of q^2. The deviation from unity measures the relative size of the derivative form factor with respect to the tensor and vector FFs. The mass used in (2.11) is the pole mass, an issue discussed in appendix A.5. For the explicit m_b mass we use the central value and do not include an error since in the $B \to V\ell\ell$ helicity amplitudes the m_b-pole is not present. The fact that the quantities tend towards one for very high q^2 is expected from the viewpoint of the Isgur-Wise relations and proves a certain robustness of the LCSR-results for high q^2. Similar ratios have been plotted in previous work in the context of Isgur-Wise relations [21] and LEL relations [26] but the observation that this might be useful for the correlating the continuum thresholds was not made. In particular the derivative form factor were not identified as a independent objects.

Based on the EOM we argue, conservatively, that the continuum thresholds for tensor and vector FF cannot differ by more than $1\,\text{GeV}^2$ in order for the continuum thresholds of the derivative FF not to take on absurdly low or high values. This argument is less compelling for the $(0+t)$-direction, as can be inferred from the plots, resulting in lower correlation and larger error bands. We stress that if we were to impose standard error bands, say $s_0 = 35(2)\,\text{GeV}^2$ for the sum rule of the $\mathcal{D}_i$ FFs then the error bands for r_i-ratios would shrink to the 1%-level.

The smallness of the derivative form factors (cf. also [4] for further references and more physical discussion) is related to the findings of Charles et al. [5] within the LEL and its extension into SCET [6, 27]. The similarity is the use of the EOM of motion but the difference is that in this work the EOM are directly implemented within QCD whereas in the prior work the EOM are used at the level of an effective theory in $1/m_b$. This results in differences at the level of $1/m_b$ corrections. For example in [6] the ratio analogous to $r_\perp$ (2.11), which we shall denote by $r_\perp^{\text{BF}} = m_B/(m_B + m_{K^*})\,(V/T_1) = 1 + \mathcal{O}(m_b^{-1}, \alpha_s m_b^0)$, differs from ours by $m_B \to (m_b + m_s)$ which is indeed $\mathcal{O}(m_b^{-1})$. For completeness let us mention that the symmetry breaking corrections to $r_\perp^{\text{BF}}$ were computed to $\mathcal{O}(\alpha_s m_b^0)$ and $\mathcal{O}(\alpha_s^2 m_b^0)$ in [6] and [28, 29] respectively. Even though the twist expansion of LCSR is not

JHEP08(2016)098

a $1/m_b$-expansion, as first stated for $B \to P$ and $B \to V$ decays in [16] and [30], it is of interest to examine the various twist-quantities from the viewpoint of the standard heavy quark scaling prescriptions [16]. At the level of all explicit calculations in the literature it is found that $T_1(0) \sim V(0)|_{\text{twist-2,3}} \sim m_b^{-3/2}$ and $T_1(0) \sim V(0)|_{\text{twist-4}} \sim m_b^{-5/2}$. The derivative FFs follow $\mathcal{D}_1(0)|_{\text{twist-2,3}} \sim m_b^{-5/2}$ [4] which is in agreement with the explicit computation in [5]. For this work we have explicitly checked that $\mathcal{D}_1(0)|_{\text{twist-4}} \sim m_b^{-7/2}$ and that $\mathcal{D}_1(0) \sim \mathcal{O}(\alpha_s) m_b^{-3/2}$, in accord with the results of Beneke and Feldmann [6]. In summary we may state that the parametric statements and the previous numeric statements give a consistent picture.

2.3 Discussion of non-resonant background effects

The signal final state in a $B \to \rho(\to \pi\pi)\ell\nu$-type decay, serving as a template for any $B \to V\ell_1\ell_2$ decay, is $\pi\pi\ell\nu$. Hence in principle the decay ought to be analysed via a $B \to \pi\pi$ type form factor.[6] The analysis of $B \to \rho\ell\nu$ therefore becomes a matter of how background, finite width and S,P-wave effects are treated or discerned. This question arises in any theoretical computation as well as in any experimental measurement. It is therefore important that both theory and experiment treat these issues in a consistent way.

Let us contrast the ρ final state with the $\pi\pi$-state from a pragmatic viewpoint relevant for this paper. The orbital angular momentum of the $\pi\pi$-state is either $l = 0, 1, \ldots$ ($S, P, \ldots$-wave). If the $\pi\pi$-state originates from a ρ-meson then it is necessarily in a P-wave state and shows a distinct angular distribution. Hence this contribution can be separated through an angular analysis from other type of partial waves.[7] We therefore conclude that the S-wave contribution is not to be included in a $B \to \rho$ FF and we therefore do not need to attribute any additional uncertainty to it.

We turn to the question of the treatment of the P-wave. For the sake of concreteness we discuss the $B \to J/\Psi\pi^+\pi^-$ measurement of the LHC collaboration [38]. In a certain window around $m_{\pi\pi}^2 \simeq m_\rho^2$ the $\pi\pi$-spectrum, in the P-wave, is fitted through an ansatz of a resonant ρ and the two excited $\rho(1450)$ and $\rho(1700)$ states. The main fit parameters are the amplitudes (complex residues) of the Breit-Wigner ansatz whose values determine the interference pattern. A non-resonant P-wave background is usually not fitted for since it is assumed that the S-wave is dominant in the non-resonant background.[8] This raises the question of how a theoretical framework like LCSR can accommodate this complex procedure. The answer is surprisingly pragramatic. As long as the experimental input into the LCSR is treated in the same way there is no systematic effect.

Let us argue this point in some more detail. In current LCSR determinations of the $B \to V$ FFs the V-meson is described by vector meson DAs. The latter are mainly

[6] Within the framework of LCSR this could be done by using the a two-pion DA [31–34]. The technology for pursuing a $B \to \pi\pi$ FF computation on the lattice has been put forward recently in reference [35].

[7] The importance of separating the S-wave, in the context of $B \to K^*\ell\ell$-type decays, was emphasised not long ago in [36]. Thereafter the S-wave FFs $B \to (K\pi)_{\text{S-wave}}$ were computed in LCSR in the tree level approximation [37].

[8] In the cases where a background has been searched for in $B \to \rho\ell\nu$, it has been found to be consistent with zero [39, 40]. Whether or not future experiments can discern the background is difficult for us to judge but we argue that from a pragmatic point of view this might not be necessary.

JHEP08(2016)098

characterised by the longitudinal and transverse decay constants $f_V^{\parallel}$ and $f_V^{\perp}$ respectively and it is therefore important to know how they are obtained. The method of choice for determining $f_V^{\parallel}$ is experiment: $e^+e^- \to V^0(\to PP)$ (for $V^0 = \rho^0, \phi, \omega$) and $\tau^+ \to V^+(\to PP)\nu$ (for $V^+ = K^{*,+}, \rho^+$) cf. appendix C. As long as the experimental treatment of the ρ-meson versus $\pi\pi$-signal event is the same as for the semileptonic decay $B \to (\rho \to \pi\pi)\ell\nu$ the decay constant encodes the same definition of the ρ-meson as used in $B \to \rho\ell\nu$. The other quantities associated with the ρ-DA are not directly accessible in experiment. For example the transverse decay constant $f_V^{\perp}$ is obtained through ratios of $f_V^{\parallel}/f_V^{\perp}$ from lattice QCD and sum rules where one would expect effects of the treatment of the ρ-meson to cancel to a large extent or to be taken care of by the respective uncertainties.

We may discuss the same reasoning from the viewpoint of a computation using a two-pion DA instead of a ρ DA. Let us consider for example the contribution of the DA that couples to the vector current. The latter is described at lowest order in the conformal spin expansion by $f_\rho^{\parallel}$ times the asymptotic DA which follows from conformal symmetry. From the formulae in [32] it is seen that the analogue of the two-pion DA is given by the pion FF $f_+^{(\pi)}(q^2)$ times the asymptotic DA. Somewhat symbolically the transitions in terms of ρ and 2-pion DAs are given by

$$\text{vector } \rho\text{-DA}: \qquad f_\rho^{\parallel} \cdot \mathrm{BW}(m_{\pi\pi}^2) \to \frac{f_\rho^{\parallel} m_\rho g_{\rho\pi\pi}}{m_{\pi\pi}^2 - m_\rho^2 - i m_\rho \Gamma_\rho} + \dots\,, \tag{2.13}$$

$$\text{vector } \pi\pi\text{-DA}: \qquad f_+^{(\pi)}(m_{\pi\pi}^2) \to \frac{f_\rho^{\parallel} m_\rho g_{\rho\pi\pi}}{m_{\pi\pi}^2 - m_\rho^2 - i m_\rho \Gamma_\rho} + \dots\,, \tag{2.14}$$

for $m_{\pi\pi}^2 \simeq m_\rho^2$ where $g_{\rho\pi\pi}$ is the $\rho \to \pi\pi$ decay constant, BW stands for some type of Breit-Wigner ansatz and the dots stand for all contributions other than the ρ-resonance from the $\pi\pi$ P-wave. Our argument is that unless one is specifically interested in the local $m_{\pi\pi}^2$-behaviour this contribution can and is effectively absorbed into $f_\rho^{\parallel}$ upon integration over the ρ mass window in the experimental analysis. For higher order conformal spin corrections, i.e. higher Gegenbauer moments, and other decay constants the same reasoning applies. The strong rescattering phases in the $\pi\pi$-channel are universal in each partial wave and do not distort the result.

In summary, from a pragmatic viewpoint as long as the treatment of the $\rho(\to \pi\pi)$-meson is the same that is used for the extraction of $f_\rho^{\parallel}$, the LCSR should not suffer from sizeable additional uncertainties. It therefore seems that in practice the uncertainty is a small fraction of the the P-wave background which itself is around 5%.[9] In view of all

[9]Despite this aspect it is of interest to estimate the non-ρ background. One can get an idea by analysing the pion FF $f_+^{(\pi)}(q^2)(p_1 - p_2)_\mu = \langle \pi(p_1)\pi(p_2)|j_\mu^{\mathrm{em}}|0\rangle$. A measure of the non-resonant background around the ρ-meson peak is given by the difference of the model-independent determination of the pion FF using data on $\pi\pi$-scattering phase shifts and the Omnès-dispersion relation versus a fitted ρ-meson Breit-Wigner ansatz. Around the ρ-meson mass window the difference is found to be $\sim 5\%$ (we are grateful to Gilberto Colangelo and Peter Stoffer for providing with the necessary plots and their insights into this matter). Similar conclusions can be reached when considering the figures in [41] with and without the $\rho(1450)$ and $\rho(1700)$ contributions. We note that 5% is of the same order as the S-wave background found in $B \to \pi\pi\ell\nu$ [42].

JHEP08(2016)098

	$f^{\parallel}$ [GeV]	$f^{\perp}$ [GeV]	$a_2^{\parallel}$	$a_2^{\perp}$	$a_1^{\parallel}$	$a_1^{\perp}$	$\zeta_3^{\parallel}$ [46]
ρ	0.213(5)	0.160(7)	0.17(7)	0.14(6)	–	–	0.030(10)
ω	0.197(8)	0.148(13)	0.15(12)	0.14(12)	–	–	idem
K^*	0.204(7)	0.159(6)	0.16(9)	0.10(8)	0.06(4)	0.04(3)	0.023(8)
ϕ	0.233(4)	0.191(4)	0.23(8)	0.14(7)	–	–	0.024(8)

Table 1. The determination of $f^{\parallel}$ is discussed in some detail in appendix C. The fine structure constant α, relevant for the extraction of $f_V^{\parallel}$, is evaluated at $\mu = 1\,\text{GeV} \sim m_V$. Scale dependent quantities, e.g. $f^{\perp}$, $a_{1,2}^{\parallel,\perp}$ and $\zeta_3^{\parallel}$, are evaluated at $\mu_F = 1\,\text{GeV}$. The parameters $a_{1,2}^{\parallel,\perp}$ are taken to be the same as in [47] which include computations from [46, 48–51]. The $f^{\perp}$ decay constants are obtained from $f^{\parallel}$ through ratios $r[X] = f_X^{\perp}(2\,\text{GeV})/f_X^{\parallel}$ with $r[\rho] = 0.687(27)$, $r[K^*] = 0.712(12)$ and $r[\phi] = 0.750(8)$ from lattice QCD [52]. For the ω-meson we adopt $r[\omega] \simeq r[\rho]$ in view of a lack of a lattice QCD determination of this quantity. Twist-3 DA parameters are taken from the values for $\omega_3^{\perp}, \omega_3^{\parallel}$ and $\tilde{\omega}_3^{\parallel}$ [46] which include $\zeta_3^{\parallel}$ (quoted in the table), $\omega_3^{\parallel}$, $\omega_3^{\perp}$. The twist-4 3-particle DA parameters are neglected since they are at the sub per mill domain. Again, for the ω-meson we adapt the same values as for the ρ-meson since a specific determination is lacking.

other sizeable uncertainties we refrain from adding any further error due to this effect and reemphasise the importance of comparing our result only with the P-wave contribution of the corresponding $\pi\pi$-pair. Whereas the analysis in this section questions the practical impact of using a two-pion DA around the the ρ-meson mass, it is of course interesting to look at the B_{ℓ_4} decay $B \to \pi\pi\ell\nu$ in other regions of phase space. For recent theoretical developments of B_{ℓ_4} we refer the reader to [43, 44] which are though not yet at the level of maturity of K_{ℓ_4} [45].

2.4 Input parameters and uncertainties

The uncertainty of the LCSR results for the FFs is determined from the uncertainties on the input parameters, the factorisation scale μ_F and the Borel parameter M^2 as well as the effective continuum threshold s_0. The values of input parameters used in our calculation, along with the errors assigned can be found in table 1. We draw the reader's attention to the fact that it is the quantity $[F(q^2) \cdot f_B]$, where F stands for any of the seven form factors, that is determined from the correlation function. Therefore one needs to divide by f_B in order to obtain the FF F. It is well known and appreciated that the uncertainty in α_s is considerably reduced when sum rule in f_B is taken to same order as for the quantity $[F \cdot f_B]$. For example f_B increases by $\sim 9\%$ at $\mathcal{O}(\alpha_s^2\beta_0)$ whereas the combination $(f_+^{B\to\pi} f_B)_{\text{LCSR}}/(f_B)_{\text{SR}}$ only increases by 2% [53]. Therefore we make use of the QCD sum rules result at $\mathcal{O}(\alpha_s)$ [54, 55] for f_B.

The two sum rule specific parameters are the Borel parameter M^2 and the effective continuum threshold s_0. For reasons of consistency the Borel parameter is to be chosen at an extremum (cf. appendix A.6) which serves as a quality control parameter. The continuum threshold is more problematic and the final result does depend on the choice. Hence our recipe for the error analysis is to assume a sizeable uncertainty for the continuum threshold. The new ingredient of our analysis is that we have argued that the EOM

JHEP08(2016)098

results in correlations between continuum thresholds of certain FFs; (cf. appendix A.2 for an elaborate discussion). The correlations used are summarised in and in between eqs. (A.8) and (A.9). The correlation of the continuum thresholds are such that the relative uncertainty is $1\,\mathrm{GeV}^2$ which has to be compared to the individual uncertainty of $2\,\mathrm{GeV}^2$ or the uncertainty of their sum which is close to $4\,\mathrm{GeV}^2$. The influence of the Borel parameter on the light-cone sum rule is negligible as compared to the continuum threshold of the light-cone sum rule and we therefore do not vary them separately for each FF. The Borel parameter dependence of the f_B-sum rule is sizeable and is taken into account and contributes to the uncertainty of the normalisation of the FFs. The intermediate states for the light-cone and the f_B sum rule are the same since they couple to the same interpolating current J_B. It would therefore seem absurd, or contradictive to the method, if the corresponding continuum thresholds were far apart. We implement this reasoning by correlating $s_0^{f_B}$ and s_0^{LC} at the 50%-level which implies that the uncertainty on the difference is $2\,\mathrm{GeV}^2$; a factor of $\sqrt{2}$ lower than without correlations.

We turn to the choice of the actual central values of the continuum threshold and the Borel parameter. It is useful to recall that if the sum rules were perfect then the LCSR FF would be independent of the Borel parameter. In reality a small Borel parameter is desirable from the viewpoint of suppressing any higher states in the spectrum whereas a large Borel parameter improves the convergence of the light-cone operator product expansion (LC-OPE). In practice one therefore chooses a compromise value which is usually found as an extremum. The flatness of the FF around this extremum as a function of the Borel parameter is a measure of the quality of the sum rule. In appendix A.6 it is shown that extremising in the Borel parameter is formally equivalent to imposing a daughter sum rule for m_B^2. From the viewpoint of the physics, the effective continuum threshold is expected to lie somewhere between $(m_B + 2m_\pi) \simeq 30.9\,\mathrm{GeV}^2$ and $(m_B + m_\rho)^2 \simeq 36.6\,\mathrm{GeV}^2$ with the true value being closer to the latter since the production of a ρ-meson is much more likely than the production of two non-resonant pions. The twist-4 contribution for $\pm$-helicity ($T_{1,2}$, V, and A_1) is around 5% whereas for 0-helicity (T_{23}, A_{12} and A_0) they are just below the 10%-range. Guided by the relative size of the twist-2 and twist-3 radiative versus tree contribution[10] we estimate the uncertainty due to the missing $\mathcal{O}(\alpha_s)$ twist-4 contribution[11] by associating a Gaussian error of 50% to the latter.

In order to limit contamination due to higher states we verify that the continuum contribution does not exceed 30%. If one assumes that semi-global quark hadron-duality itself works at the 30%-level the additional suppression reduces this error to just below the 10%-level. The sum rule parameters, with some more details in the caption, are given in table 2.

2.5 Series expansion fits to LCSR form factors

As mentioned in the introduction, for phenomenological analyses of rare decays, it is crucial to take into account the theoretical uncertainties of the $B \to V$ FFs and the correlations

[10] We remind the reader that the actual impact of the radiative corrections on the FF result is considerably smaller since a large part is absorbed by the radiative corrections to f_B (cf. the beginning of this subsection).

[11] More precisely no $\mathcal{O}(m_V^2)$ are included at $\mathcal{O}(\alpha_s)$. (cf. table II in [2]). We impose a 50% uncertainty on the corresponding tree-level terms.

JHEP08(2016)098

B_q	$M^2_{f_{B_q}}$	$s_0^{f_{B_q}}$	$M^2_{\rm LC}$	$s_0^{\rm LC}$
B_d	4.1(1)	34.2(2)	$c_c/\langle u\rangle_{q^2} M^2_{f_{B_d}}$	35(2)
B_s	4.4(1)	35.4(2)	$c_c/\langle u\rangle_{q^2} M^2_{f_{B_s}}$	36(2)

Table 2. Sum rule parameters for B_d and B_s sum rules. All numbers are in units of GeV^2, $M^2_{f_B(\text{LC})}$ and $s_0^{f_B(\text{LC})}$ denote the Borel parameter and continuum threshold of the f_B sum rule and the LCSR of $f_B F(q^2)$ (where F stands for a FF) respectively. The difference between the B_d and B_s continuum thresholds follows $(m_{B_d}+\Delta)^2 = s_0|_{B_d}$ and $(m_{B_s}+\Delta)^2 = s_0|_{B_s}$. The average momentum fraction of the transition quark $\langle u\rangle_{q^2}$ (cf. [19] for the definition) varies smoothly from 0.86 at $q^2 = 0\,\text{GeV}^2$ to 0.77 at $q^2 = 14\,\text{GeV}^2$. Dividing the sum rule parameter by this quantity serves to take into account q^2-dependence the Borel parameter under the extremisation procedure. The value $c_c = 2.2$ is determined through the mentioned procedure of extremisation. The criteria in the text imply that the Borel parameter of the LCSR is considerably higher than that from the f_B-sum rule [19].

F_i	J^P	$m_{R,i}^{b\to d}/\text{GeV}$	$m_{R,i}^{b\to s}/\text{GeV}$
A_0	0^-	5.279	5.366
T_1, V	1^-	5.325	5.415
T_2, T_{23}, A_1, A_{12}	1^+	5.724	5.829

Table 3. Masses of resonances of quantum numbers J^P as indicated necessary for the parameterisation of FF F_i for $b\to d$ and $b\to s$ transitions.

among them. In order to facilitate the use of the LCSR results, we perform fits of the full analytical result to a simplified series expansion (SSE), which is based on a rapidly converging series in the parameter

$$z(t) = \frac{\sqrt{t_+ - t} - \sqrt{t_+ - t_0}}{\sqrt{t_+ - t} + \sqrt{t_+ - t_0}}\,, \tag{2.15}$$

where $t_\pm \equiv (m_B \pm m_V)^2$ and $t_0 \equiv t_+(1-\sqrt{1-t_-/t_+})$. We write the FFs as

$$F_i(q^2) = P_i(q^2) \sum_k \alpha_k^i \big[z(q^2) - z(0)\big]^k, \tag{2.16}$$

where $P_i(q^2) = (1-q^2/m^2_{R,i})^{-1}$ is a simple pole corresponding to the first resonance in the spectrum. The appropriate resonance masses are given in table 3. We consider fits that are truncated after the quadratic term in z, i.e. we will have three fit parameters $\alpha_{0,1,2}$ for each of the seven FFs. We will see in section 2.6 that a three-parameter fit is sufficient for a combined fit to lattice and LCSR results in the entire kinematic range relevant for $B\to V\ell^+\ell^-$ decays.

Note that the parameterisation (2.16) differs from that used in [10, 11]. It has the advantage that the value of the FF at $q^2 = 0$ is among the fit parameters, $F_i(0) = \alpha_0^i$. We prefer this parameterisation as it allows to impose the exact kinematical relations $A_0(0) = (8m_B m_V)/(m_B^2 - m_V^2)\, A_{12}(0)$ (which is equivalent to $A_0(0) = A_3(0)$) and $T_1(0) = T_2(0)$ at

JHEP08(2016)098

	$B \to K^*$	$B \to \rho$	$B \to \omega$	$B_s \to \phi$	$B_s \to K^*$
$A_0(0)$	0.356 ± 0.046	0.356 ± 0.042	0.328 ± 0.048	0.389 ± 0.045	0.314 ± 0.048
$A_1(0)$	0.269 ± 0.029	0.262 ± 0.026	0.243 ± 0.031	0.296 ± 0.027	0.230 ± 0.025
$A_{12}(0)$	0.256 ± 0.033	0.297 ± 0.035	0.270 ± 0.040	0.246 ± 0.029	0.229 ± 0.035
$V(0)$	0.341 ± 0.036	0.327 ± 0.031	0.304 ± 0.038	0.387 ± 0.033	0.296 ± 0.030
$T_1(0)$	0.282 ± 0.031	0.272 ± 0.026	0.251 ± 0.031	0.309 ± 0.027	0.239 ± 0.024
$T_2(0)$	0.282 ± 0.031	0.272 ± 0.026	0.251 ± 0.031	0.309 ± 0.027	0.239 ± 0.024
$T_{23}(0)$	0.668 ± 0.083	0.747 ± 0.076	0.683 ± 0.090	0.676 ± 0.071	0.597 ± 0.076

Table 4. Values of the FFs at $q^2 = 0$ and their uncertainties. The tensor FFs are renormalised at the pole mass of the b-quark $\mu_{\rm UV} = 4.8\,\text{GeV}$. For a more detailed error breakdown we refer the reader to the table 7 of the previous LCSR FF work [2].

the level of the SSE coefficients as

$$\alpha_0^{A_0} = \frac{8 m_B m_V}{m_B^2 - m_V^2}\, \alpha_0^{A_{12}}\,, \qquad \alpha_0^{T_1} = \alpha_0^{T_2}\,. \tag{2.17}$$

The results for the FFs at $q^2 = 0$ are provided in table 4. To determine the fit coefficients α_i, the uncertainties, and the correlations between them, we first generate an ensemble of $N = 500$ input parameter sets where the values of the input parameters are randomly distributed according to a multivariate normal distribution with the location given by the central values and the covariance given by the uncertainties and correlations of the input parameters discussed above. We then compute all FFs at integer values of q^2 between 0 and $14\,\text{GeV}^2$. Finally, we fit the z expansion to all seven FFs for the N ensembles of FF values and extract the mean, variance, and correlation of the z expansion coefficients $\alpha_{0,1,2}$. Since we impose the exact conditions (2.17) throughout, the number of independent fit parameters is 19.

The resulting mean and variance are shown in table 14. We do not reproduce the full 21×21 correlation matrices in the paper but rather provide them as downloadable ancillary files which are available on the arXiv preprint page (see appendix F for details). Here we merely note that these correlations are sizeable and it is crucial to include them when using the FFs in phenomenological analyses.

With these results at hand, the uncertainty of an observable Ψ (e.g. angular observable) can be computed via

$$\sigma^2(\Psi) = \sum_{k,l,i,j} \frac{\partial \Psi(F_i)}{\partial \alpha_k^i}\, \text{cov}(\alpha_k^i, \alpha_l^j)\, \frac{\partial \Psi(F_i)}{\partial \alpha_l^j}\,. \tag{2.18}$$

where $i, j = 1 \ldots 7$ denotes the FF index and $k, l = 0 \ldots 2$ parameterises the expansion coefficients of the z-series. The covariance matrix is defined as

$$\text{cov}(\alpha_k^i, \alpha_l^j) = \text{corr}(\alpha_k^i, \alpha_l^j)\, \sigma(\alpha_k^i)\, \sigma(\alpha_l^j) \qquad \text{(no sums)} \tag{2.19}$$

in terms of the correlation matrix and the variances.

JHEP08(2016)098

As an example let us write the formula relevant to the ratio $\mathcal{R}_1(q^2) = (m_B + m_V)/m_B T_1(q^2)/V(q^2)$ whose difference from 1 marks difference from the large energy limit [6]. At $q^2 = 0$ the error of the FF ratio is given by

$$\sigma\left(\frac{T_1(0)}{V(0)}\right)^2 = \left(\frac{\alpha_0^{T_1}}{\alpha_0^V}\right)^2\left[\left(\frac{\sigma(\alpha_0^{T_1})}{\alpha_0^{T_1}}\right)^2 + \left(\frac{\sigma(\alpha_0^V)}{\alpha_0^V}\right)^2 - 2\frac{\sigma(\alpha_0^{T_1})\sigma(\alpha_0^V)}{\alpha_0^{T_1}\alpha_0^V}\,\mathrm{corr}(\alpha_0^{T_1}, \alpha_0^V)\right] \tag{2.20}$$

from which we obtain $\mathcal{R}_1(0)^{B\to K^*} = 0.97 \pm 0.04$.

2.6 Interpolating between lattice and LCSR form factors

The LCSR and lattice FF calculations are complementary since the former is valid at low q^2 and the latter at high q^2. Performing a combined fit of the SSE parameterisation to both lattice and LCSR results is useful for two reasons. First, whether a good fit to two completely independent methods in two different kinematical regions is possible at all is a powerful consistency check of those methods. Second, in phenomenological analyses constraining physics beyond the SM combining both observables at low and at high q^2, one needs a consistent set of FFs for the full q^2 range.

To obtain this combined fit, we first generate pseudo-data points with correlated theoretical uncertainties at three q^2 values both at low and at high q^2. For LCSR at low q^2, we proceed as in the previous subsection. For the lattice FFs at high q^2, we make use of the parameterisation of lattice FFs provided in [11]. We generate an ensemble of series expansion coefficient sets randomly distributed according to a multivariate normal distribution, using the fitted central values and covariance given in [11]. For each of the sets, we then evaluate the FFs at the three q^2 values and extract the uncertainties and correlation of these pseudo-data points.

We then construct a χ^2 function

$$\begin{aligned}\chi^2(\alpha_0^1, \ldots, \alpha_2^7) = &+ \sum_{ijkl}\left[F^i_{\mathrm{LCSR}}(q_k^2) - F^i_{\mathrm{fit}}(q_k^2; \alpha_m^i)\right](C^{ijkl}_{\mathrm{LCSR}})^{-1}\left[F^j_{\mathrm{LCSR}}(q_l^2) - F^j_{\mathrm{fit}}(q_l^2; \alpha_n^j)\right] \\ &+ \sum_{ijkl}\left[F^i_{\mathrm{latt}}(q_k^2) - F^i_{\mathrm{fit}}(q_k^2; \alpha_m^i)\right](C^{ijkl}_{\mathrm{latt}})^{-1}\left[F^j_{\mathrm{latt}}(q_l^2) - F^j_{\mathrm{fit}}(q_l^2; \alpha_n^j)\right]\end{aligned} \tag{2.21}$$

where F^i_X are the central values of the pseudo data points of FF i and C^{ijkl}_X the corresponding covariance matrices (taking into account both the correlation between different FFs and different q^2 values). We then sample a likelihood $L = e^{-\chi^2/2}$ using a Markov Chain Monte Carlo (MCMC) approach with flat priors for the series expansion coefficients. From the stationary distribution of the MCMC, we extract the central values and covariance of the coefficients.

Figure 2 shows the fit result for the $B \to K^*$ FFs in the variable q^2. The FF plots, in the $z(q^2)$-variable, for the modes $B \to K^*$, $B_s \to \phi$ and $B_s \to \bar{K}^*$ are shown in figures 5, 6, 7 of appendix E. The LCSR and lattice pseudo-data points are shown in blue and red. The light red dashed band shows the 2-parameter fit from [11]. The solid gray band is our combined 3-parameter fit result. The numerical fit coefficients, of both fits, are reproduced in table 15 in appendix F. As for the pure LCSR fit, the central values, the

JHEP08(2016)098

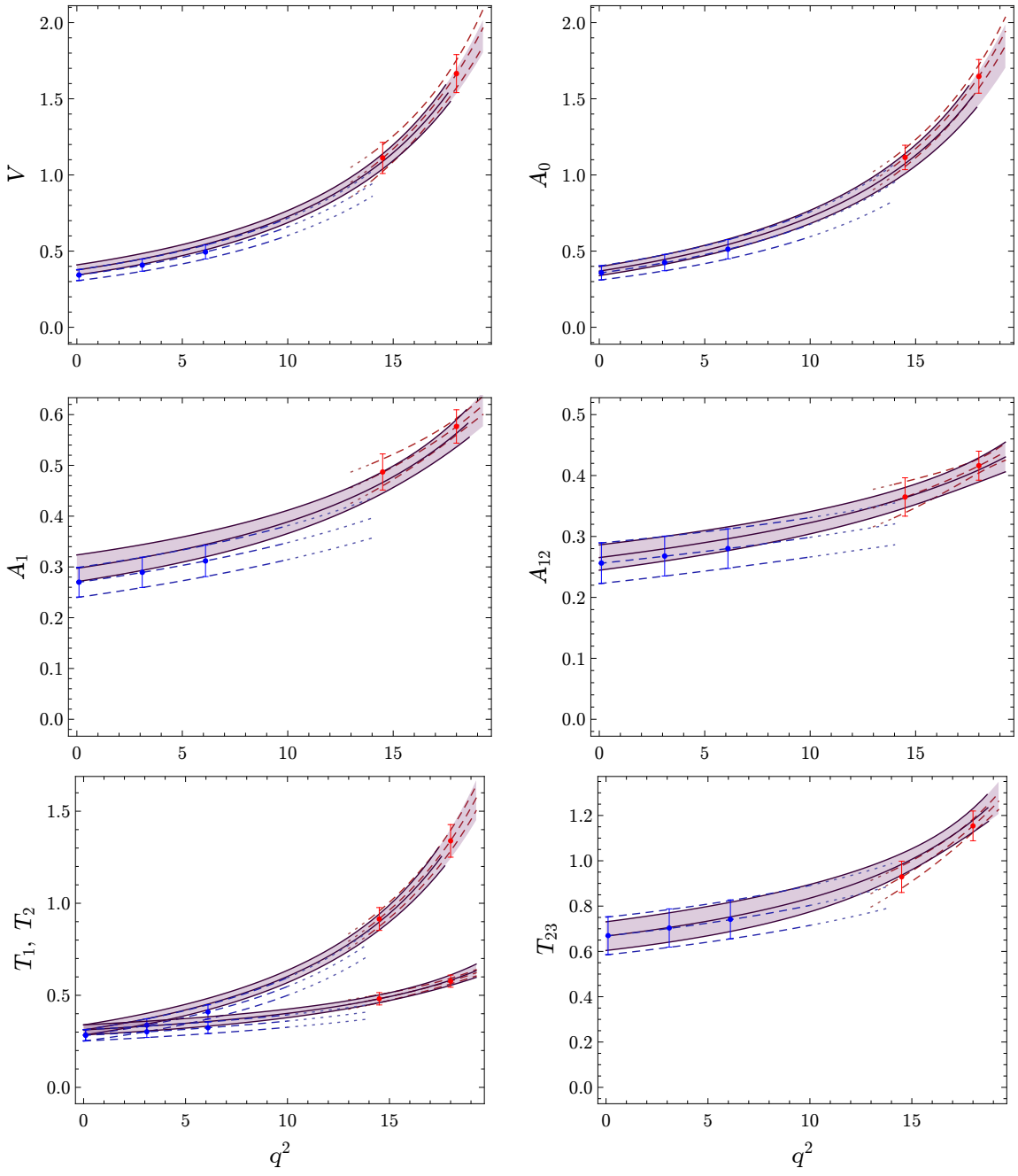

Figure 2. Combined LCSR and lattice fit to $B \to K^*$ FFs, where lattice data points are indicated in red, LCSR points in blue, the gray solid band shows the combined 3-parameter fit and the red dashed band the 2-parameter lattice fit from ref. [11]. In the lower left plot $T_1 > T_2$ for $q^2 > 0\,\text{GeV}^2$ above.

uncertainties and all correlations are provided as ancillary files on the arXiv preprint page (see appendix F).

We would like to add that the fits are valid under the premise that the LCSR and lattice QCD data points and their uncertainties, including correlations, are valid as well

JHEP08(2016)098

as the z-expansion being a reasonable model function. There is no evidence against the latter, as we have found that adding higher orders in the z expansion and using different parameterisations does not change matters. This is an aspect that could change in the future with more precise FF determination from LCSR or lattice QCD. Overall the agreement is good. For the central values, we find a χ^2 of 7.0 for $B \to K^*$, 10.2 for $B_s \to \phi$, and 19.5 for $B_s \to K^*$, for 16 degrees of freedom. The fits in the $z(q^2)$-variable, shown in figures 5, 6, 7, are particularly useful in judging the quality of the fits. In these figures the FFs times $P = (q^2 - m_R^2)$ is plotted. The latter serves to cancel the first physical pole, at the resonance R, in the q^2-spectrum. The remaining slope therefore is a measure of the behaviour of the higher poles or cuts in the q^2-spectrum.

An interesting qualitative feature is the behaviour of the $B \to K^*$ versus $B_s \to \phi$ lattice FFs $P \cdot T_{23}(q^2)$ (and to some extent also $P \cdot A_{12}$). From figures 5, 6 is seen that the slopes are opposite in direction for the two cases. In a LCSR computation, valid at low q^2, such a qualitative difference cannot arise since the main difference between the FFs for $B \to K^*$ versus $B_s \to \phi$ is due to hadronic input data (which is numerically similar). It is possible that by going closer to the hadronic spectrum, at high q^2, a more distinct pattern arises in accordance with the lattice QCD computation. It will be interesting to see whether this qualitative feature which is not yet statistically significant is confirmed in future lattice predictions with higher statistics and a more complete treatment of the vector mesons (e.g. physical quark masses).

To this end we would like to add that differences in normalisation of $\parallel, \perp$ (V, A_1 and $T_{1,2}$) versus 0-helicity (A_0 A_{12} and T_{23}) in the LCSR computation are highly sensitive to $f_V^{\parallel}$ and $f_V^{\perp}$ decay constants. For instance the 0-helicity FFs depend to $\sim 75\%$ on the normalisation of $f_V^{\parallel}$ with the situation being just the opposite for the $\parallel, \perp$-helicity FFs.

3 Phenomenological applications

We make use of the updated FFs and their error correlations in predicting experimentally accessible observables. More specifically we consider the $b \to s$ flavour-changing neutral current transitions (FCNC) $B \to K^* \mu^+ \mu^-$, $B \to K^* \gamma$, $B_s \to \phi \mu^+ \mu^-$ sensitive to physics beyond the SM and the branching fractions of the tree-level decays $B \to (\rho, \omega) \ell \nu$. The latter are of interest to extract the CKM matrix element $|V_{\rm ub}|$ and conversely serve as a test of the FF normalisation (and shape) when $|V_{\rm ub}|$ is taken as an input from other channels and global fits.

3.1 $B \to K^* \mu^+ \mu^-$ at low q^2

The decay $B \to K^* \mu^+ \mu^-$, being one of the golden channels of LHCb, requires no introduction. It has received a great deal of attention, particularly in the last decade. By making use of the large energy relation [5], observables have been identified which have reduced uncertainties with respect to FFs (e.g. [9]). Recent measurements and analyses of several of these observables by LHCb [56–59], CMS [60], ATLAS [61] and Belle [62] have revealed a number of potential tensions with the SM predictions. Whether or not this is

JHEP08(2016)098

due to new physics or hadronic effects is a subject of vital debate [7, 8, 63–67]. This motivates reinvestigation into predictions of hadronic quantities such as the FFs undertaken in this work.

In the SM, neglecting the muon mass, the differential decay distribution of $B \to K^*\mu^+\mu^-$ can be written in terms of of six helicity amplitudes

$$H_\iota^V = N\sqrt{q^2}\left(C_9^{\text{eff}}(q^2)\,\mathcal{V}^{(\iota)}(q^2) + \frac{2m_b}{q^2}\,C_7^{\text{eff}}(q^2)\,T^{(\iota)}(q^2) + i\sqrt{\lambda}\,\frac{2m_b}{q^2}\,\Delta_\iota(q^2)\right), \tag{3.1}$$

$$H_\iota^A = N\sqrt{q^2}\,C_{10}\,\mathcal{V}^{(\iota)}(q^2), \tag{3.2}$$

where $\iota = +, -, 0$ denotes the polarisation of the K^*-meson. The helicity FFs $T^{(\iota)}, \mathcal{V}^{(\iota)}$ are defined as in appendix D and Δ_ι stands for various corrections to be discussed further below. The quantity

$$N \equiv V_{\text{tb}}V_{\text{ts}}^*\left[\frac{G_F^2\alpha^2}{3\cdot 2^{10}\pi^5 m_B^3}\lambda^{1/2}\right]^{1/2}, \tag{3.3}$$

is a normalisation factor where G_F stand for Fermi's constant, e for the electric charge and $V_{\text{tb(s)}}$ are CKM matrix elements. The differential branching ratio is then given by

$$\frac{d\text{BR}(B_q \to K^*\mu^+\mu^-)}{dq^2} = \tau_{B_q}\frac{1}{2}\sum_{\iota=\pm,0}\sum_{X=V,A}|H_\iota^X|^2. \tag{3.4}$$

Factorisable quark loop contributions are absorbed into Wilson coefficients C_7^{eff} and C_9^{eff} which therefore become q^2-dependent (e.g. [26] for the definition). The quantities Δ_ι contain the NNLL corrections to the matrix elements of the current-current operators [68] as well as various "non-factorisable" contributions. The latter entail the effect of weak annihilation, the chromomagnetic operator contribution both computed in LCSR [12, 47] as well as hard spectator scattering taken from QCD factorisation [69, 70].

An important contribution arises due to the final state leptons emerging from charm quarks; so called charm loops. At high q^2 the effect of the broad charmonium resonances measured by the LHCb-collaboration [71] has turned out to be substantially more sizeable than anticipated [66]. More precisely, for $\text{BR}(B \to K\mu\mu)$ the resonance residues are found to be ~ 2.5 larger with opposite sign from naive factorisation indicating sizeable duality violations [66]. It therefore seems well-motivated to discuss the various contributions in some detail. At low $q^2 < 6\,\text{GeV}^2$ such effects are thought to be captured in the partonic language of charm quarks and gluons. The $\mathcal{O}(\alpha_s)$ hard vertex corrections [68] factorise in the heavy quark limit into a q^2-dependent function times the FF. The part which does not contain gluon exchanges between the hadron transition and the charm loop factorises non-perturbatively by definition and the q^2-dependent function is given by the vacuum polarisation. The latter can be extracted in a model-independent way from $e^+e^- \to$ hadrons-data.[12] These contributions, as mentioned above, are included in the central values of the predictions of our work. In addition there is soft gluon emission from the charm loop into the B-meson as well as the K^*-meson. Both effects have been assessed in LCSR, the former

[12] Cf. [66] for a recent determination.

JHEP08(2016)098

with a B-meson DA [72] and the latter with K^*-meson DA (for $B \to K^*\gamma$ only) [73, 74]. The combination of the two results is not completely free from model-dependence.[13] At q^2 approaching the charmonium resonance region, the contribution is predicted to be significantly enhanced, rendering the partonic theory prediction unreliable above about $6\,\text{GeV}^2$. These two effects, the soft gluon emission and the charmonium effect, can be captured in the region $q^2 \in [0, 6\,\text{GeV}^2]$ by a linear parameterisation

$$\Delta_\iota^{c\bar{c}}(q^2) = \frac{i}{\sqrt{\lambda}}\, C_7^{\text{eff}}\, T^{(\iota)} \left[a_\iota e^{i\phi_{a_\iota}} + b_\iota e^{i\phi_{b_\iota}} \left(\frac{q^2}{6\,\text{GeV}^2} \right) \right], \tag{3.5}$$

where a, b are positive numbers and $\phi_{a,b}$ are strong phases whose parameter ranges we discuss further below. Note that (3.5) and the replacement of

$$C_7^{\text{eff}} \to C_7^{\text{eff}} \left[1 + a_\iota e^{i\phi_{a_\iota}} + b_\iota e^{i\phi_{b_\iota}} \left(\frac{q^2}{6\,\text{GeV}^2} \right) \right] \tag{3.6}$$

in (3.1) are equivalent to each other. The parameterisation (3.5) is convenient for low q^2 since it incorporates the helicity hierarchy $\Delta_+ \ll \Delta_-$[14] through the FF parameterisation. This results in $a_+ \simeq a_-$ and $b_+ \simeq b_-$. We find[15]

$$\begin{aligned} a_\pm &\in [0, 0.05]\,, \qquad & b_\pm &\in [0, 0.2]\,, \\ a_0 &\in [0, 0.2]\,, & b_0 &\in [0, 0.05]\,. \end{aligned} \tag{3.7}$$

where a_ι is mainly fixed at low q^2 by the soft gluon emission [72–74] and b_ι is then determined to cover the J/Ψ uncertainty. We vary the phase of the J/Ψ-residue in the dispersion representation in the full range motivated by the findings in [66]. Note that the absolute value of the residues are known from the polarisation specific branching fractions $B \to J/\Psi K^*$. The asymmetry between the parameter values of a_0, b_0 and $a_\pm, b_\pm$ is due to the $\pm$ directions being sensitive to the photon pole (contrary to the 0-helicity direction). At intermediate q^2 this hierarchy disappears which can for example be seen from the polarisation fractions of the $B \to J/\Psi K^*$ amplitudes or the general result that the helicity amplitudes are degenerate at the kinematic endpoint [76]. In summary the uncertainty due to soft gluon emission and nearby resonances is covered by the parameterisation (3.6) with parameter ranges as given in (3.7) and varying the phases $\phi_{a,b}$ in the full range.

Numerical predictions in different q^2 bins for $B^0 \to K^{*0}\mu^+\mu^-$ observables (see e.g. refs. [26, 77, 78] for definitions of the angular observables) and the $B^+ \to K^{*+}\mu^+\mu^-$ branching ratio are given in tables 6, 7 and 8 respectively. Crucially uncertainties are split into parametric,[16] FF and non-factorisable charm uncertainties as parameterised in

[13] The problem is that the two effects are computed in two, slightly, different frameworks. It would be best to compute, in either of the two frameworks, the radiative corrections which would then include both effects as well as the $\mathcal{O}(\alpha_s)$ vertex corrections. This could be a rather challenging as it would seem to require analytic results in order to be verify the dispersion relation.

[14] We refer the reader to the appendix of [47] and [75] for recent theoretical discussions of this topic.

[15] Compared to the parameterisation used in [67] the value of b_0 is considerably reduced. For the observables presented in this paper this effect has a negligible influence on the values of the uncertainty.

[16] The parametric uncertainties, with values adopted from the PDG [79], include $|V_{\text{tb}}V_{\text{ts}}^*| = (4.01 \pm 0.10) \cdot 10^{-2}$, the scale variation $\mu = 4.8 \pm 0.8\,\text{GeV}$, the b-quark $\overline{\text{MS}}$ mass $m_b(m_b) = 4.18 \pm 0.03\,\text{GeV}$ and the pole mass of the charm quark $m_c = 1.4 \pm 0.2\,\text{GeV}$.

JHEP08(2016)098

Parameter	Value	Ref.
τ_{B^0}	1.520(4) ps	[80]
$\tau_{B^\pm}$	1.638(4) ps	[80]
τ_{B_s}	1.604(10) ps	[80]
$\Delta\Gamma_s/\Gamma_s \equiv 2y_s$	0.124(9)	[80]
$\lvert V_{cb}\rvert$	$4.221(78) \times 10^{-2}$	[79]
$\lvert V_{tb}V_{ts}^*/V_{cb}\rvert$	0.980(2)	

Table 5. Numerical inputs for the SM predictions.

eq. (3.5). It is observed that the dominant uncertainty of the branching fraction is due to FFs and amounts to about 20% relative to the central value. In the case of the angular observables the error is considerably reduced by the inclusion of the correlations. Comparing the angular observables $S_{4,5}$ with the related observables $P_{4',5'}$ it is noted that the FF uncertainties are comparable. This improvement for $S_{4,5}$ observables is due to the inclusion of correlated uncertainties in the FFs. The error due to the Δ-corrections results in comparable uncertainties in both bases. The advantage of using fully correlated errors in explicit computation over general parameterisation can be seen by comparing the uncertainties in our work versus those of ref. [8].

For comparison of the $B \to K^*\mu^+\mu^-$ observables to existing experimental measurements of $3\,\text{fb}^{-1}$ LHCb data and the implications for new physics, we refer the reader to [67], where the FF results of this work were used for a global analysis of $b \to s$ transitions.

Values of important parameters used for all the SM predictions are given in table 5.

3.2 $B \to K^*\gamma$

The precise experimental determination of the branching ratio for $B \to K^*\gamma$ provides a good opportunity to compare our results for the FFs to experiment. The branching ratio of $B \to K^*\gamma$ is given by

$$\text{BR}(B_q \to K^*\gamma) = \tau_{B_q} 48\pi^2 \left(|H_+^q|^2 + |H_-^q|^2\right), \tag{3.8}$$

where $q = u, d$. We have introduced the superscript q in addition to the previous section because we give separate predictions for charged and neutral modes. The amplitudes are related to the limit of the vector helicity amplitudes of $B \to K^*\ell^+\ell^-$ at vanishing dilepton invariant mass,

$$H_\pm^q(B \to K^*\gamma) = \lim_{q^2\to 0} \frac{q^2}{e} H_\pm^{V,q}(B \to K^*\ell^+\ell^-). \tag{3.9}$$

They can be written as

$$H_\pm^q = \frac{N}{e}\sqrt{\lambda_0}\Big(2m_b\, C_7^{\text{eff}}\left(T_\pm(0) + i\,2\,m_b\,\Delta_\pm^q(0)\right)\Big), \tag{3.10}$$

where and $\lambda_0 = \lambda|_{q^2=0} = (m_B^2 - m_{K^*}^2)^2$ is the Källén-function for the photon final state and $T_\pm(0) = T^{(\pm)}(q^2)/\sqrt{\lambda(q^2)}|_{q^2=0}$ which results in $T_+(0) = 2T_1(0)$ and $T_-(0) = 0$. The quantity $T^{(\pm)}$ is defined in appendix D. For $\Delta_\pm(0)$, the following contributions are included,

JHEP08(2016)098

$B^0 \to K^{*0}\mu^+\mu^-$		
Observable	q^2 bin	SM prediction
$10^7 \frac{d\text{BR}}{dq^2}$	$[0.1, 1]$	$0.897 \pm 0.035 \pm 0.147 \pm 0.050$
	$[1, 2]$	$0.436 \pm 0.017 \pm 0.094 \pm 0.014$
	$[2, 3]$	$0.400 \pm 0.015 \pm 0.091 \pm 0.010$
	$[3, 4]$	$0.409 \pm 0.016 \pm 0.091 \pm 0.008$
	$[4, 5]$	$0.432 \pm 0.016 \pm 0.091 \pm 0.010$
	$[5, 6]$	$0.461 \pm 0.018 \pm 0.093 \pm 0.012$
	$[1.1, 2.5]$	$0.420 \pm 0.016 \pm 0.093 \pm 0.013$
	$[2.5, 4]$	$0.406 \pm 0.088 \pm 0.087 \pm 0.094$
	$[4, 6]$	$0.447 \pm 0.017 \pm 0.092 \pm 0.011$
	$[1.1, 6]$	$0.426 \pm 0.016 \pm 0.091 \pm 0.009$
A_{FB}	$[0.1, 1]$	$-0.093 \pm 0.000 \pm 0.012 \pm 0.001$
	$[1, 2]$	$-0.140 \pm 0.002 \pm 0.036 \pm 0.010$
	$[2, 3]$	$-0.072 \pm 0.002 \pm 0.021 \pm 0.020$
	$[3, 4]$	$0.010 \pm 0.002 \pm 0.011 \pm 0.026$
	$[4, 5]$	$0.085 \pm 0.002 \pm 0.023 \pm 0.030$
	$[5, 6]$	$0.152 \pm 0.002 \pm 0.034 \pm 0.031$
	$[1.1, 2.5]$	$-0.122 \pm 0.002 \pm 0.033 \pm 0.013$
	$[2.5, 4]$	$-0.010 \pm 0.011 \pm 0.011 \pm 0.010$
	$[4, 6]$	$0.120 \pm 0.002 \pm 0.029 \pm 0.031$
	$[1.1, 6]$	$0.014 \pm 0.002 \pm 0.011 \pm 0.025$
F_L	$[0.1, 1]$	$0.330 \pm 0.004 \pm 0.064 \pm 0.018$
	$[1, 2]$	$0.749 \pm 0.004 \pm 0.053 \pm 0.019$
	$[2, 3]$	$0.825 \pm 0.001 \pm 0.041 \pm 0.009$
	$[3, 4]$	$0.805 \pm 0.000 \pm 0.046 \pm 0.005$
	$[4, 5]$	$0.757 \pm 0.000 \pm 0.055 \pm 0.011$
	$[5, 6]$	$0.702 \pm 0.001 \pm 0.062 \pm 0.016$
	$[1.1, 2.5]$	$0.782 \pm 0.003 \pm 0.048 \pm 0.016$
	$[2.5, 4]$	$0.812 \pm 0.044 \pm 0.047 \pm 0.046$
	$[4, 6]$	$0.728 \pm 0.001 \pm 0.059 \pm 0.013$
	$[1.1, 6]$	$0.768 \pm 0.001 \pm 0.051 \pm 0.006$

Table 6. Standard model predictions for binned $B^0 \to K^{*0}\mu^+\mu^-$ observables, where the uncertainties are split into parametric uncertainties, FF uncertainties, and our estimate of the uncertainties due to missing hadronic effects.

- corrections to the matrix elements of current-current operators [68];
- hard scattering contributions computed in QCD factorisation [69, 70];
- non-factorisable contributions of the chromomagnetic penguin operator O_8 computed in LCSR [47];
- weak annihilation computed in LCSR [12].

JHEP08(2016)098

$B^0 \to K^{*0}\mu^+\mu^-$		
Observable	q^2 bin	SM prediction
S_4	$[0.1, 1]$	$0.093 \pm 0.000 \pm 0.005 \pm 0.003$
	$[1, 2]$	$0.005 \pm 0.001 \pm 0.009 \pm 0.010$
	$[2, 3]$	$-0.096 \pm 0.001 \pm 0.015 \pm 0.013$
	$[3, 4]$	$-0.163 \pm 0.001 \pm 0.019 \pm 0.013$
	$[4, 5]$	$-0.206 \pm 0.001 \pm 0.019 \pm 0.011$
	$[5, 6]$	$-0.233 \pm 0.000 \pm 0.017 \pm 0.009$
	$[1.1, 2.5]$	$-0.027 \pm 0.001 \pm 0.010 \pm 0.011$
	$[2.5, 4]$	$-0.148 \pm 0.018 \pm 0.019 \pm 0.018$
	$[4, 6]$	$-0.220 \pm 0.001 \pm 0.018 \pm 0.010$
	$[1.1, 6]$	$-0.145 \pm 0.001 \pm 0.016 \pm 0.012$
S_5	$[0.1, 1]$	$0.254 \pm 0.000 \pm 0.009 \pm 0.004$
	$[1, 2]$	$0.110 \pm 0.004 \pm 0.017 \pm 0.020$
	$[2, 3]$	$-0.090 \pm 0.004 \pm 0.017 \pm 0.027$
	$[3, 4]$	$-0.222 \pm 0.003 \pm 0.024 \pm 0.028$
	$[4, 5]$	$-0.306 \pm 0.002 \pm 0.025 \pm 0.025$
	$[5, 6]$	$-0.360 \pm 0.002 \pm 0.022 \pm 0.022$
	$[1.1, 2.5]$	$0.048 \pm 0.004 \pm 0.016 \pm 0.023$
	$[2.5, 4]$	$-0.192 \pm 0.023 \pm 0.023 \pm 0.023$
	$[4, 6]$	$-0.334 \pm 0.002 \pm 0.023 \pm 0.024$
	$[1.1, 6]$	$-0.185 \pm 0.003 \pm 0.019 \pm 0.026$
P_4'	$[0.1, 1]$	$0.240 \pm 0.001 \pm 0.006 \pm 0.007$
	$[1, 2]$	$0.014 \pm 0.003 \pm 0.022 \pm 0.025$
	$[2, 3]$	$-0.273 \pm 0.005 \pm 0.029 \pm 0.042$
	$[3, 4]$	$-0.430 \pm 0.003 \pm 0.021 \pm 0.031$
	$[4, 5]$	$-0.491 \pm 0.001 \pm 0.016 \pm 0.020$
	$[5, 6]$	$-0.518 \pm 0.001 \pm 0.014 \pm 0.013$
	$[1.1, 2.5]$	$-0.070 \pm 0.004 \pm 0.026 \pm 0.032$
	$[2.5, 4]$	$-0.398 \pm 0.022 \pm 0.022 \pm 0.022$
	$[4, 6]$	$-0.504 \pm 0.001 \pm 0.015 \pm 0.016$
	$[1.1, 6]$	$-0.358 \pm 0.003 \pm 0.022 \pm 0.029$
P_5'	$[0.1, 1]$	$0.653 \pm 0.002 \pm 0.009 \pm 0.012$
	$[1, 2]$	$0.280 \pm 0.008 \pm 0.031 \pm 0.043$
	$[2, 3]$	$-0.254 \pm 0.011 \pm 0.044 \pm 0.082$
	$[3, 4]$	$-0.585 \pm 0.008 \pm 0.035 \pm 0.070$
	$[4, 5]$	$-0.732 \pm 0.005 \pm 0.029 \pm 0.051$
	$[5, 6]$	$-0.799 \pm 0.003 \pm 0.028 \pm 0.039$
	$[1.1, 2.5]$	$0.126 \pm 0.009 \pm 0.038 \pm 0.057$
	$[2.5, 4]$	$-0.517 \pm 0.043 \pm 0.040 \pm 0.039$
	$[4, 6]$	$-0.765 \pm 0.004 \pm 0.028 \pm 0.044$
	$[1.1, 6]$	$-0.459 \pm 0.008 \pm 0.034 \pm 0.064$

Table 7. Standard model predictions for binned angular $B^0 \to K^{*0}\mu^+\mu^-$ observables, where the uncertainties are split into parametric uncertainties, FF uncertainties, and our estimate of the uncertainties due to missing hadronic effects.

JHEP08(2016)098

$B^+ \to K^{*+}\mu^+\mu^-$		
Observable	q^2 bin	SM prediction
$10^7 \frac{d\text{BR}}{dq^2}$	$[0.1, 1]$	$0.923 \pm 0.036 \pm 0.155 \pm 0.052$
	$[1, 2]$	$0.474 \pm 0.018 \pm 0.102 \pm 0.015$
	$[2, 3]$	$0.438 \pm 0.017 \pm 0.099 \pm 0.010$
	$[3, 4]$	$0.448 \pm 0.017 \pm 0.098 \pm 0.009$
	$[4, 5]$	$0.472 \pm 0.018 \pm 0.099 \pm 0.011$
	$[5, 6]$	$0.502 \pm 0.019 \pm 0.100 \pm 0.014$
	$[1.1, 2.5]$	$0.458 \pm 0.017 \pm 0.101 \pm 0.013$
	$[2.5, 4]$	$0.445 \pm 0.095 \pm 0.094 \pm 0.102$
	$[4, 6]$	$0.487 \pm 0.018 \pm 0.099 \pm 0.012$
	$[1.1, 6]$	$0.466 \pm 0.018 \pm 0.099 \pm 0.009$

Table 8. Standard model predictions for the differential branching ratio of $B^+ \to K^{*+}\mu^+\mu^-$, where the uncertainties are split into parametric uncertainties, FF uncertainties, and our estimate of the uncertainties due to missing hadronic effects.

	Theory	Experiment
$10^5 \times \text{BR}(B^0 \to K^{*0}\gamma)$	$3.39 \pm 0.14 \pm 0.70 \pm 0.28$	4.33 ± 0.18
$10^5 \times \text{BR}(B^+ \to K^{*+}\gamma)$	$3.33 \pm 0.13 \pm 0.72 \pm 0.29$	4.21 ± 0.15

Table 9. SM predictions and experimental world averages for the branching ratios of $B^0 \to K^{*0}\gamma$ and $B^+ \to K^{*+}\gamma$. The theory uncertainty is split into parametric, FF, and non-factorisable power correction uncertainties.

The first of these corrections is by far the dominant one, leading to a +60% shift in the branching ratios. The three remaining ones contribute to the isospin asymmetry (e.g. [12]) of which WA is the one which is most sizeable.

Our predictions for the branching ratios are listed in table 9 along with the experimental world averages and are consistent with the experimental results at around 1σ. We would like to emphasise that the $B \to K^*\gamma$ is a FCNC and that the consistency cannot be taken to be one to one with a FF measurement. The $B \to (\rho, \omega)\ell\nu$ decays, discussed in section 3.5, are more favourable in this respect.

Another cross-check is the branching ratio of the decay $B \to K^* e^+ e^-$ at very low q^2 that is dominated by the photon pole and that has been measured recently by LHCb [81],

$$\text{BR}(B \to K^* e^+ e^-)^{30\text{–}1000\,\text{MeV}}_{\text{exp}} = \left(3.1^{+0.9+0.2}_{-0.8-0.3} \pm 0.2\right) \times 10^{-7}, \tag{3.11}$$

where the superscript refers to $\sqrt{q^2}$. An interesting observable is the ratio of this branching ratio to the $B \to K^*\gamma$ branching ratio, since theoretical uncertainties, factorisable or non-factorisable, cancel to a high degree. In the SM, we predict

$$R_{ee,\gamma} \equiv \frac{\text{BR}(B^0 \to K^{*0} e^+ e^-)^{30\text{–}1000\,\text{MeV}}}{\text{BR}(B^0 \to K^{*0}\gamma)} = (6.3 \pm 0.2) \times 10^{-3}, \tag{3.12}$$

where the residual error is dominated by FF uncertainties. Combining experimental errors in quadrature, from the LHCb measurement and the world average of $\text{BR}(B^0 \to K^{*0}\gamma)$,

JHEP08(2016)098

we obtain

$$R_{ee,\gamma}^{\text{exp}} = (7.2 \pm 2.1) \times 10^{-3}, \tag{3.13}$$

which is consistent with the prediction, albeit with sizeable uncertainties. Finally, for the angular observable F_L, that has been measured recently in $B^0 \to K^* e^+ e^-$ at low q^2 [82], we predict

$$F_L(B \to K^* e^+ e^-)^{45\text{–}1058\,\text{MeV}} = 0.203 \pm 0.003 \pm 0.058 \pm 0.017\,. \tag{3.14}$$

This is in very good agreement with the experimental value,

$$F_L(B \to K^* e^+ e^-)^{45\text{–}1058\,\text{MeV}}_{\text{exp}} = 0.16 \pm 0.06 \pm 0.03\,. \tag{3.15}$$

3.3 $B_s \to \phi\mu^+\mu^-$ at low q^2

The decay channel $B_s \to \phi\mu^+\mu^-$ is proceeds via the same quark level transition as $B \to K^*\mu^+\mu^-$ and may serve to compare possible deviations. An important difference between the two channels is that the ϕ-meson decays to K^+K^-, implying that the decay is not self-tagging in contrast to $B_d \to K^*\mu^+\mu^-$, where the flavour of the initial B-meson can be inferred from the charge of the $K\pi$ decay products of the K^*. As a consequence, among the observables discussed for $B \to K^*\mu^+\mu^-$, A_{FB} and S_5 cannot be measured at a hadron collider.

Other than CP asymmetries, the most interesting observables are then the differential branching ratio, F_L, and S_4, in the SM and beyond. For these observables, the three possible sources of difference between the results for $B_s \to \phi\mu^+\mu^-$ and those for $B \to K^*\mu^+\mu^-$ are as follows,

- the FFs are different;
- differences induced by spectator effects, e.g. weak annihilation;
- effects due to the sizeable B_s-$\bar{B}_s$ lifetime difference.

The FFs have already been discussed in sections 2.5 and 2.6. The spectator effects turn out to be very small in the SM and are not relevant compared to the FF uncertainties. For a discussion of effects beyond the SM we refer the reader to the appendix of ref. [12]. The lifetime effects are due to the B_s and $\bar{B}_s$ lifetime difference of roughly 6% absent for B_d-mesons. This leads to a difference between the observables defined in the absence of neutral meson oscillations, as used in the case of $B_d \to K^*\mu^+\mu^-$, and time-integrated observables, as measured experimentally [83]. This difference has to be taken into account when comparing theory predictions to experimental data. Details are discussed in appendix G.

In table 10, we list our numerical predictions for the differential branching ratio and angular observables accessible from an untagged measurement $B_s \to \phi\mu^+\mu^-$. The uncertainties are treated in the same way as for $B \to K^*\mu^+\mu^-$.

JHEP08(2016)098

$B_s \to \phi\mu^+\mu^-$		
Observable	q^2 bin	SM prediction
$10^7 \frac{d\text{BR}}{dq^2}$	$[0.1, 1]$	$1.067 \pm 0.042 \pm 0.155 \pm 0.058$
	$[1, 2]$	$0.497 \pm 0.019 \pm 0.099 \pm 0.017$
	$[2, 3]$	$0.450 \pm 0.017 \pm 0.096 \pm 0.011$
	$[3, 4]$	$0.459 \pm 0.017 \pm 0.096 \pm 0.009$
	$[4, 5]$	$0.484 \pm 0.018 \pm 0.097 \pm 0.011$
	$[5, 6]$	$0.516 \pm 0.019 \pm 0.099 \pm 0.015$
	$[1.1, 2.5]$	$0.476 \pm 0.018 \pm 0.098 \pm 0.014$
	$[2.5, 4]$	$0.455 \pm 0.017 \pm 0.096 \pm 0.009$
	$[4, 6]$	$0.500 \pm 0.019 \pm 0.098 \pm 0.013$
	$[1.1, 6]$	$0.479 \pm 0.018 \pm 0.097 \pm 0.010$
F_L	$[0.1, 1]$	$0.311 \pm 0.004 \pm 0.057 \pm 0.017$
	$[1, 2]$	$0.732 \pm 0.003 \pm 0.051 \pm 0.020$
	$[2, 3]$	$0.813 \pm 0.001 \pm 0.039 \pm 0.010$
	$[3, 4]$	$0.791 \pm 0.001 \pm 0.045 \pm 0.006$
	$[4, 5]$	$0.739 \pm 0.001 \pm 0.054 \pm 0.011$
	$[5, 6]$	$0.682 \pm 0.001 \pm 0.060 \pm 0.016$
	$[1.1, 2.5]$	$0.767 \pm 0.003 \pm 0.046 \pm 0.017$
	$[2.5, 4]$	$0.799 \pm 0.001 \pm 0.043 \pm 0.006$
	$[4, 6]$	$0.710 \pm 0.001 \pm 0.057 \pm 0.014$
	$[1.1, 6]$	$0.752 \pm 0.001 \pm 0.050 \pm 0.006$
S_4	$[0.1, 1]$	$0.088 \pm 0.000 \pm 0.005 \pm 0.002$
	$[1, 2]$	$0.003 \pm 0.001 \pm 0.009 \pm 0.010$
	$[2, 3]$	$-0.099 \pm 0.001 \pm 0.016 \pm 0.013$
	$[3, 4]$	$-0.166 \pm 0.001 \pm 0.019 \pm 0.012$
	$[4, 5]$	$-0.208 \pm 0.001 \pm 0.018 \pm 0.010$
	$[5, 6]$	$-0.234 \pm 0.000 \pm 0.016 \pm 0.008$
	$[1.1, 2.5]$	$-0.029 \pm 0.001 \pm 0.011 \pm 0.011$
	$[2.5, 4]$	$-0.151 \pm 0.001 \pm 0.018 \pm 0.013$
	$[4, 6]$	$-0.221 \pm 0.000 \pm 0.017 \pm 0.009$
	$[1.1, 6]$	$-0.146 \pm 0.001 \pm 0.016 \pm 0.012$

Table 10. Standard model predictions for binned, time-integrated $B_s \to \phi\mu^+\mu^-$ observables, where the uncertainties are split into parametric uncertainties, FF uncertainties, and our estimate of the uncertainties due to missing hadronic effects.

3.4 $R_{K^*\phi}$: $B \to K^*\mu^+\mu^-$ versus $B_s \to \phi\mu^+\mu^-$

The similarity of the $B \to K^*\mu^+\mu^-$ and $B_s \to \phi\mu^+\mu^-$ channels implies that the uncertainties of ratios of these observables should be strongly reduced.[17] Theory predicts $B_s \to \phi\mu^+\mu^-$ to have a higher transition than $B \to K^*\mu^+\mu^-$ which essentially comes from

[17] In this work we have not performed an error analysis on the ratios themselves. The latter would greatly reduce the error and could be undertaken if the experimental central values persist with smaller uncertainties.

JHEP08(2016)098

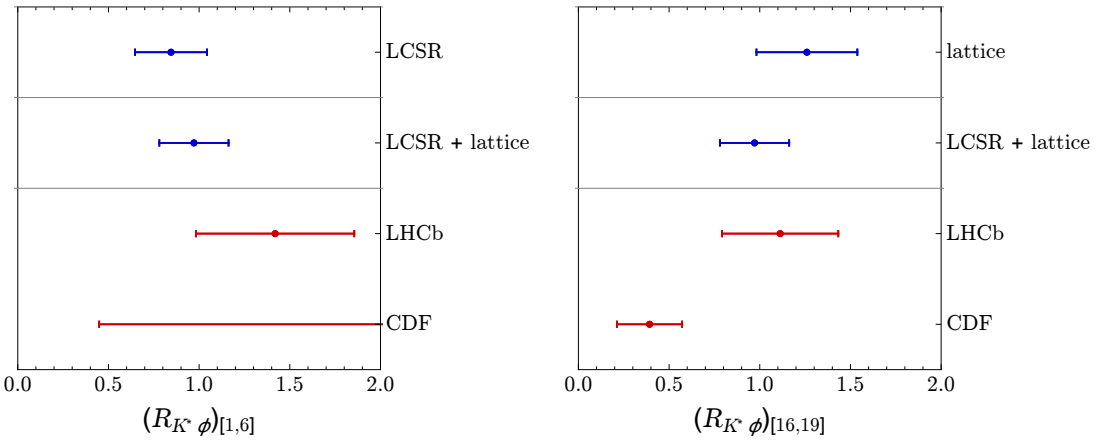

Figure 3. Our predictions for $R_{\phi K^*}$ at low and high q^2 using LCSR, Lattice and a combination of the two, compared to experimental results from LHCb with and integrated luminosity of $1\,\text{fb}^{-1}$ [56, 85] and CDF [86].

the decay constants (cf. table 1) showing this hierarchy. At low q^2 and for $\phi(K^*)\gamma$ final state (i.e. $q^2 = 0$) the central values of the LHCb results show the opposite effect.

First, we recapitulate the prediction for the branching ratio of $B_s \to \phi\gamma$ (see appendix A of ref. [12] for more details) versus $B \to K^*\gamma$. The effect is driven by $T_1^{B\to K^*}(0)/T_1^{B_s\to\phi}(0) = 0.89 \pm 0.10$,[18] resulting from the above mentioned decay constants, leads to

$$R_{K^*\phi}^{(\gamma)} = \frac{\text{BR}(B^0 \to K^{*0}\gamma)}{\text{BR}(B_s \to \phi\gamma)} = 0.78 \pm 0.18\,, \tag{3.16}$$

which is roughly 1.5 standard deviations below the LHCb measurement for this ratio, 1.23 ± 0.32 [84]. Such a deviation can, of course, not be regarded as statistically significant.

A similar ratio can also be considered for the decay to leptons,

$$R_{K^*\phi}[q_1, q_2] \equiv \frac{d\text{BR}(B^0 \to K^{*0}\ell^+\ell^-)/dq^2|_{[q_1,q_2]}}{d\text{BR}(B_s \to \phi\ell^+\ell^-)/dq^2|_{[q_1,q_2]}}\,, \tag{3.17}$$

by considering ratios of the differential branching ratios integrated over specified ranges in q^2. We show a graphical comparison of our predictions using LCSR, lattice and combinations of the two for the ratio $R_{\phi K^*}$ to the results of LHCb [56, 85] and CDF [86] at both low and high q^2 in figure 3. Again, the results per se are not statistically significant. On the qualitative level it is though interesting that the theoretical and the experimental ratio are below and above unity respectively. It is hard to see how the theoretical value can move above one, through redetermination of parameters, without uncovering a new physical effect. We stress once more that we have not undertaken an analysis with correlated errors for this quantity. One could easily expect the theory error to reduce down by a factor of two which would result in $R_{K^*\phi}|_{[1,6]} < 1$ within uncertainties. We are looking forward to the $3\,\text{fb}^{-1}$ results to reexamine this issue.

[18] The central value of this work, which is a more complete update, is $T_1^{B\to K^*}(0)/T_1^{B_s\to\phi}(0) = 0.91$.

JHEP08(2016)098

3.5 $|V_{\rm ub}|$ from $B \to (\rho, \omega)\ell\nu$

FCNC decays such as $B \to K^*\mu^+\mu^-$ and $B_s \to \phi\mu^+\mu^-$ are potentially affected by new physics and therefore do not provide an unambiguous environment to test FF predictions. The semi-leptonic decays $B \to (\omega, \rho)\ell^+\nu$ based on the charged current $b \to u$ transition occur at tree-level, and are therefore less likely to be affected by new physics and serve to test FF predictions. In particular in view of the current discrepancies between the $B \to K^*\mu^+\mu^-$ and $B_s \to \phi\mu^+\mu^-$ branching fraction measurements the normalisation of the FFs per se has become an issue of considerable interest.

The differential branching ratios of these decays, for $m_\ell = 0$, are given by

$$\frac{d\mathrm{BR}(B^0 \to \rho^-\ell^+\nu)}{dq^2} = \tau_{B^0}|V_{\rm ub}|^2 \frac{G_F^2}{192\pi^3 m_B^3}\sqrt{\lambda}\big(|\mathcal{V}^{(+)}|^2 + |\mathcal{V}^{(-)}|^2 + |\mathcal{V}^{(0)}|^2\big)\,, \tag{3.18}$$

$$\frac{d\mathrm{BR}(B^+ \to \rho^0\ell^+\nu)}{dq^2} = \frac{\tau_{B^+}}{2\tau_{B^0}}\frac{d\mathrm{BR}(B^0 \to \rho^-\ell^+\nu)}{dq^2}\,, \tag{3.19}$$

where definitions of $\mathcal{V}^{(\iota)}$ for $\iota = +, -, 0$ as well as λ, the Källén-function, can be found in appendix D, with the adaption $m_{K^*} \to m_\rho$. The one for $B^+ \to \omega\ell^+\nu$ is analogous to $B^+ \to \rho^0\ell^+\nu$ with obvious replacements.

The most recent measurements of the branching ratios have been performed for $B \to \rho\ell\nu$ by BaBar [87] and Belle [88] and for $B \to \omega\ell\nu$ by BaBar [89, 90] and Belle [88] respectively. We extract $|V_{\rm ub}|$ from the BaBar and Belle data by minimizing the χ^2 function that reads in both cases

$$\chi^2(|V_{\rm ub}|) = \sum_{ij}\big[B^i_{\rm exp} - B^i_{\rm th}(|V_{\rm ub}|)\big](C^{ij}_{\rm exp} + C^{ij}_{\rm th})^{-1}\big[B^j_{\rm exp} - B^j_{\rm th}(|V_{\rm ub}|)\big]\,, \tag{3.20}$$

where $B^i_{\rm exp}$ and $B^i_{\rm th}$ are the experimental and theoretical central values for the branching ratios in one q^2-bin and the sum runs over all bins for the charged and neutral mode. $C_{\rm th}$ is the theoretical covariance matrix that includes in particular the correlated FF uncertainties.[19] In the case of Belle, we use the data up to $q^2 = 8\,\mathrm{GeV}^2$ or $12\,\mathrm{GeV}^2$ and take the full covariance matrix provided in ref. [88]. The BaBar dataset consists of a single bin in the low-q^2 region from 0 to $8\,\mathrm{GeV}^2$ and the correlation between the charged and neutral decay is not provided. For $B \to \rho\ell\nu$ we obtain

$$|V_{\rm ub}|^{B\to\rho\ell\nu}_{\text{Belle, } q^2<8\,\mathrm{GeV}^2} = (3.36 \pm 0.17 \pm 0.34) \times 10^{-3}, \tag{3.21}$$

$$|V_{\rm ub}|^{B\to\rho\ell\nu}_{\text{Belle, } q^2<12\,\mathrm{GeV}^2} = (3.25 \pm 0.14 \pm 0.34) \times 10^{-3}, \tag{3.22}$$

$$|V_{\rm ub}|^{B\to\rho\ell\nu}_{\text{BaBar, } q^2<8\,\mathrm{GeV}^2} = (2.52 \pm 0.42 \pm 0.56) \times 10^{-3}, \tag{3.23}$$

and those from $B^+ \to \omega\ell^+\nu$ we get

$$|V_{\rm ub}|^{B\to\omega\ell\nu}_{\text{Belle, } q^2<7\,\mathrm{GeV}^2} = (2.49 \pm 0.34 \pm 0.32) \times 10^{-3}, \tag{3.24}$$

$$|V_{\rm ub}|^{B\to\omega\ell\nu}_{\text{BaBar, } q^2<8\,\mathrm{GeV}^2} = (3.25 \pm 0.36 \pm 0.53) \times 10^{-3}, \tag{3.25}$$

$$|V_{\rm ub}|^{B\to\omega\ell\nu}_{\text{BaBar, } q^2<12\,\mathrm{GeV}^2} = (3.25 \pm 0.29 \pm 0.46) \times 10^{-3}, \tag{3.26}$$

[19] In ref. [91], the importance of uncertainty correlations to extract V_{ub} from $B \to \rho\ell\nu$ decays has been emphasized.

JHEP08(2016)098

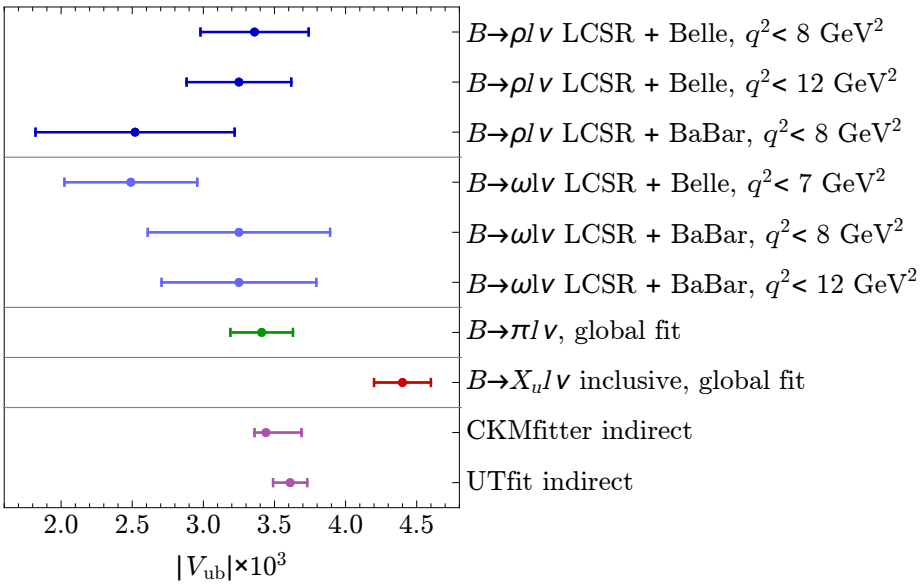

Figure 4. Our predictions for $|V_{\rm ub}|$ from $B \to \rho\ell\nu$ and $B \to \omega\ell\nu$ (blue) compared to global fits to $V_{\rm ub}$ from exclusive [79] and inclusive channels [88] and indirect determinations from fits of the unitarity triangle [92, 93].

where the first error is experimental and the second theoretical. For the FF $B \to \rho$ and $B \to \omega$ we have taken into account that it is a $b \to u$ and not a $b \to d$ transition by scaling the FFs as in (C.16).

Our results can be compared to the value extracted from $B \to \pi\ell\nu$ decays, obtained in ref. [88] from a global fit of BaBar and Belle data to lattice and LCSR computations,

$$|V_{\rm ub}|^{B\to\pi\ell\nu} = (3.41 \pm 0.22) \times 10^{-3}, \tag{3.27}$$

or the average of the inclusive semi-leptonic $b \to u$ determinations [79]

$$|V_{\rm ub}|^{\rm incl.} = \left(4.41 \pm 15^{+15}_{-17}\right) \times 10^{-3}, \tag{3.28}$$

where the first error is experimental and the second error is theoretical. Finally we also compare our results to the values obtained indirectly from global fits of the CKM matrix [92, 93],

$$|V_{\rm ub}|_{\rm CKMfitter} = \left(3.44^{+0.25}_{-0.08}\right) \times 10^{-3}, \qquad |V_{\rm ub}|_{\rm UTfit} = (3.61 \pm 0.12) \times 10^{-3}. \tag{3.29}$$

The various values for $|V_{\rm ub}|$ quoted in this section are summarised graphically in figure 4.

The $B \to (\rho, \omega)$ FFs do not, and should not, incorporate an S-wave contribution since the $(\rho, \omega) \to \pi\pi$ is necessarily in a P-wave (cf. section 2.3). Hence the experimental branching ratios might be too large which in turn leads to a systematic upward shift of $|V_{\rm ub}|$ as extracted from these analyses. In ref. [42] (cf. figure 9 of that reference) this effect has been analysed and it has been found that the integrated line-shapes of the S-wave over the interval $[m_\rho - \Gamma_\rho, m_\rho + \Gamma_\rho]$ is around 12% of the corresponding P-wave contribution.

JHEP08(2016)098

This means that if the S-wave is neglected altogether then we can expect an upward shift of $\sim 6\%$ of the $|V_{\rm ub}|$ values. In the BaBar and Belle analysis the S-wave has not been subtracted systematically. Hence if the precision below the 10%-level is to be reached then the experimental analyses have to perform an angular analysis[20] in order to subtract the S-wave.

Leaving aside the inclusive determinations we conclude that our $|V_{\rm ub}|$-values from the combined Belle and BaBar analysis are somewhat lower but surely consistent with $B \to \pi\ell\nu$ determinations as well as the global CKM fits. The values of $|V_{\rm ub}|$ which are considerably lower than the average come with large experimental uncertainties and are consistent at the level of one standard deviation. The uncertainty is rather large and an updated analysis with the full BaBar data set will be more telling.

4 Conclusions

In this paper we present an update of the light-cone sum rules FFs relevant for the $B \to V$ transitions $B_{d,s} \to K^*, \rho, \omega, \phi$ using new hadronic inputs such as decay constants (appendix C), the newly determined light-cone DAs $\mathbb{G}_\perp^{v,a}$ (twist-5) (appendix B) with explicit results given in appendix A.4 as well as in form of a Mathematica notebook. To corroborate the robustness of our predictions, we have discussed in detail the role of the equations of motion in reducing the uncertainties of tensor-to-vector FF ratios and mass scheme dependence in section 2.2 and appendix A.5 respectively. The impact of the V-meson being an unstable particle is analysed in section 2.3.

An important point of this work are the easy-to-use numerical expressions of the FFs, provided to the phenomenological community, that allow to retain all the uncertainty correlations among the FFs in phenomenological analyses. This is of particular importance for predicting angular observables that involve ratios of FFs. A z-expansion fit, eq. (2.16), to the FFs is provided along central values, uncertainties, and correlation matrices for the expansion coefficients; available in electronic form as ancillary files on the arXiv webages (see appendix F for details and table 14 for the central values). The parameterisation is chosen to transparently fulfil the two exact relations among the FFs at $q^2 = 0$. In addition we performed combined fits to LCSR and lattice computations of the FFs. This serves on the one hand to obtain predictions for the FFs valid in the full kinematic range, on the other hand as a cross-check of the consistency between the two complementary approaches, as they have to coincide for intermediate q^2 values; good agreement is observed between the two. Likewise the z-expansion coefficients and the correlated uncertainties of the combined fits are downloadable as ancillary files (and central values in table 15).

A phenomenological analysis is performed using the updated predictions and a new treatment of theoretical uncertainties. In sections 3.1 and 3.2, we have given updated Standard Model predictions for $B \to K^*\mu^+\mu^-$ and $B \to K^*\gamma$ observables, taking into account LCSR calculations of several hadronic effects beyond FFs and an estimate of the uncertainties due to missing hadronic effects, notably contributions from charm quarks. Potentially

[20] For the $\pi\pi$ final state one can make use of the isospin in order to deduce whether it is an S- or P-wave contribution [39].

JHEP08(2016)098

relevant long-distance effects which have not been fully computed are the complete $\mathcal{O}(\alpha_s)$ charm loops effects in one single framework as well as weak annihilation at $\mathcal{O}(\alpha_s)$. The latter could be sizeable since the chiral suppression might be relieved for radiative corrections. Likewise, in section 3.3 we have given predictions for $B_s \to \phi\mu^+\mu^-$ observables, showing (in appendix G) that the effect of the finite B_s-lifetime difference is negligible in the Standard Model. Our predictions are particularly relevant in view of several apparent tensions between Standard Model expectations and experimental measurements observed recently. A crucial question to address in the near future will be whether these tensions are due to underestimated hadronic effects or physics beyond the Standard Model. Our improved FF predictions can play an important role in answering this question.

In section 3.5, the new FF predictions were used to extract the CKM element $|V_{\rm ub}|$ from BaBar and Belle measurements of $B \to (\rho,\omega)\ell\nu$ decays. Barring some disagreement among the experiments, we find good agreement of our predictions with other exclusive predictions, e.g. $B \to \pi\ell\nu$ and global fits. Our results contribute to the enhancement of the ongoing tension between the exclusive and inclusive determination of $|V_{\rm ub}|$. From another viewpoint the encouraging agreement with other exclusive channels serve as a test of the FF normalisation which might become particularly important if the disagreement of $B \to K^*\ell^+\ell^-$ versus $B_s \to \phi\ell^+\ell^-$ becomes more significant. Our predictions for $|V_{\rm ub}|$ have a relative theory uncertainty at the level of 10% from $B \to \rho$ and 12–15% from $B \to \omega$, showing the potential of future, more precise measurements of these semi-leptonic decays to improve the precision on $|V_{\rm ub}|$.

We conclude by emphasising that our improved FF predictions are important for the tensions in both $b \to s$ channels and the determination of $|V_{\rm ub}|$. These questions can be further examined with future experimental data to which we look forward.

Acknowledgments

We thank Wolfgang Altmannshofer, Frederik Beaujean, Martin Beneke, Christoph Bobeth, Peter Boyle, Vladimir Braun, Gerhard Buchalla, Jérôme Charles, Gilberto Colangelo, Greig Cowan, Luigi Del Debbio, Jochen Dingfelder, Thorsten Feldmann, Gudrun Hiller, Lars Hofer, Fred Jegerlehner, Alex Khodjamirian, Andreas Kronfeld, Vera Luth, Kim Maltman, Stefan Meinel, Mikolai Misiak, Matthias Neubert, Nils Offen, Steve Playfer, Christoph Schwanda, Peter Stoffer, Javier Virto, Yuming Wang, and Matthew Wingate for useful discussions. R.Z. is particularly grateful to Patricia Ball for collaboration on $B \to V$ form factor computations in the past. The research of D.S. is supported by the DFG cluster of excellence "Origin and Structure of the Universe".

A Aspects of the LCSR determination of the form factors

A.1 Equation of motion and correlation functions

The LCSR FFs are computed from a correlation function of the type

$$C[\Gamma] = i \int d^4x e^{ip_B x} \langle K^*(p)|T\{\bar{s}\Gamma b(0) J_B(x)\}|0\rangle \,, \tag{A.1}$$

JHEP08(2016)098

where Γ is the Dirac-structure and $J_B \equiv m_b \bar{b} i\gamma_5 q$ an interpolating field for the B-meson. In fact, the projection on the B-meson through a dispersion relation and the Borel transformation can be seen as the substitute of the LSZ-formalism for the B-meson. It is well-known that at the level of correlation functions EOM (2.5) are corrected by contact terms. This results in

$$q^\nu C[i\sigma_{\mu\nu}(\gamma_5)] + \Delta_\mu^{(5)} = -(m_s \pm m_b) C[\gamma_\mu(\gamma_5)] + C[i(\overleftarrow{\partial} + \overrightarrow{\partial})_\mu(\gamma_5)] - 2iC[\overleftarrow{D}_\mu\,(\gamma_5)]\,, \tag{A.2}$$

where $\Delta_\mu^{(5)}$ denote the contact terms. A heuristic derivation of the contact term follows from the time derivative acting on the time ordering of the operators which leads to a commutator expression

$$\Delta_\mu^{(5)} = -\int d^3x e^{-ip\vec{_B}\cdot\vec{x}} \langle K^*(p,\eta)|[\bar{s} i\sigma_{\mu 0}(\gamma_5) b(0), J_B(\vec{x},0)]|0\rangle\,. \tag{A.3}$$

Using the canonical equal-time commutation relation for the b-quarks, $\{b_\alpha^\dagger(\vec{x},0), b_\beta(0)\} = \delta^{(3)}(\vec{x})\delta_{\alpha\beta}$, leads to[21]

$$\Delta_\mu = 0 \text{ and } \Delta_\mu^5 = -im_b f_V^{\parallel} \eta_\mu^*\,. \tag{A.4}$$

The crucial point is that the contact term is a local term which does not affect the extraction of the FFs at all since it does not enter the dispersion relation. Hence the FFs which are determined from the correlation function in LCSR obey the EOM. More precisely the EOM impose constraints/correlations on Borel parameters and continuum thresholds of sum rule parameters.

A.2 Correlation of continuum thresholds and Borel parameters

Each correlation function obeys a dispersion relation. Using the notation $C[\gamma^\mu] = C_1[\gamma^\mu]P_1^\mu + \ldots$, $C_1[\gamma^\mu]$ can be written as

$$C_1[\gamma^\mu] = \int_{\text{cut}}^\infty ds \frac{\rho_1[\gamma^\mu](s)}{s - p_B^2 - i0} = \frac{m_B^2 \mathcal{V}_1(q^2) f_B}{p_B^2 - m_B^2 + i0} + \int_{s_c}^\infty ds \frac{\rho_1[\gamma^\mu](s)}{s - p_B^2 - i0}\,, \tag{A.5}$$

where s_c marks the continuum threshold and "cut" stands for the beginning of the discontinuity which is just below $p_B^2 = m_B^2$. Since (A.2) is valid for any p_B^2 it follows from the representation (A.5) that the EOM are valid for the densities $\rho_1(s)$ point by point, i.e. locally. In particular subtracting the FF EOM (2.6) from (A.2) we obtain

$$q^\nu \int_{s_c}^\infty ds \frac{\rho_1[i\sigma_{\mu\nu}(\gamma_5)](s)}{s - p_B^2 - i0} = -(m_s + m_b) \int_{s_c}^\infty ds \frac{\rho_1[\gamma^\mu](s)}{s - p_B^2 - i0} - 2i \int_{s_c}^\infty ds \frac{\rho_1[\overleftarrow{D}_\mu](s)}{s - p_B^2 - i0} \tag{A.6}$$

for the direction P_1^μ with somewhat elaborate notation. This is of course true for the exact density as well as for the density $\rho_1^{\text{LC-OPE}}$ computed from the light-cone OPE. The semi-global quark-hadron duality, or sum rule approximation, consists of replacing the integral

[21] In the computation we have assumed that the vector meson is at rest. The result (A.4) is the covariantised version. Alternatively we could have derived the contact term directly from the path integral through field transformations or the (covariant) T^*-product. Both of which should directly yield a covariant result.

JHEP08(2016)098

on the right-hand side of (A.5) by:

$$\int_{s_c}^{\infty} ds \frac{\rho_1(s)}{s - p_B^2 - i0} \simeq \int_{s_0^V}^{\infty} ds \frac{\rho_1^{\text{LC-OPE}}(s)}{s - p_B^2 - i0}\,, \tag{A.7}$$

where s_0^V is some effective threshold parameter which is expected to lie somewhere between $(m_B{+}2m_\pi) \simeq 30.9\,\text{GeV}^2$ and $(m_B{+}m_\rho)^2 \simeq 36.6\,\text{GeV}^2$. A simple way to achieve consistency with the EOM (A.2) is to impose $s_0^V = s_0^{T_1} = s_0^{\mathcal{D}_1}$. From a physical perspective this is a natural choice since the currents are of identical quantum numbers and therefore couple to the same spectrum of states. Below, it is argued that the EOM strengthen this point implying a high degree of correlation of the continuum thresholds.

Our main point is that since $\mathcal{D}_1 \ll T_1, V$, which we infer from the closeness of $r_\perp$ (2.11) to unity (cf. figure 1), a relative difference between s_0^V and $s_0^{T_1}$ can only be compensated by a much larger change in $s_0^{\mathcal{D}_1}$. The latter corresponds to a gross violation of semi-global quark hadron duality which we exclude; partly on grounds of past experience with LCSR.

Let us illustrate this more quantitatively by considering r-ratio which are not accidentally close to zero cf. figure 1. Let us choose $r_\perp(0) \simeq 0.957$, for $s_0^V = 35\,\text{GeV}^2$ and $s_0^{T_1} = s_0^V \pm 0.5\,\text{GeV}^2$, with fixed Borel parameters, the EOM (2.6) requires $s_0^{\mathcal{D}_1} = (35^{+6}_{-4})\,\text{GeV}^2$ which are considerable shifts. This corresponds to a change in the FF $\mathcal{D}_1$ of roughly 50% in both directions. The situation is similar for the other directions.[22,23] From this we infer that a difference of $1\,\text{GeV}^2$ on the two continuum thresholds $s_0^{T_1} - s_0^V$ is at the upper boundary of what seems plausible. For $s_0^{T_1,V} = 35(2)\,\text{GeV}^2$ this can be imposed by correlating the two FFs by 7/8 (i.e. 87.5%). The same line of reasoning applies to $r_\parallel$ and r_{0+t} (2.11). Yet for r_{0+t} the numerics are less compelling (cf footnote above) and we restrict the correlation between to 50%. There are two further correlations at $q^2 = 0$, namely $T_1(0) = T_2(0)$ which is of the algebraic type and $A_0(0) = A_3(0)$ which is required to avoid an unphysical pole at $q^2 = 0$. This leads to $s_0^{T_1} = s_0^{T_2}$ and $s_0^{\mathcal{V}_0} = s_0^{A_0}$. Strictly speaking the latter two are only exact at $q^2 = 0$ but since we refrain from assigning a q^2-dependence to s_0 the relation is assumed throughout.

In summary the following correlations are imposed,

$$\text{corr}(s_0^{T_1}, s_0^V) = 7/8\,, \qquad \text{corr}(s_0^{T_2}, s_0^{A_1}) = 7/8\,, \qquad \text{corr}(s_0^{A_{12}}, s_0^{T_{23}}) = 1/2\,, \tag{A.8}$$

and the full correlations $\text{corr}(s_0^{T_1}, s_0^{T_2}) = 1$ and $\text{corr}(s_0^{A_0}, s_0^{A_3}) = 1$ together with (A.8) imply

$$\text{corr}(s_0^{T_1}, s_0^{A_1}) = 7/8\,, \qquad \text{corr}(s_0^{T_2}, s_0^V) = 7/8\,, \qquad \text{corr}(s_0^{A_{12}}, s_0^{A_0}) = 1/2\,. \tag{A.9}$$

The reader is reminded that we have argued in section 2.4 for a correlation of the type $\text{corr}(s_0^F, s_0^{f_B}) = 1/2$ where F stands for any FF and $s_0^{f_B}$ is the continuum threshold for the f_B sum rule.

[22] With respect to v1 of our paper the argument is even stronger as the twist-4 contributions do all satisfy the EOM.

[23] The main conclusions remain unchanged when other points are chosen. For example $r_\parallel(10\,\text{GeV}^2) \simeq 1.022$ requires shifts of $s_0^{\mathcal{D}_1} = 35(^{-5.5}_{+10})\,\text{GeV}^2$ for $s_0^{T_2} = 35 \pm 0.5\,\text{GeV}^2$ again corresponding to shift of around 50% of $\mathcal{D}_2(10\,\text{GeV}^2)$. In fact the $+10\,\text{GeV}^2$ is only compatible within 10% with the EOM. The EOM are only satisfied asymptotically for this case. The situation for r_{0+t} is less compelling and requires shift of $\pm 2\,\text{GeV}^2$ for an original deviation of $0.5\,\text{GeV}^2$ which is still remarkable though.

JHEP08(2016)098

So far we have not discussed the role of the Borel parameter. In principle one could argue that the Borel parameter and the continuum threshold could conspire to satisfy the EOM. Whereas this does not seem to be very viable from the point of view of physics it is in addition not credible on grounds of the actual numerics. For example doubling the Borel parameter of the light-cone sum rule $M^2_{\rm LC}$, keeping the Borel parameter $M^2_{f_B}$ of the f_B sum rule fixed, leads to a change in the FFs T_1 and V of just one percent. Doubling the sum rule parameter is outside the validity range since it enhances the continuum contributions relative to the B-pole contribution. For example for $T_1(0)$ the continuum contribution becomes 42% by doubling $M^2_{\rm LC}$. Hence the Borel parameter cannot balance a change in the continuum threshold of s_0 of $1\,\text{GeV}^2$. Hence it is legitimate not to enter the $M^2_{\rm LC}$ in the discussion. The sensitivity of the f_B sum rule to the Borel parameter $M^2_{f_B}$ is slightly higher presumably because the local condensates are more vulnerable to (semi-global) quark hadron duality violations. This uncertainty is important for the FF prediction per se but only enters the EOM by a global factor and is therefore not relevant for the discussion of this section. Hence, we fully correlate the uncertainties of the Borel parameters $\text{corr}(M^2_{f_B}, M^2_F) = 1$ which is justified since the variation in s_0 are responsible for the bulk part of the uncertainty. It should be added that it is the variation of the parameters M^2 and s_0 that addresses the validity of the semi-global quark hadron duality.

A.3 Remarks on the explicit verification of the EOM at tree level

In view of the importance of the EOM for the determination of the ratio of tensor-to-vector FFs we discuss in some more detail the DAs that enter the EOM and the consistent handling of the projection of the correlation functions on the FFs. We have explicitly verified the EOM at the tree level for all five structures appearing in (A.2) including the derivative FFs as well as the strange quark mass terms at twist-3. The strange quark mass terms cancel non-trivially between the explicit term in (2.5) and $\mathcal{O}(m_s)$-correction in the DAs. More detail on the latter can be found in section B. The mechanism that guarantees this interplay of light and heavy quark mass are the EOM of the light DAs. Explicit results are given in the next subsection A.4 and in form of a Mathematica notebook. In addition we have verified that the renormalisation of the composite operators (cf. section A.5.1) are compatible with the EOM as expected from first principles. We remind the reader that the completely tractable issue of contact terms has been discussed and resolved in section A.1. Let us add that the covariant derivative between the strange and beauty quark can be exchanged by using the following algebraic identity

$$C[i(\overleftarrow{\partial} + \overrightarrow{\partial})_\mu] - 2iC[\overleftarrow{D}_\mu] = -C[i(\overleftarrow{\partial} + \overrightarrow{\partial})_\mu] + 2iC[\overrightarrow{D}_\mu]\,. \tag{A.10}$$

To this end we would like to discuss the consistent handling of the projection onto the structures P_i^μ (2.2). First, we note that for the EOM to be satisfied the projection on the Lorentz structures ought to be handled consistently for all structures appearing in (A.2). For $P^\mu_{2,3}$ extra care is in order, see e.g. discussion in [47], since $q\cdot(p+p_B) = p_B^2 - m_V^2$ equals $m_B^2 - m_V^2$ only if p_B^2 is on-shell. Hence in the computation the following projectors

JHEP08(2016)098

ought to be used

$$p_2^\mu = i\{q\cdot(p+p_B)\eta^{*\mu} - (\eta^*\cdot q)(p+p_B)^\mu\}\,,$$
$$p_3^\mu = i(\eta^*\cdot q)\left\{q^\mu - \frac{q^2}{q\cdot(p+p_B)}(p+p_B)^\mu\right\}, \tag{A.11}$$

which we denote by a lower case p. The important point is that these projectors are transverse $q\cdot p_i = 0$ even in the case where $p_B^2 \neq m_B^2$ (off-shell). We should add that the actual effect on the standard tensor and vector FFs due to the difference of using either $p_{2,3}^\mu$ or $P_{2,3}^\mu$ is rather small (numerically around 2%) since the the sum rule aims at imposing $p_B^2 \simeq m_B^2$ by construction. The latter might be taken as a measure of the quality of the sum rule. See also the discussion on the optimisation of the Borel parameter given in appendix A.6.

A.4 Explicit tree level results

The FF densities $R_{T_{1,2,3},\mathcal{V}_{1,2,3,P}}$, given in appendix A.4.2 relate to the FFs as follows

$$F(q^2) = c_F \frac{m_b\, e^{m_B^2/M^2}}{m_B^2 f_B}\hat{B}\left[\int_0^1 \big(R_F(u,q^2)\big)du\right] \tag{A.12}$$

with

$$c_{T_{1,2,3}} = 1\,, \qquad c_{V,A_1} = -(m_B \pm m_V)\,, \qquad c_{A_{3,0}} = \pm\frac{q^2}{m_V}\,, \tag{A.13}$$

being a matching factor, with a slight abuse of notation, to translate from $\{V, A_1, A_3, A_0\} \leftrightarrow \{\mathcal{V}_1, \mathcal{V}_2, \mathcal{V}_3, \mathcal{V}_P\}$, cf. (2.3). The symbol $\hat{B}$ denotes the subtracted Borel transformation explained in the next subsection. As an example we write

$$\begin{aligned} V(q^2) &= -(m_B+m_V)\frac{m_b\, e^{m_B^2/M^2}}{m_B^2 f_B}\hat{B}\left[\int_0^1 du \frac{-f_V^\perp}{2\Delta}\phi_\perp(u) + \mathcal{O}(m_V^2) + \dots\right] \\ &= (m_B+m_V)\frac{m_b}{m_B^2 f_B}\int_{u_0}^1 \frac{du}{u} e^{(m_B^2 - h(u,q^2))/M^2}\, f_V^\perp \phi_\perp(u) + \mathcal{O}(m_V^2) + \dots\,, \end{aligned} \tag{A.14}$$

where the dots stand for contributions from other DAs and $h(u,q^2)$ and u_0 are defined in eqs. (A.17) and (A.18) respectively. Simpler and more definite expression for the DAs $\phi_{\perp,\parallel}$, $g_{v,a}^\perp$ can be found in v1 of this paper which fully agree with the current version. Those results agree with the expressions given in [26] for $T_1(0)$, $V(q^2)$ and $A_0(q^2)$ but differs slightly for $A_1(q^2)$ due to the previously discussed handling of the projections (cf. section A.3). In practice the results for each FF are numerically small but for this work is of importance since we are interested in a precise determination of the ratio of tensor-to-vector FF. For example A_1 differs by a prefactor $(m_B^2 - m_V^2)/\big(q\cdot(p+p_B)\big) = (m_B^2 - m_V^2)/(p_B^2 - m_V^2) = (m_b^2 - \bar{u}q^2)/(um_B^2) + \mathcal{O}(m_V^2)$.

A.4.1 The subtracted Borel transformation

The correlation functions of the explicit tree-level results are given by integrals of the type

$$I_n = \int_0^1 du \frac{F(u)}{\Delta^n}\,, \qquad \Delta \equiv m_b^2 - up_B^2 - \bar{u}q^2. \tag{A.15}$$

The subtracted Borel transformation $\hat{B}$ is defined as the two-fold operation of taking the Borel transformation B followed by the so-called continuum subtraction. From $\hat{B}[I_1]$ the higher $\hat{B}[I_{n\geq 1}]$ can be found by

$$\hat{B}[I_n] = \frac{1}{\Gamma[n]}\left(-\frac{d}{dm_b^2}\right)^{(n-1)}\hat{B}[I_1]\,. \tag{A.16}$$

Hence, if $\hat{B}[I_1]$ is found explicitly then the problem is solved. To do so one can write

$$I_1 = \int_0^1 du\frac{F(u)}{\Delta} = \int_0^1 \frac{du}{u}\frac{F(u)}{h(u)-p_B^2}\,, \qquad h(u,q^2) = \frac{1}{u}(m_b^2-\bar{u}q^2)\,, \tag{A.17}$$

and apply the standard Borel transformation $B[1/(m^2-p_B^2)] = e^{-m^2/M^2}$ and the subtraction (corresponding to cutting of the dispersion integral at $s=s_0$) is implemented by imposing $u \geq u_0$

$$\hat{B}[I_1] = \int_{u_0}^1 \frac{F(u)e^{-\frac{h(u,q^2)}{M^2}}}{u}du\,, \qquad u_0 \equiv \frac{m_b^2-q^2}{s_0-q^2}\,. \tag{A.18}$$

Using formula (A.16), taking into account the m_b-dependence of u_0 and h, results in

$$\begin{aligned}
\hat{B}[I_2] &= \left(\int_{u_0}^1 \frac{F(u)e^{-\frac{h(u,q^2)}{M^2}}}{M^2u^2}\,du + \frac{F(u_0)e^{-\frac{s_0}{M^2}}}{u_0(s_0-q^2)}\right),\\
\hat{B}[I_3] &= \frac{1}{2}\left(\int_{u_0}^1 \frac{F(u)e^{-\frac{h(u,q^2)}{M^2}}}{M^4u^3}\,du + \frac{e^{-\frac{s_0}{M^2}}}{u_0^2(s_0-q^2)^2}\big(F(u_0)(1+x_{s_0})-u_0F'(u_0)\big)\right),\\
\hat{B}[I_4] &= \frac{1}{6}\left(\int_{u_0}^1 \frac{F(u)e^{-\frac{h(u,q^2)}{M^2}}}{M^6u^4}\,du + \frac{e^{-\frac{s_0}{M^2}}}{u_0^3(s_0-q^2)^3}\right.\\
&\qquad \left.\times\big(F(u_0)(2+2x_{s_0}+x_{s_0}^2)-u_0F'(u_0)(2+x_{s_0})+u_0^2F''(u_0)\big)\right),
\end{aligned} \tag{A.19}$$

where $x_{s_0} \equiv (s_0-q^2)/M^2$.

To this end we wish to comment on the different techniques of Borel transformation. Method i): substitute explicit DAs and then integrate over the DA-parameters to obtain analytic functions in p_B^2 (and q^2), take the discontinuity, obtain the dispersion relation and then perform the Borel transform on the dispersion relation which corresponds to the standard Borel transformation. This method has been pursued for example in [2] for the radiative corrections. Method ii): using partial integration rewrite the integrals over the DA-parameters such that they take the form of a dispersion relation and then apply the standard Borel transformation. This method has been applied in [26] and the v1 of this paper to present tree-level results of a few DAs. Method iii): the one described above and used here. Methods ii) and iii) have an advantage in that one can substitute other DAs after performing the Borel transformation. It should be added though that with method ii) that for performing the Borel transformation assumptions on the endpoint behaviour of the DAs might have been made.

JHEP08(2016)098

A.4.2 Explicit tree-level correlation functions

The relation of the correlation functions R_F (cf. also Mathematica notebook `notebookBSZ.nb`) given below to the FFs is given in (A.12) and $\Delta \equiv m_b^2 - up_B^2 - \bar{u}q^2$. The definition of the DAs and the actual form and values chosen are described in section B. We find (with $R_{T_P} = 0$ by definition)

$$
\begin{aligned}
R_{T_1} &= \frac{m_b f_V^\perp (u\bar{u}m_V^2 + \Delta)\phi_\perp}{2\Delta^2} - \frac{u m_b m_V^2 f_V^\perp h_{\perp,3}^{(1)}}{2\Delta^2} + \frac{f_V^\parallel m_V \phi_\parallel^{(1)}}{2\Delta} \\
&\quad + \frac{f_V^\parallel m_V (m_b^2 + \Delta + q^2)\tilde{g}_a^\perp}{8\Delta^2} - \frac{m_b^3 m_V^2 f_V^\perp A_\perp}{4\Delta^3} - \frac{m_b m_V^2 f_V^\perp h_\parallel^{(\mathrm{t},2)}}{\Delta^2} + \frac{u f_V^\parallel m_V g_v^\perp}{2\Delta}\,, \\
R_{T_2} &= -\frac{u m_b m_V^2 f_V^\perp \big(q^2\big(q^2\bar{u} - \Delta(u-2)\big) + q^2 u m_b^2 + m_b^4\big) h_{\perp,3}^{(1)}}{2\Delta^2 (q^2\bar{u} + m_b^2)^2} + \frac{f_V^\parallel m_V (m_b^2 - q^2)\phi_\parallel^{(1)}}{2\Delta(q^2\bar{u} + m_b^2)} \\
&\quad + \frac{\big(q^2(q^4\bar{u}^2 + \Delta q^2 u\bar{u} + \Delta^2 u) + q^2 m_b^2\big(\Delta u - q^2(u^2 - 4u + 3)\big) + q^2(3-2u)m_b^4 - m_b^6\big) m_b^3 m_V^2 f_V^\perp A_\perp}{4\Delta^3 (q^2\bar{u} + m_b^2)^3} \\
&\quad + \frac{f_V^\parallel m_V (m_b^2 - q^2)^2 (q^2\bar{u} + m_b^2 + \Delta) g_a^\perp}{8\Delta^2 (q^2\bar{u} + m_b^2)^2} + \frac{u f_V m_V (m_b^2 + q^2) g_v^\perp}{2\Delta(q^2\bar{u} + m_b^2)} \\
&\quad - \frac{m_b m_V^2 f_V^\perp \big(q^2(u-2)m_b^2 + m_b^4 + q^2\big(q^2(-u) + q^2 - \Delta u\big)\big) h_\parallel^{(\mathrm{t},2)}}{\Delta^2 (q^2\bar{u} + m_b^2)^2} \\
&\quad + \frac{m_b f_V^\perp \big(q^2(u-2)m_b^2(u\bar{u}m_V^2 + \Delta) + m_b^4(u\bar{u}m_V^2 + \Delta) - q^2\big(q^2\bar{u}(u\bar{u}m_V^2 + \Delta) + \Delta u^3 m_V^2\big)\big)\phi_\perp}{2\Delta^2 (q^2\bar{u} + m_b^2)^2}\,, \\
R_{T_3} &= -\frac{\big(q^2\big(q^2\bar{u} - \Delta(u-2)\big) + q^2 u m_b^2 + m_b^4\big) u m_b m_V^2 f_V^\perp h_3^{(1)}}{2\Delta^2 (q^2\bar{u} + m_b^2)^2} + \frac{(m_b^2 - q^2) f_V^\parallel m_V \Phi \mathrm{g}_v^{(1)}}{2\Delta(q^2\bar{u} + m_b^2)} \\
&\quad + \frac{(m_b^2 - q^2)^2 (q^2\bar{u} + m_b^2 + \Delta) f_V^\parallel m_V g_a^\perp}{8\Delta^2 (q^2\bar{u} + m_b^2)^2} + m_b^3 m_V^2 f_V^\perp A_\perp \\
&\quad \times \frac{\big(q^2(q^4\bar{u}^2 + \Delta q^2 u\bar{u} + \Delta^2 u) + q^2 m_b^2\big(\Delta u - q^2(u^2 - 4u + 3)\big) + q^2(3-2u)m_b^4 - m_b^6\big)}{4\Delta^3 (q^2\bar{u} + m_b^2)^3} \\
&\quad + \frac{(m_b^2 + q^2) u f_V m_V g_v^\perp}{2\Delta(q^2\bar{u} + m_b^2)} - \frac{\big(q^2(u-2)m_b^2 + m_b^4 + q^2\big(q^2(-u) + q^2 - \Delta u\big)\big) m_b m_V^2 f_V^\perp h_L^{(\mathrm{t},2)}}{\Delta^2 (q^2\bar{u} + m_b^2)^2} \\
&\quad + \frac{\big(q^2(u-2)m_b^2(u\bar{u}m_V^2 + \Delta) + m_b^4(u\bar{u}m_V^2 + \Delta) - q^2\big(q^2\bar{u}(u\bar{u}m_V^2 + \Delta) + \Delta u^3 m_V^2\big)\big) m_b f_V^\perp \phi_\perp}{2\Delta^2 (q^2\bar{u} + m_b^2)^2}\,, \\
R_{\mathcal{V}_1} &= -\frac{f_V^\perp (u\bar{u}m_V^2 + \Delta)\phi_\perp}{2\Delta^2} - \frac{m_b f_V^\parallel m_V \tilde{g}_a^\perp}{4\Delta^2} + \frac{m_V^2 (2m_b^2 + \Delta) f_V^\perp A_\perp}{8\Delta^3}\,, \\
R_{\mathcal{V}_2} &= \frac{u m_V^2 f_V^\perp \big(m_b^2(2q^2\bar{u} + 3\Delta) + \Delta q^2\bar{u} + 2m_b^4\big) h_{\perp,3}^{(1)}}{2\Delta^2 (q^2\bar{u} + m_b^2)^2} - \frac{u m_b f_V^\parallel m_V g_v^\perp}{\Delta(q^2\bar{u} + m_b^2)} \\
&\quad + \frac{m_V^2 f_V^\perp \big(q^2(u-2)m_b^2 + m_b^4 + q^2\big(q^2(-u) + q^2 - \Delta u\big)\big) h_\parallel^{(\mathrm{t},2)}}{\Delta^2 (q^2\bar{u} + m_b^2)^2} - \frac{u m_V^2 f_V^\perp \tilde{h}_\parallel^{(s)}}{2\Delta(q^2\bar{u} + m_b^2)} \\
&\quad - \Big(m_b^2\big(q^2(u-2)(u\bar{u}m_V^2 + \Delta) + 2\Delta u^2 m_V^2\big) + m_b^4(u\bar{u}m_V^2 + \Delta) - q^2\big(q^2\bar{u}(u\bar{u}m_V^2 + \Delta) \\
&\quad - \Delta(u-2)u^2 m_V^2\big)\Big)\frac{f_V^\perp \phi_\perp}{2\Delta^2 (q^2\bar{u} + m_b^2)^2} + \Big(-q^2 m_b^2\big(2q^4\bar{u}^2 + \Delta q^2(u^2 + 2u - 3) + 3\Delta^2 u\big) \\
&\quad - \Delta q^4\bar{u}(q^2\bar{u} + \Delta u) + q^2 m_b^4\big(2q^2(u^2 - 4u + 3) - 3\Delta\big) + m_b^6\big(\Delta + q^2(4u - 6)\big) + 2m_b^8\Big) \\
&\quad \times \frac{m_V^2 f_V^\perp A_\perp}{8\Delta^3 (q^2\bar{u} + m_b^2)^3}\,,
\end{aligned}
$$

$$
\begin{aligned}
R_{\mathcal{V}_3} = &\frac{(q^2\bar{u}+m_b^2-\Delta)3m_b^3 f_V^{\parallel} m_V^3 A_{\parallel}^{(1)}}{2\Delta^4 q^2 u} + \frac{(q^2\bar{u}+m_b^2)m_V^2 f_V^{\perp} h_{\parallel}^{s}}{2\Delta^2 q^2} \\
&+ \frac{\big(-m_b^2(2u\bar{u}m_V^2+\Delta)+q^2(-\bar{u})(2u\bar{u}m_V^2+\Delta)+\Delta\big(\Delta+u(2u-1)m_V^2\big)\big)m_b f_V^{\parallel} m_V \Phi \mathrm{g}_v^{(1)}}{\Delta^3 q^2 u} \\
&+ \frac{(-2q^2\bar{u}-2m_b^2+\Delta)m_b f_V m_V^3 g_3^{(2)}}{\Delta^3 q^2} + \frac{(u\bar{u}m_V^2+\Delta)m_b f_V^{\parallel} m_V g_{\perp}^{v}}{\Delta^2 q^2} \\
&+ \frac{\big(2q^4\bar{u}+2q^2 u m_b^2+2m_b^4-2\Delta^2+\Delta q^2(3u-4)\big)m_V^2 f_V^{\perp} h_{\parallel}^{(\mathrm{t},2)}}{\Delta^3 q^2 u} \\
&+ \frac{\big(2\Delta u m_V^2 - q^2(u\bar{u}m_V^2+\Delta)\big)f_V^{\perp}\phi_{\perp}}{2\Delta^2 q^2} - \frac{\big(m_b^2+2\Delta+q^2(-u)+q^2\big)m_V^2 h_3^{(1)} f_V^{\perp}}{2\Delta^2 q^2} \\
&+ \frac{m_V^2(2m_b^2+\Delta)f_V^{\perp}A_{\perp}}{8\Delta^3} - \frac{m_b^3 f_V^{\parallel} m_V^3 \mathbb{G}_{\perp}^{v}}{2\Delta^3 q^2}\,, \\
R_{\mathcal{V}_P} = &\frac{m_b f_V^{\parallel} m_V\big(m_b^2(2u\bar{u}m_V^2+\Delta)+q^2\big(-(2u\bar{u}m_V^2+\Delta)\big)-\Delta\big(\Delta+u(2u-1)m_V^2\big)\big)\phi_{\parallel}^{(1)}}{\Delta^3 q^2 u} \\
&- \frac{m_b f_V^{\parallel} m_V(u\bar{u}m_V^2+\Delta)g_v^{\perp}}{\Delta^2 q^2} + \frac{3m_b^3 f_V m_V^3(-m_b^2+\Delta+q^2)A_{\parallel}^{(1)}}{2\Delta^4 q^2 u} \\
&+ \frac{m_V^2 h_{\perp,3}^{(1)} f_V^{\perp}(m_b^2+2\Delta-q^2)}{2\Delta^2 q^2} + \frac{m_b f_V^{\parallel} m_V^3(2m_b^2-\Delta+2q^2)g_{\parallel,3}^{(2)}}{\Delta_{\parallel,3}^{g} 3q^2} \\
&- \frac{2m_V^2 f_V^{\perp}(-2q^2m_b^2+m_b^4-\Delta^2+q^4)h_{\parallel}^{(\mathrm{t},2)}}{\Delta^3 q^2 u} - \frac{m_V^2(m_b^2+q^2)f_V^{\perp}\tilde{h}_{\parallel}^{(s)}}{2\Delta^2 q^2} \\
&+ \frac{m_b^3 f_V^{\parallel} m_V^3 \mathbb{G}_{\perp}^{v}}{2\Delta^3 q^2} - \frac{u m_V^2 f_V^{\perp}\phi_{\perp}}{\Delta q^2}\,, \\
R_{\mathcal{D}_1} = &-\frac{f_V^{\parallel} m_V \tilde{g}_a^{\perp}}{4\Delta}\,, \\
R_{\mathcal{D}_2} = &\frac{f_V^{\parallel} m_V(q^2-m_b^2)\Phi_{\parallel}^{(1)}}{\Delta(q^2\bar{u}+m_b^2)} + \frac{u m_b m_V^2 f_V^{\perp} h_{\parallel}^{s}}{\Delta(q^2\bar{u}+m_b^2)}\,, \\
R_{\mathcal{D}_3} = &\frac{\big(m_b^2(6q^4\bar{u}+2\Delta q^2\bar{u}+\Delta^2)-\Delta\big(\Delta^2+\Delta q^2(5-3u)-4q^4\bar{u}\big)+6m_b^4\big(\Delta-q^2(u-2)\big)-6m_b^6\big)}{4\Delta^4 q^2 u} \\
&\times f_V^{\parallel} m_V^3 A_{\parallel}^{(1)} - \frac{\big(m_b^2(u\bar{u}m_V^2+\Delta)+q^2\bar{u}(u\bar{u}m_V^2+\Delta)-\Delta u^2 m_V^2\big)f_V^{\parallel} m_V g_{\perp}^{v}}{\Delta^2 q^2} \\
&+ \frac{f_V^{\parallel} m_V^3\big(m_b^2(4q^2\bar{u}+\Delta)+3\Delta q^2\bar{u}+4m_b^4\big)g_3^{(2)}}{\Delta^3 q^2} - \frac{m_b m_V^2 f_V^{\perp}(q^2\bar{u}+m_b^2)h_{\parallel}^{s}}{\Delta^2 q^2} \\
&+ \frac{\big(2q^2\bar{u}m_b^2-\Delta(\Delta-2q^2\bar{u})+2m_b^4\big)f_V^{\parallel} m_V^3 \mathbb{G}_{\perp}^{v}}{4\Delta^3 q^2} + \Big(m_b^2\big(q^2(u-2)(2u\bar{u}m_V^2+\Delta) \\
&- \Delta(u\bar{u}m_V^2+\Delta)\big) + m_b^4(2u\bar{u}m_V^2+\Delta) - \bar{u}q^4(2u\bar{u}m_V^2+\Delta) + \Delta^2 u^2 m_V^2 \\
&+ \Delta q^2\big(\Delta+u(2u-1)m_V^2-\Delta u\big)\Big)\frac{f_V^{\parallel} m_V \Phi \mathrm{g}_v^{(1)}}{\Delta^3 q^2 u}\,,
\end{aligned}
$$

JHEP08(2016)098

$$
\begin{aligned}
R_{\mathcal{D}_P} = & \frac{\big(m_b^2(u\bar{u}m_V^2+\Delta)+q^2\big(-(u\bar{u}m_V^2+\Delta)\big)-\Delta u^2 m_V^2\big) f_V^{\parallel} m_V g_\perp^v}{\Delta^2 q^2} \\
& - \Big(- m_b^2\big(2q^2(2u\bar{u}m_V^2+\Delta)+\Delta(u\bar{u}m_V^2+\Delta)\big) + m_b^4(2u\bar{u}m_V^2+\Delta) + q^4(2u\bar{u}m_V^2+\Delta) \\
& \quad + \Delta q^2\big(\Delta+u(5u-1)m_V^2\big)+\Delta^2 u^2 m_V^2\Big)\frac{f_V^{\parallel} m_V \Phi \mathbb{g}_v^{(1)}}{\Delta^3 q^2 u} \\
& + \frac{\big(-6m_b^4(\Delta+2q^2)+m_b^2(-\Delta^2+6q^4+10\Delta q^2)+6m_b^6+\Delta(\Delta^2-4q^4-3\Delta q^2)\big) f_V^{\parallel} m_V^3 A_{\parallel}^{(1)}}{4\Delta^4 q^2 u} \\
& + \frac{(m_b^2+2\Delta-q^2)m_V^2 f_V^{\perp} h_3^{(1)}}{\Delta^2 m_b} - \frac{\big(\Delta m_b^2+4m_b^4+q^2(5\Delta-4q^2)\big) f_V^{\parallel} m_V^3 g_3^{(2)}}{\Delta^3 q^2} \\
& + \frac{(m_b^4-q^4)m_V^2 f_V^{\perp} h_{\parallel}^s}{\Delta^2 q^2 m_b} - \frac{4(-2q^2 m_b^2+m_b^4-\Delta^2+q^4)m_V^2 f_V^{\perp} h_{\parallel}^{(\mathrm{t},2)}}{\Delta^3 u m_b} \\
& - \frac{\big(-2q^2 m_b^2+2m_b^4+\Delta(2q^2-\Delta)\big) f_V^{\parallel} m_V^3 \mathbb{G}_\perp^v}{4\Delta^3 q^2} - \frac{2um_V^2 f_V^{\perp}\phi_\perp}{\Delta m_b}\,.
\end{aligned}
$$

A.5 Scheme dependence of the form factors

In many determinations of $B \to V, P$ FF calculation in LCSR the pole mass scheme is assumed to be the appropriate scheme for the b-quark mass. For $B \to \pi$ FFs it has been found that a conversion to the $\overline{\text{MS}}$-scheme leads to minor changes only [20, 53]. The explicit appearance of m_b in the EOM (2.6)–(2.9) deserves a reinvestigation of the issue of scheme dependence.

In LCSR calculations one distinguishes between a factorisation scale $\mu_F^2 \simeq m_B^2 - m_b^2 \simeq \mathcal{O}(m_b \Lambda_{\text{QCD}})$ and a renormalisation scale $\mu_{\text{UV}} = m_b$. The former is the separation scale of the LC-OPE and the latter is the scale of the composite operators e.g. the tensor or vector bilinear quark currents. For the analysis in this appendix, and throughout the paper, we adopt the strategy to lower μ_{UV} to μ_F in the actual computation and then use renormalisation group running to scale the tensor FFs from $T_i(q^2)|_{\mu_{\text{UV}}=\mu_F}$ to $T_i(q^2)|_{\mu_{\text{UV}}=m_b}$. This makes it clear how the EOM are obeyed at any step of the computation. More details on the renormalisation of the composite operators are given in the next section.

One can switch back and forth between the pole and $\overline{\text{MS}}$-scheme by replacing $m_b^{\text{pole}} = \bar{m}_b(\mu_m) Z_m^{\overline{\text{MS}}} / Z_m^{\text{pole}} = \bar{m}_b(\mu_m)\big(1 + \frac{\alpha_s(\mu)}{4\pi} C_F\big(4 - 3\ln(m_b^2/\mu_m^2)\big) + \mathcal{O}(\alpha_s^2)\big)$ (with $C_F = 4/3$ in QCD) in the tree-level computation and expanding to first order in α_s. The additional scale μ_m is introduced (through the $\overline{\text{MS}}$ -scheme) for the same reasons as μ_F-scale mentioned above. In table 11 examples of FF determinations in both schemes are given. We infer that the impact of changing from the pole to the $\overline{\text{MS}}$-scheme for the FFs is around 4% which is sizeable but controlled. Yet the ratio of FFs changes by only 1% which is rather small and therefore substantiates the robustness of the tensor-to-vector FF ratio which is one of the main points of this paper. The μ-dependence entering through the μ-dependent $\overline{\text{MS}}$-mass is reflected in the pole scheme through a larger uncertainty in the pole mass itself; $m_b^{\text{pole}} = 4.8(1)\,\text{GeV}$ as compared to $\bar{m}_b(\bar{m}_b) = 4.18(3)\,\text{GeV}$ [79].

JHEP08(2016)098

$B \to K^*$	μ^2 [GeV^2]	$T_1(0)$	$V(0)$	$T_1(0)/V(0)$
pole	4.8	0.282	0.341	0.828
$\overline{\text{MS}}$	4.8	0.271	0.330	0.821
$\overline{\text{MS}}$	8	0.293	0.349	0.840

Table 11. As mentioned in the text the tensor FFs are understood to be evaluated at the scale $\mu_{\text{UV}} = m_b$ by one-loop renormalisation group running. Note $\mu^2 = m_B^2 - m_b^2 \simeq 4.8\,\text{GeV}^2$ is the standard factorisation scale of the LC-OPE used throughout. The values are for central values of the input parameters and differ slightly from that obtained from the Markov Chain Monte Carlo.

A.5.1 Renormalisation of composite operators and compatibility with EOM

The aim of this section is to clarify the renormalisation of the composite operators entering the EOM (2.5) with particular focus on the m_b quark mass. The following shorthand notations for the operators

$$\begin{aligned} O_1 &= O_D = 2\bar{s}i\overleftarrow{D}_\mu\, b\,, & O_2 &= O_{\partial T} = i\partial^\nu(\bar{s}i\sigma_{\mu\nu}b)\,,\\ O_3 &= O_{mV} = (m_s+m_b)\bar{s}\gamma_\mu b\,, & O_4 &= O_{\partial S} = i\partial_\mu(\bar{s}b)\,, \end{aligned} \tag{A.20}$$

is introduced. The mixing matrix is defined by

$$O_i^{(0)} = Z_q Z_{ij} O_j\,, \tag{A.21}$$

where Z_q is the external leg or wavefunction renormalisation. Through an explicit computation it is found that

$$Z_{ij} = \delta_{ij} + C_F\frac{\alpha_s}{4\pi}\frac{1}{4-d}\begin{pmatrix} 2 & 2 & 6 & 6\\ 0 & 0 & 0 & 0\\ 0 & 0 & (2-6) & 0\\ 0 & 0 & 0 & 8\end{pmatrix}. \tag{A.22}$$

It is noteworthy that the renormalisation of the operator O_D requires the additional diagrams where a gluon originates from the vertex through the covariant derivative. The operators $O_{mV,\partial T,\partial S}$ do renormalise multiplicatively since they are of lowest dimension (effectively three) and differ in quantum numbers when the contraction of the total derivative is undone. The operator O_D is of dimension four and the dimension three operators can and do mix with O_D. In the notation (A.20), the operator identity (2.5) reads

$$O_D + O_{mV} + O_{\partial T} - O_{\partial S} = 0\,. \tag{A.23}$$

It is readily verified that the renormalisation (A.22) is compatible with the EOM (A.23). As an additional check let us mention that from the diagonal elements $Z_q \cdot \text{diag}(Z) \equiv (Z_D, Z_{\partial T}, Z_m Z_V, Z_{\partial S})$ one infers $Z_S \equiv Z_{\partial_S} = 1+6\Delta$, $Z_V = 1$ and $Z_T \equiv Z_{\partial T} = 1-2\Delta$ with $\Delta \equiv C_F\frac{\alpha_s}{4\pi}\frac{1}{\epsilon}$, $Z_m = 1-6\Delta$. From the latter the well-known anomalous dimensions $\gamma_S^{(0)} = -6C_F$, $\gamma_V^{(0)} = 0$ and $\gamma_T^{(0)} = 2C_F$ of these operators follow (notation: $\gamma_X = \gamma_X^{(0)}\frac{\alpha_s}{4\pi} + \mathcal{O}(\alpha_s^2)$).

At last we turn to the issue of the impact of the mass renormalisation on the composite operators. From the mixing of operators in (A.22) it is clear that the renormalisation of O_D

is affected by a mass scheme change. This can be seen by writing somewhat symbolically $Z_{13} = Z_{D(mV)} = Z_m Z_{DV}$. So in summary going to the pole scheme enforces a finite renormalisation of the operator O_D since changing from $\overline{\text{MS}}$ to the pole scheme corresponds to a finite shift in the ratio of the Z_m-factors. Most importantly the renormalisation of the composite operators O_V, O_T and O_S, on the other hand, is not affected by the mass scheme. Hence it is legitimate to use the $\overline{\text{MS}}$-scheme to renormalise them. This is fortunate since the Wilson coefficients are evaluated in the $\overline{\text{MS}}$-scheme and together this guarantees the cancellation of the μ_{UV}-scale between the Wilson coefficients and the matrix elements. The scheme independence of the operators O_V, O_T underlies or partly explains the small changes in the FFs when going from the pole- to the $\overline{\text{MS}}$-scheme (cf. table 11).

A.6 Remarks on fixing the Borel parameter

A sum rule for a FF $F(q^2)$ of a process $B \to P, V$-transition may be written as

$$F(q^2)_{M^2} = \int_{m_b^2}^{s_0} \rho_F(s, q^2) e^{\frac{m_B^2 - s}{M^2}} ds \,, \tag{A.24}$$

where M^2 is the Borel parameter. The goal of this section is to show that two seemingly different methods for fixing M^2 are equivalent. For this purpose we introduce the following notation

$$\langle x(s) \rangle_{q^2, M^2} \equiv \int_{m_b^2}^{s_0} x(s) \rho_F(s, q^2) e^{\frac{m_B^2 - s}{M^2}} ds \,. \tag{A.25}$$

We note that $F(q^2)_{M^2} = \langle 1 \rangle_{q^2, M^2}$. The two methods are:

- *Extremising the Borel parameter*: if one were to succeed in computing the sum rule exactly, which would imply[24]

$$\rho_F(s, q^2) = \delta(s - m_B^2) F(q^2) + \Theta(s - s_c) \sigma_F(s) \,, \tag{A.26}$$

  then eq. (A.24) would remain valid for any Borel parameter. In practice the partonic evaluation through the OPE is optimised by using a large Borel parameter, with just the opposite being true for the projection on the lowest hadronic state. Hence a compromise value has to be found, ideally in a region where $F(q^2)_{M^2}$ shows an extremum in M^2. This is imposed by

$$0 = \frac{d}{d(1/M^2)} \ln F(q^2)_{M^2} = \frac{m_B^2 \langle 1 \rangle_{q^2, M^2} - \langle s \rangle_{q^2, M^2}}{\langle 1 \rangle_{q^2, M^2}} \,. \tag{A.27}$$

- *Daughter sum rule in* m_B^2: one may write a daughter sum rule for m_B^2 as follows

$$(m_B^2)_{M^2} = \frac{\langle s \rangle_{q^2, M^2}}{\langle 1 \rangle_{q^2, M^2}} \,. \tag{A.28}$$

  Note that using eq. (A.26) satisfies (A.28) exactly as it should.

It is readily seen that eqs. (A.27), (A.28) are the same and hence the two methods are equivalent.

[24] For the sake of illustration we employ the narrow width approximation which is justified for the B-meson.

JHEP08(2016)098

B Light-cone distribution amplitudes

B.1 Distribution amplitudes including $\mathbb{A}_\parallel$ and the new twist-5 $\mathbb{G}_\perp^{v,a}$ DAs

A general review on the subject of LCDAs can be found in [94] which is by now over thirty years old. The main concepts for the vector DAs are explained, in some details, in the more modern write-up [95].

Light-cone physics is conventionally discussed by introducing two light-like vectors say z and $\hat{p}$ (i.e. $z^2 = \hat{p}^2 = 0$).[25] The close to light-like separation x and the meson momentum p ($p^2 = m_V^2$) can be expressed as linear combinations of z and p

$$z_\mu = x_\mu - p_\mu \frac{1}{m_V^2}\big(xp - \sqrt{(xp)^2 - x^2 m_V^2}\big)\,, \qquad \hat{p}_\mu = p_\mu - \frac{1}{2}\frac{m_V^2}{\hat{p}z} z_\mu\,, \tag{B.1}$$

whereas any vector such as the vector meson polarisation $\eta(p)$ is decomposed

$$\eta_\mu = \frac{\eta z}{\hat{p}z}\hat{p}_\mu + \frac{\eta\hat{p}}{\hat{p}z} z_\mu + \eta_\mu^\perp\,, \tag{B.2}$$

into $\eta^\perp$ and the $\hat{p}$ and z direction e.g. [95]. Above $\hat{p}z \equiv \hat{p}\cdot z$ etc. is understood.

The rigorous definition of the LCDAs is given for quark bilinears with light-like separation (e.g. [95]). Applying the decomposition in (B.2) to the vector Dirac structure leads to the following parameterisation

$$\langle V(p)|\bar{q}_1(0)\gamma_\mu\, q_2(z)|0\rangle = f_V^\parallel m_V \int du\, e^{i\bar{u}\hat{p}z}\left\{\frac{\eta z}{\hat{p}z}\hat{p}_\mu\,\phi_\parallel(u) + \eta_\mu^\perp g_\perp^v(u) - \frac{\eta z\, m_V^2}{2(\hat{p}z)^2} z_\mu\, g_{\parallel,3}(u)\right\}, \tag{B.3}$$

for a vector meson $V[q_1\bar{q}_2]$ coupling to a light-like separated vector quark-bilinear.[26] Considering all Dirac structures this amounts to a total of eight DAs $\phi_{\parallel,\perp}, g_\perp^{v,a}, h_\parallel^{(s,t)}, g_{\parallel,3}$ and $h_{\perp,3}$ which loosely follow the nomenclature of the nucleon parton distributions functions. It is readily verified, using $\eta p = 0$, $\int_0^1 f(u) = 1$ for $f = \phi_\parallel, g_\perp^v, g_{\parallel,3}$ and (B.2), that in the limit $z \to 0$ the left hand side of (B.3) reduces to $\eta_\mu f_V^\parallel m_V$ as required. Using (B.1) and (B.2) this can be written in terms of the actual momentum of the vector meson p and the near light-like distance x as follows[27,28,29]

$$\begin{aligned}\langle V(p)|\bar{q}_1(0)\gamma_\mu q_2(x)|0\rangle = f_V^\parallel m_V \int du\, e^{i\bar{u}px}\Bigg\{ & p_\mu \frac{\eta x}{px}\left(\phi_\parallel(u) - g_\perp^v(u) + \frac{1}{16} m_V^2 x^2\big(\mathbb{A}_\parallel(u) - \mathbb{G}_\perp^v(u)\big)\right) \\ & + \eta_\mu\left(g_\perp^v(u) + \frac{m_V^2 x^2}{16}\mathbb{G}_\perp^v(u)\right) - \frac{\eta x\, m_V^2}{2(px)^2}\, x_\mu\big(g_{\parallel,3}(u) - 2g_\perp^v(u) + \phi_\parallel(u)\big)\Bigg\}\,,\end{aligned}$$

[25] The latter are often denoted by $n_\pm$ or $[n,\bar{n}]$ with the two remaining directions being labelled by $\perp$.

[26] Above the Wilson line between 0 and z, rendering the matrix element gauge invariant, is omitted for brevity.

[27] Note that $\langle V(p)|\bar{q}_1(0)\gamma_5 q_2(x)|0\rangle = 0$ by parity conservation of QCD.

[28] With due apologies we follow the notation in [95] and not the newer and more systematic notation introduced in [96] because of reasons of familiarity. A dictionary between the two notations is shown in table 12.

[29] The definition of $\mathbb{G}_\perp^v$ is adapted such that $\mathbb{A}_\parallel$ remains as in [97] and $(\phi_\parallel,\, g_\perp^v)$ and $(\mathbb{A}_\parallel,\, \mathbb{G}_\perp^v)$ take on an analoguous role.

JHEP08(2016)098

DA	$\phi_\perp$	$\phi_\parallel$	$g_\perp^v$	$\tilde{g}_\perp^a$	$\tilde{h}_\parallel^{(s)}$	$h_\parallel^{(t)}$	$g_3^{(\parallel)}$	$h_3^{(\perp)}$	$\mathbb{A}_\perp$	$\mathbb{A}_\parallel$	$\mathbb{G}_\perp^v$	$\mathbb{G}_\perp^a$
NN	$\phi_{2,V}^\perp$	$\phi_{2,V}^\parallel$	$\phi_{3,V}^\perp$	$\psi_{3,V}^\perp$	$\psi_{3,V}^\parallel$	$\phi_{3,V}^\parallel$	$\psi_{4,V}^\parallel$	$\psi_{4,V}^\perp$	$\phi_{4,V}^\perp$	$\phi_{4,V}^\parallel$	$\phi_{5,V}^\perp$	$\psi_{5,V}^\perp$
form	–	–	3.9	3.9	3.7	3.7	3.24	4.21	4.22	–	–	–
expl	(B.14)	(B.14)	3.18	3.17	3.16	3.15	3.27	4.24	4.25	(B.12)	(B.12)	(B.12)
Dirac	$\sigma_{\mu\nu}$	γ_μ	γ_μ	$\gamma_\mu\gamma_5$	**1**	$\sigma_{\mu\nu}$	γ_μ	$\sigma_{\mu\nu}$	$\sigma_{\mu\nu}$	γ_μ	γ_μ	$\gamma_\mu\gamma_5$
twist	2	2	3	3	3	3	4	4	4	4	5	5

Table 12. Translation table between old [95, 97] and new notation (NN) [46, 96]. The third and fourth line indicate the reference to the formal and explicit solution of the DAs. The twist-3,4 DAs refer to refs. [46, 96] respectively. The first two DAs are of leading twist 2 and are not referenced since they have been known for a long time e.g. [94]. The last three DAs are obtained in this work. The second last line denotes the Dirac structure of the DA with $\mathbf{1}, \sigma_{\mu\nu}$ and $\gamma_\mu, \gamma_\mu\gamma_5$ being chiral odd and chiral even respectively.

$$
\begin{aligned}
\langle V(p)|\bar{q}_1(0)\sigma_{\mu\nu}q_2(x)|0\rangle &= -if_V^\perp \int du\, e^{i\bar{u}px}\Big\{(\eta_\mu p_\nu - \eta_\nu p_\mu)\Big(\phi_\perp(u) + \frac{1}{16}\, m_V^2 x^2 \mathbb{A}_\perp(u)\Big) \\
&\quad + (p_\mu x_\nu - p_\nu x_\mu)\frac{\eta x}{(px)^2}\, m_V^2\Big(h_\parallel^{(t)}(u) - \frac{1}{2}\,\phi_\perp(u) - \frac{1}{2}\, h_{\perp,3}(u)\Big) \\
&\quad + \frac{m_V^2}{2px}(\eta_\mu x_\nu - \eta_\nu x_\mu)\big(h_{\perp,3}(u) - \phi_\perp(u)\big)\Big\}\,, \\
\langle V(p)|\bar{q}_1(0)\gamma_\mu\gamma_5 q_2(x)|0\rangle &= \frac{1}{4}\, f_V^\parallel m_V\, \epsilon_{\mu\nu\rho\sigma}\eta^{*\nu}p^\rho x^\sigma \int_0^1 du\, e^{i\bar{u}px}\Big(\tilde{g}_\perp^a(u) + \frac{m_V^2 x^2}{16}\tilde{\mathbb{G}}_\perp^a(u)\Big)\,, \\
\langle V(p)|\bar{q}_1(0)q_2(x)|0\rangle &= \frac{i}{2}\, f_V^\perp\,(\eta x) m_V^2 \int_0^1 du\, e^{i\bar{u}px}\,\tilde{h}_\parallel^{(s)}(u)\,,
\end{aligned}
\tag{B.4}
$$

where the notation $g_{\parallel,3} = g_3$ and $h_{\perp,3} = h_3$ has been introduced (w.r.t. to ref. [95]) in order to declare the polarisation of the DAs. Additionally

$$
\tilde{h}_\parallel^{(s)} = (1-\delta_+)h_\parallel^{(s)}, \qquad \tilde{g}_\perp^a(u) = (1-\tilde{\delta}_+)g_\perp^a(u)\,, \qquad \tilde{\mathbb{G}}_\perp^a = (1-\tilde{\delta}_+)\mathbb{G}_\perp^a\,, \tag{B.5}
$$

take into account valence quark mass corrections

$$
\delta_\pm \equiv \frac{f_V^\parallel(m_{q_2} \pm m_{q_1})}{(f_V^\perp m_V)}\,, \qquad \tilde{\delta}_\pm \equiv \frac{f_V^\perp(m_{q_2} \pm m_{q_1})}{(f_V^\parallel m_V)}\,, \tag{B.6}
$$

consistent with the normalisation

$$
I_1[\phi](1) = 1\,, \qquad \phi = \{\phi_{\parallel,\perp}, g_\perp^{v,a}, h_\parallel^{(s,t)}, g_{\parallel,3}, h_{\perp,3}\}\,, \qquad I_1[\phi](u) \equiv \int_0^u dv\,\phi(v)\,, \tag{B.7}
$$

and the EOM of the LCDAs. The twist-4 meson mass corrections $\mathbb{A}_{\parallel,\perp}$ (w.r.t. $\phi_{\parallel,\perp}$ DAs) have been introduced in [97]. The twist-5 meson mass corrections $\mathbb{G}_\perp^{v,a}$ (w.r.t. $g_{v,a}^\perp$ DAs) are introduced in this work for the first time. The DAs $\mathbb{G}_\perp^{a,v}$ and $\mathbb{A}_{\parallel,\perp}$ are not subject to a particular normalisation whereas $I_1[\mathbb{A}_\parallel - \mathbb{G}_\perp^v](1) = 0$ is necessary and partly motivated the reinvestigation of the twist-4,5 DA in this work. More details follow just below. We will see in section B.2 that the four additional DAs $\mathbb{A}_{\parallel,\perp}$ and $\mathbb{G}_\perp^{v,a}$ can be obtained from the eight basic ones (at least in the asymptotic limit).

JHEP08(2016)098

A striking feature are the $(px)^{-1}$- and $(px)^{-2}$-terms which originate from the change of variables (B.1) and (B.2). From a conceptual viewpoint the limit $px \to 0$ ought to exist and imply conditions on the DA which have to be obeyed automatically by the solutions.

More concretely the $1/px$ factors are removed by

$$\frac{1}{px}\int_0^1 du\, e^{i\bar{u}px}\phi(u) \overset{I_1[\phi](1)=0}{\longrightarrow} i\int_0^1 du\, e^{i\bar{u}px} I_1[\phi](u)\,, \tag{B.8}$$

with the normalisation condition as indicated. In eq. (B.4) this concerns the following five functions combintations

$$\begin{aligned}
\frac{1}{i(px)}(\phi_\parallel - g_\perp^v) &\to \quad \phi_\parallel^{(1)}(u) = I_1[\phi_\parallel - g_\perp^v](u)\,,\\
\frac{1}{i^2(px)^2}\left(h_\parallel^{(t)} - \frac{1}{2}\,\phi_\perp - \frac{1}{2}\,h_{\perp,3}\right) &\to h_\parallel^{(t,2)}(u) = I_2\left[h_\parallel^{(t)} - \frac{1}{2}\,\phi_\perp - \frac{1}{2}\,h_{\perp,3}\right](u)\,,\\
\frac{1}{i(px)}(h_{\perp,3} - \phi_\perp) &\to \quad h_{\perp,3}^{(1)}(u) = I_1[h_{\perp,3} - \phi_\perp](u)\,,\\
\frac{1}{i^2(px)^2}(g_{\parallel,3} - 2g_\perp^v + \phi_\parallel]) &\to \quad g_{\parallel,3}^{(2)}(u) = I_2[g_{\parallel,3} - 2g_\perp^v + \phi_\parallel](u)\,,\\
\frac{1}{i(px)}(\mathbb{A}_\parallel - \mathbb{G}_\perp^v) &\to \quad \mathbb{A}_\parallel^{(1)}(u) = I_1[\mathbb{A}_\parallel - \mathbb{G}_\perp^v](u)\,,
\end{aligned} \tag{B.9}$$

where $\xi = 2u - 1$ and $I_2 = I_1 \circ I_1$ is a double application of (B.8). The asymptotic form of the DAs has been indicated and the dots stand for non-asymptotic corrections. As stated earlier all DAs are such that unwanted boundary terms disappear which is guaranteed provided that

$$I_1[\phi](1) = 0\,, \qquad I_2[\phi](1) = 0\,, \tag{B.10}$$

with the first and both conditions applying to the case where the DA in (B.9) is written in terms of I_1 and I_2 respectively. The integrated DAs are those that appear in the explicit results quoted in section A.4.2.

B.2 Determination of m_V^2-LCDA in asymptotic limit

Introducing more LCDA means that more information is needed to solve for the DAs. We did not systematically aim to do this but present an alternative and possibly new way to determine the asymptotic form of the DA directly from (B.3). We expand all quantities systematically to first order in m_V^2, using eq. (B.1), including in particular the $\hat{p}z$ in exponential factor in (B.3),

$$\hat{p}z = px\left(1 - \frac{x^2 m_V^2}{(px)^2}\right)^{1/2} = px - \frac{1}{2}\frac{x^2 m_V^2}{px} + \mathcal{O}(m_V^4)\,. \tag{B.11}$$

By matching the first power in m_V^2 this leads to the following identifications at the level of *asymptotic DAs* (cf. footnote 29)

$$\begin{aligned}
\mathbb{A}_\parallel(u) &= -4I_1[\xi(\phi_\parallel)](u) + 4I_2[4g_\perp^v - g_{\parallel,3} - 3\phi_\parallel](u) &&= 24u^2\bar{u}^2 + \dots\,,\\
\mathbb{A}_\perp(u) &= -4I_1[\xi\phi_\perp](u) + 4I_2[h_{\perp,3} - \phi_\perp](u) &&= 24u^2\bar{u}^2 + \dots\,,\\
\mathbb{G}_\perp^v(u) &= -4I_1[\xi g_\perp^v](u)\,, &&= 6u\bar{u}(1 - u\bar{u}) + \dots\,,\\
\mathbb{G}_\perp^a(u) &= -4I_1[\xi g_\perp^a](u)\,, &&= 12u^2\bar{u}^2 + \dots\,,
\end{aligned} \tag{B.12}$$

where the dots stand for non-asymptotic corrections. This method, convenient as it is, can not determine non-asymptotic corrections since one would need to expand in the z-coordinate of the quarks as well as the Wilson line. This leads to higher dimensional local operators and 3-particle DAs which are both non-asymptotic. Hence if only the asymptotic DAs are required then we do not need to do this expansion. We might turn to a more systematic study of this method in future work. Our confidence in this alternative method, for determining the asymptotic DAs, is borne out of several consistency checks.

- The DA $\mathbb{A}_\parallel$ is such $I_1[\mathbb{A}_\parallel - \mathbb{G}^v_\perp](1) = 0$ which guarantees the, previously discussed, finite limit $p \cdot x \to 0$. The latter allows for the substitution (B.9), i.e. the $1/px$-pole is removed by partial integration.[30]

- The asymptotic form $\mathbb{A}_\perp$ from the literature is reproduced.

- We adapt the moment equation [95] (eq. (4.7)) for $g^{a,v}_\perp$ to $\mathbb{G}^{a,v}_\perp$ which can be done by replacing $(n+2) \to (n+4)$ where the extra additive factor of 2 originates from the extra power of x^2 in the LCDA expansion. The adapted moment equation in the limit of vanishing quark mass and no 3-particle DA becomes

$$\frac{1}{2}(n+4)M_n^{(\mathbb{G}^a)} = M_n^{(\mathbb{G}^v)}, \qquad M_n^{(\mathbb{G}^x)} \equiv \int_0^1 du\, \xi^n\, \mathbb{G}^x_\perp(u)\,, \qquad (\xi \equiv 2u-1)\,. \tag{B.13}$$

  It is readily verified that the asymptotic DAs given in (B.12) satisfy the moment equation exactly.

- Last but not least the obtained asymptotic DAs do verify the EOM (2.5) at the level of the correlation function and therefore FFs. This was our original motivation to look into this matter.

B.3 Explicit DAs used for this work

In this section we provide the actual DAs used in this paper to the given approximation. For more complete solutions for the lower DAs we refer to the references in table 12. The conventional approach for twist-2 and twist-3 DAs is the expansion in conformal spin (e.g. Gegenbauer moments) analogous to the partial wave expansion of SO(3). For the twist 4 there is the conformal spin expansion as well as a renormalon model e.g. [96]. In this work we only solve for the asymptotic DA for twist 4 which is the lowest order in the conformal expansion. We estimate the effect of this to be at the 1%-level which is well beyond the uncertainty.

For the twist-2 DA we expand up to second order in the Gegenbauer polynomials $C_n^{3/2}(\xi = 2u-1)$

$$\phi_{\perp,\parallel}(u) = 6u(1-u)\big(1 + a_1^{\perp,\parallel} C_1^{3/2}(\xi) + a_2^{\perp,\parallel} C_2^{3/2}(\xi)\big)\,, \tag{B.14}$$

[30] We remind the reader that $I_1[\mathbb{A}_\parallel|_{\text{BBL}}](1) \neq 0$ was our motivation to investigate the DAs. It should be mentioned that it is possible that the EOM can be satisfied to the given order in m_V by using the ultrarelatvistic approximatoin $\eta(p) \to p/m$ for $\mathbb{A}_\parallel$. For consistency one should use the same approximation to determine the light-cone DAs.

JHEP08(2016)098

which is a standard approximation in view of the lack of reliable knowledge on higher moments. The twist-3 DAs are obtained from the twist-2 and the leading twist-3 3-particle DAs [95]

$$\begin{aligned}
\tilde{g}_\perp^a &= \bar{u}\int_0^u dv\,\frac{\Psi_g(v)}{\bar{v}} + u\int_u^1 dv\,\frac{\Psi_g(v)}{v} + 6u\bar{u}\left(\frac{10}{9}\zeta_3^\parallel + \frac{5}{12}(\omega_3^\parallel - \tilde{\omega}_3^\parallel/2)\right)C_2^{3/2}(\xi)\\
g_\perp^v &= \frac{1}{4}\left[\int_0^u dv\,\frac{\Psi_g(v)}{\bar{v}} + \int_u^1 dv\,\frac{\Psi_g(v)}{v}\right] + 5\zeta_3^\parallel(3\xi^2-1) + \frac{15}{32}(\omega_3^\parallel - \tilde{\omega}_3^\parallel/2)(3-30\xi^2+35\xi^4)\,,\\
h_\parallel^{(t)} &= \frac{1}{2}\left[\int_0^u dv\,\frac{\Psi_h(v)}{\bar{v}} + \int_u^1 dv\,\frac{\Psi_h(v)}{v}\right] + \frac{15}{8}\omega_3^\perp(3-30\xi^2+35\xi^4)\,,\\
\tilde{h}_\parallel^{(s)} &= \bar{u}\int_0^u dv\,\frac{\Psi_h(v)}{\bar{v}} + u\int_u^1 dv\,\frac{\Psi_h(v)}{v} + 6u\bar{u}\left(\frac{5}{18}\,\omega_3^\perp C_2^{3/2}(\xi)\right).
\end{aligned} \tag{B.15}$$

with $\Psi_g(u) \equiv 2\phi_\parallel(u) + \tilde{\delta}_+\xi\phi_\perp'(u) + \tilde{\delta}_-\phi_\perp'(u)$ and $\Psi_h(u) \equiv 2\phi_\perp(u) - \delta_+\big(\phi_\perp'(u) - \xi/2\phi_\perp'(u)\big) + 1/2\delta_-\phi_\perp'(u)$. The contributions of the 2-particle DAs are given implicitly whereas the 3-particle DA-contributions have been given explicitly. The four parameters $\zeta_3, \omega_3^\perp, \omega_3^\parallel$ and $\tilde{\omega}_3^\parallel$ are G-parity even parameters of the three twist-3 3-particle DAs as given in (eq. (3.11)) in [46]. SU(3)-breaking parameters can be neglected at the current level of precision.

As stated above for the twist-4 and twist-5 DAs we employ the asymptotic form which means that we set the Gegenbauer moments $a_{1,2}$, the 3-particle DA parameters and the quark masses to zero with respect to the more general solution. The asymptotic twist-4 DAs are given by

$$h_{\perp,3} = 6u\bar{u}\,, \qquad g_{\parallel,3} = 6u\bar{u}\,, \qquad \mathbb{A}_\perp = 24u^2\bar{u}^2, \qquad \mathbb{A}_\parallel = 24u^2\bar{u}^2 \tag{B.16}$$

and the newly introduced twist-5 DAs

$$\mathbb{G}_\perp^v = 6u\bar{u}(1-u\bar{u})\,, \qquad \mathbb{G}_\perp^a = 12u^2\bar{u}^2. \tag{B.17}$$

The determination of $\mathbb{A}_\parallel$ and $\mathbb{G}_\perp^{v,a}$ are new and discussed in the previous section. The numerical input is given in table 1 except for the values for $\omega_3^\perp$, $\omega_3^\parallel$ and $\tilde{\omega}_3^\parallel$ which are taken from table one in [46] and are related to the parameters previously used (e.g. [2]) as follows $3/2\zeta_3^\parallel\omega_3^V = \omega_3^\parallel$, $3/2\zeta_3^\parallel\omega_3^T = \omega_\perp^\parallel$ and $1/2\zeta_3^\parallel\omega_3^A = \tilde{\omega}_3^\parallel$. For the sake of completeness and clarity we give the form of the integrated asymptotic DAs given in (B.9):

$$\begin{aligned}
\phi_\parallel^{(1)}(u) &= \frac{3}{2}\bar{u}u\xi\,, \qquad & h_\parallel^{(t,2)}(u) &= \frac{3}{2}u^2\bar{u}^2, \qquad & h_{\perp,3}^{(1)}(u) &= 0\,,\\
g_{\parallel,3}^{(2)}(u) &= -\frac{3}{2}u^2\bar{u}^2, \qquad & \mathbb{A}_\parallel^{(1)}(u) &= 3\xi u^2\bar{u}^2.
\end{aligned} \tag{B.18}$$

C Decay constants from experiment

C.1 The neutral decay constants $f_{\rho^0,\omega,\phi}$ from $V^0 \to e^+e^-$

We improve the discussion on the extraction of the decay constants of the ρ^0, ω and ϕ from $V^0 \to e^+e^-$ with respect to the earlier work [73]. The effects on the decay constants due

JHEP08(2016)098

to mixing are taken into account at the level of matrix elements. Previously the mixing was abstracted from the state mixing. The relation between the two is commented on in section C.1.3.

The three vector mesons ρ^0, ω and ϕ are flavour neutral and can therefore mix into each other through QCD and QED. The mixing of ϕ–ω is driven by QCD, ρ–ω is due to QED and $m_{u,d}$-quark mass difference whereas ϕ–ρ requires both forces and can therefore be neglected. In $V^0 \to e^+e^-$ the meson couple to the electromagnetic current as follows

$$j_\mu^{\text{em}} = Q_s V_\mu^{\phi_I} + \frac{Q_u + Q_d}{\sqrt{2}} V_\mu^{\omega_I} + \frac{Q_u - Q_d}{\sqrt{2}} V_\mu^{\rho_I} \tag{C.1}$$

with $Q_{u,d,s}$ being the charges of the quarks and the quark currents are defined by

$$V_\mu^{\omega_I, \rho_I^0} = \frac{1}{\sqrt{2}}(\bar{u}\gamma_\mu u \pm \bar{d}\gamma_\mu d)\,, \qquad V_\mu^{\phi_I} = \bar{s}\gamma_\mu s\,. \tag{C.2}$$

The label I stands for isospin as well as ideal mixing (i.e. ϕ being a pure $s\bar{s}$-state). The currents $V_\mu^{\omega_I, \phi_I}$ and $V_\mu^{\rho_I^0}$ are of isospin $I = 0$ and $I = 1$ for respectively.

It is our goal to extract the following decay constants

$$\langle \phi | V_\mu^{\phi_I} | 0 \rangle = \eta_\mu m_\phi f_\phi^{\phi_I}, \qquad \hat{c}_\omega^q \langle \omega | \bar{q}\gamma_\mu q | 0 \rangle = \eta_\mu m_\omega f_\omega^{(q)}, \qquad \hat{c}_{\rho^0}^q \langle \rho^0 | \bar{q}\gamma_\mu q | 0 \rangle = \eta_\mu m_{\rho^0} f_{\rho^0}^{(q)}, \tag{C.3}$$

relevant for the description of flavour transition via the weak force. Above η denotes the polarisation vectors, the $\parallel$ superscript on $f_V^\parallel$ is omitted and $\hat{c}_{\rho^0}^u = -\hat{c}_{\rho^0}^d = \hat{c}_\omega^u = \hat{c}_\omega^d = \sqrt{2}$ are prefactors taking into account the quark composition of the wave functions. The effect of the mixing is investigated in a two step procedure of ϕ–ω and ρ–ω mixing.

C.1.1 Effective couplings to the electromagnetic current

ϕ–ω mixing. In order to asses the effect of the ϕ–ω mixing the following matrix elements are needed

$$\begin{aligned} \langle \phi | V_\mu^{\omega_I} | 0 \rangle &= \eta_\mu m_\phi f_\phi^{\omega_I} \equiv \epsilon(m_\phi) \eta_\mu m_\phi f_\phi^{\phi_I}\,, \\ \langle \omega | V_\mu^{\phi_I} | 0 \rangle &= \eta_\mu m_\omega f_\omega^{\phi_I} \equiv -\epsilon(m_\omega) \eta_\mu m_\omega f_\omega^{\omega_I}\,. \end{aligned} \tag{C.4}$$

They have been computed to be $\epsilon \equiv \epsilon(m_\phi) \simeq \epsilon(m_\omega) = 0.05(2)$ in the pioneering papers of QCD sum rules [14]. Note, the effect is driven by contributions of four quark condensates, estimated in the vacuum saturation approximation, and we have therefore assigned a conservative 40% error to ϵ.

ρ–ω mixing. The analogous ρ, ω decay constants have been computed in reference [98] by using finite energy sum rules. Effects are due to different QED and $m_{u,d}$-quark mass differences.[31] Their results, neglecting the ρ–ϕ mixing, translates into the notation analogous to (C.4) as follows: $f_\rho^{\omega_I} = \sqrt{6} F_\rho^8 \simeq 5.9(12)\,\text{MeV}$ and $f_\omega^{\rho_I} = \sqrt{2} F_\omega^3 = -4.8(10)\,\text{MeV}$. We have enlarged the uncertainty in view of possible duality violation of finite energy sum rules [99].

[31] Note computing the QED corrections to the local matrix element, i.e. which we call decay constant, is not the same as computing the QED corrections to the corresponding leptonic decays themselves. The latter are more complex, requiring the computation of virtual and real corrections taken into account in the experimental analysis.

JHEP08(2016)098

C.1.2 Scaling factors due to mixing

We parameterise the mixing effects in terms of correction factors, denoted by κ, to the matrix element to the electromagnetic current,

$$\langle\omega|j_\mu^{\rm em}|0\rangle = \eta_\mu m_\omega f_\omega^{\omega_I}\frac{Q_u+Q_d}{\sqrt{2}}\kappa^{\omega[\phi]}\kappa^{\omega[\rho]}, \qquad \langle\rho^0|j_\mu^{\rm em}|0\rangle = \eta_\mu m_{\rho^0} f_{\rho^0}^{\rho_I^0}\frac{Q_u-Q_d}{\sqrt{2}}\kappa^{\rho[\omega]},$$
$$\langle\phi|j_\mu^{\rm em}|0\rangle = \eta_\mu m_\phi f_\phi^{\phi_I} Q_s \kappa^{\phi[\omega]}. \tag{C.5}$$

Using the numerical input of the previous section we get

$$\begin{aligned}
\kappa^{\phi[\omega]} &\equiv \left(1+\frac{f_\phi^{\omega_I}}{f_\phi^{\phi_I}}\frac{Q_u+Q_d}{\sqrt{2}Q_s}\right) \simeq \left(1+\epsilon\frac{Q_u+Q_d}{\sqrt{2}Q_s}\right) \simeq 1/\big(1.037(16)\big)\,,\\
\kappa^{\omega[\phi]} &\equiv \left(1+\frac{f_\omega^{\phi_I}}{f_\omega^{\omega_I}}\frac{\sqrt{2}Q_s}{Q_u+Q_d}\right) \simeq \left(1-\epsilon\frac{\sqrt{2}Q_s}{Q_u+Q_d}\right) \simeq 1/\big(0.933(28)\big)\,,\\
\kappa^{\omega[\rho]} &\equiv \left(1+\frac{f_\omega^{\rho_I^0}}{f_\omega^{\omega_I}}\frac{Q_u-Q_d}{Q_u+Q_d}\right) \qquad\qquad \simeq 1/\big(1.08(2)\big)\,,\\
\kappa^{\rho[\omega]} &\equiv \left(1+\frac{f_{\rho^0}^{\omega_I}}{f_{\rho^0}^{\rho_I^0}}\frac{Q_u+Q_d}{Q_u-Q_d}\right) \qquad\qquad \simeq 1/\big(0.990(2)\big)\,.
\end{aligned} \tag{C.6}$$

The impact of the mixing on the extraction of the decay constants is heavily affected by the charge ratios $\sqrt{2}Q_s/(Q_u+Q_d) = -\sqrt{2}$ and $(Q_u-Q_d)/(Q_u+Q_d) = 3$. The reader is reminded that ρ–ϕ mixing is neglected since it requires the strong as well as the electromagnetic force which is expected to be a small effect.

The experimental branching ratios are [79]

$$\begin{aligned}
&{\rm BR}(\rho^0\to e^+e^-) = (4.72\pm0.05)\times10^{-5}, \qquad {\rm BR}(\omega\to e^+e^-) = (7.28\pm0.14)\times10^{-5},\\
&{\rm BR}(\phi\to e^+e^-) = (2.95\pm0.30)\times10^{-5}.
\end{aligned} \tag{C.7}$$

The theoretical expression for the decay rate is given by

$$\Gamma(V^0\to e^+e^-) = \frac{4\pi}{3}\frac{\alpha^2}{m_V}f_V^2 c_V + O\left(\alpha,\frac{m_V^2}{M_W^2}\right), \tag{C.8}$$

where the coefficients c_V in the limit of no mixing (i.e. $\kappa\to0$) can be read-off from (C.1) $c_{\rho_I^0} = (Q_u-Q_d)^2/2 = 1/2$, $c_{\omega_I} = (Q_u+Q_d)^2/2 = 1/18$ and $c_{\phi_I} = Q_s^2 = 1/9$. The effect of mixing leads to the following replacements

$$c_{\rho_I^0}\to c_{\rho_I^0}\big(\kappa^{\rho[\omega]}\big)^2, \qquad c_{\omega_I}\to c_{\omega_I}\big(\kappa^{\omega[\rho]}\kappa^{\omega[\phi]}\big)^2, \qquad c_{\phi_I}\to c_{\phi_I}\big(\kappa^{\phi[\omega]}\big)^2,$$

and results in a shift of ρ, ω and ϕ decay constant of roughly -1%, 0.5% and 4% respectively. It is noticed that the individual effects of the ω–ρ and the ω–ϕ mixing are around $\pm8\%$ but do almost cancel each other out.

Including the mixing effects we get the following decay constants for the currents (C.2)

$$\begin{aligned}
f_{\rho^0}^{\rho_I} &= (215.6\pm2_{\rm Br}\pm1_{\Gamma_\rho}\pm1_{\omega\text{–}\rho}\pm0)\,{\rm MeV} &&= 216(3)\,{\rm MeV},\\
f_\omega^{\omega_I} &= (196.5\pm2_{\rm Br}\pm1_{\Gamma_\omega}\pm4_{\omega\text{–}\rho}\pm6_{\omega\text{–}\phi})\,{\rm MeV} &&= 197(8)\,{\rm MeV},\\
f_\phi^{\phi_I} &= (233.0\pm2_{\rm Br}\pm1_{\Gamma_\phi}\pm3_{\phi\text{–}\omega}\pm0)\,{\rm MeV} &&= 233(4)\,{\rm MeV},
\end{aligned} \tag{C.9}$$

JHEP08(2016)098

where the uncertainties in the other input parameters are irrelevant. Errors are added in quadrature in the final result. To clarify the notation we quote the example $f_{\rho^0}^{\rho_I} = f_{\rho^0}/\kappa^{\rho[\omega]} \simeq 0.99 f_{\rho^0}$ with f_{ρ^0} from (C.8).

Finally we get for the ρ and ω decay constants coupling directly to u and d quark currents

$$\begin{aligned} f_{\rho^0}^{(u)} &= f_{\rho^0}^{\rho_I^0} + f_{\rho^0}^{\omega_I} = (215.6 + 5.9)\,\text{MeV} = 221.5(3)\,\text{MeV}, \\ f_{\rho^0}^{(d)} &= f_{\rho^0}^{\rho_I^0} - f_{\rho^0}^{\omega_I} = (215.6 - 5.9)\,\text{MeV} = 209.7(3)\,\text{MeV}, \\ f_{\omega}^{(u)} &= f_{\omega}^{\omega_I} + f_{\omega}^{\rho_I^0} = (196.5 - 4.8)\,\text{MeV} = 191.7(8)\,\text{MeV}, \\ f_{\omega}^{(d)} &= f_{\omega}^{\omega_I} - f_{\omega}^{\rho_I^0} = (196.5 + 4.8)\,\text{MeV} = 201.3(8)\,\text{MeV}, \end{aligned} \tag{C.10}$$

where we have taken the same uncertainties as in (C.9).

C.1.3 Comment on state mixing versus decay constant mixing

The mixing of states and decay constants are related but can be quantitatively different.[32] The former is one of the effects contributing to the latter. Below we present evidence that in reality the mixing of states dominates the mixing of the $\omega - \phi$ decay constants.

For example if one assumes that $f_{\omega}^{\omega_I} \simeq f_{\phi}^{\phi_I}$ ($\text{SU}(3)_F$-symmetry for which there is empirical evidence), $|f_{\omega_I}^{\phi_I}| \ll |f_{\omega_I}^{\phi}|$ and takes into account the ϕ–ω state mixing

$$|\omega\rangle \sim |\omega_I\rangle - \epsilon_{\omega\phi}|\phi_I\rangle\,, \qquad |\phi\rangle \sim |\phi_I\rangle + \epsilon_{\omega\phi}|\omega_I\rangle\,, \tag{C.11}$$

one arrives at

$$\epsilon_{\omega\phi}\frac{m_\omega}{m_\phi} \simeq \epsilon(m_\phi)\,, \qquad \epsilon_{\omega\phi}\frac{m_\phi}{m_\omega} \simeq \epsilon(m_\omega)\,, \tag{C.12}$$

which is reasonably well satisfied. A recent determination of the mixing angle by the KLOE collaboration is given by $\epsilon_{\omega\phi} = 3.32(9)^\circ \simeq 0.58(2)$. Using, as previously [14], $\epsilon \equiv \epsilon(m_\phi) \simeq \epsilon(m_\omega) = 0.05(2)$, eq. (C.12) is equivalent to $0.45 \simeq 0.5(2)$ and $0.7 \simeq 0.5(2)$ which is satisfied within errors. It is to be concluded that the effect of ϕ–ω decay constant mixing is driven by the state-mixing.

One could put forward the same procedure for the ρ–ω system but there are complications. The ρ–ω system is more delicate since the closeness of the two states means that the mixing angle is effectively a complex number because diagonal and off-diagonal self energies are complex. The off-diagonal self energy acquires an imaginary part through the isospin violating $\omega \to \pi\pi \to \rho$ transition; a circumstance which has been neglected in the literature for a long time! The off-diagonal self energy has been determined to be $\Pi_{\rho\omega}(m_\rho^2) \simeq (-4620 \pm 220_{\text{model}} \pm 170_{\text{data}}) + (-6100 \pm 1800_{\text{model}} \pm 1110_{\text{data}})i\,\text{MeV}^2$ [100] by using a recent BaBar analysis [101]. The value of the mixing angle through $\epsilon_{\rho\omega} = \Pi_{\rho\omega}(m_\rho^2)/\big((m_\omega - i\Gamma_\omega/2)^2 - (m_\rho - i\Gamma_\rho/2)^2\big)$ then comes with a large error; especially on the real part which is decisive. The small error on previous determinations turned out to be an artefact of neglecting the imaginary part of the off-diagonal self energy [98]. In view of this situation we chose to directly use the computations on the mixing of the decay constants and abandon the mixing of state picture.

[32] This is particularly enhanced for η–η' system because of the effect of the chiral anomaly.

JHEP08(2016)098

C.2 Charged decay constants from $\tau^+ \to V^+\nu$ decays

The same standard procedure is applied as in [73] including in addition the sizeable leading electroweak corrections (due to a $\ln(m_Z/m_\tau)$-term) [102, 103]. Implementing this amounts to making the replacement $\text{BR}(\tau^+ \to K^{*+}\nu)_{\text{here}} = 1.015 \cdot \text{BR}(\tau^+ \to K^{*+}\nu)_{[73]}$. Using the input parameters $|V_{\text{us}}| \simeq 0.225$, $|V_{\text{ud}}| \simeq 0.974$, $\text{BR}(\tau^+ \to \rho^+\nu) = 25.22 \pm 0.33$ and $\text{BR}(\tau^+ \to K^{*+}\nu) = 1.20 \pm 0.07$, $\alpha(m_V) \simeq 1/135.4$ and the τ lifetime $\tau_\tau = (290.3 \pm 0.5) \cdot 10^{-15}\,\text{s}$ [79] we get

$$f_{K^*} = 204(7)\,\text{MeV}, \qquad f_{\rho^+} = 210(4)\,\text{MeV}. \tag{C.13}$$

C.3 Final results summarised

In view of the many details discussed and numbers quoted we summarise our results for the reader's convenience. The difference in the charged and neutral ρ decay constants is 6 MeV and we therefore choose to average them $\bar{f}_\rho^{\rho_I} = 213(5)\,\text{MeV}$ slightly enhancing the uncertainty. The final results for the decay constants coupling to the currents (C.2) are then taken from (C.9), (C.13) and the above mentioned average

$$\begin{aligned} \bar{f}_\rho^{\rho^I} &= 213(5)\,\text{MeV}, & f_\omega^{\omega_I} &= 197(8)\,\text{MeV}, \\ f_\phi^{\phi_I} &= 233(4)\,\text{MeV}, & f_{K^*} &= 204(7)\,\text{MeV}. \end{aligned} \tag{C.14}$$

The decay constant for the pure flavour currents to the ρ^0- and ω-meson are (C.10)

$$\begin{aligned} f_{\rho^0}^{(u)} &= 221.5(3)\,\text{MeV}, & f_{\rho^0}^{(d)} &= 209.7(3)\,\text{MeV} \\ f_\omega^{(u)} &= 191.7(8)\,\text{MeV} & f_\omega^{(d)} &= 201.3(8)\,\text{MeV}. \end{aligned} \tag{C.15}$$

In our tables and computation we will use the decay constants (C.14) omitting the additional labels. The results of f_{K^*} is consistent with [103], ϕ–ω is treated similarly to [104], whereas our discussion on ρ–ω mixing is more detailed in terms of explicit results. We would like to add a comment concerning QED corrections. The experimental analyses are performed using photon showers (e.g. photos [105]) and subtracting the large part of the final state photons. A fully consistent treatment of QED corrections might be carried out in the future for which we may expect a global shift (i.e. multiplicative factor in front of all decay constants) at or below the 1%-level.

As for the flavour specific decay constants we leave it to the reader to scale the $B \to \rho^0, \omega$ FFs appropriately. For example for

$$\begin{aligned} F_{b\to u}^{B\to\rho^0} &= k_{(\rho^0,u)} F^{B\to\rho^0} \simeq 1.040\, F^{B\to\rho^0}, \\ F_{b\to u}^{B\to\omega} &= k_{(\omega,u)} F^{B\to\omega} \simeq 0.973\, F^{B\to\omega}, \end{aligned} \tag{C.16}$$

where F stands for any of the seven FFs. The scale factors k are $k_{(\rho^0,q)} = f_{\rho^0}^{(q)}/\bar{f}_\rho^{\rho^I}$ and $k_{(\rho^0,q)} = f_\omega^{(q)}/f_\omega^{\omega^I}$ which upon using (C.14) and (C.15) amount to

$$k_{(\rho^0,u)} = 1.040\,, \qquad k_{(\rho^0,d)} = 0.985\,, \qquad k_{(\omega,u)} = 0.973\,, \qquad k_{(\omega,d)} = 1.022\,. \tag{C.17}$$

Scaling the FF as in (C.16) is a reasonable procedure since, in practical computations, all input parameters of the DA are made dependent on the normalisation of the longitudinal decay constant.

JHEP08(2016)098

D Conversion between form factor bases

D.1 Helicity basis

In this appendix we give the projection of the FFs onto the helicity basis which is convenient for the computation of angular observables. Using the Jacob Wick polarisation tensors[33] we define:

$$X^{(\rho)} = \epsilon_\mu(\rho)\langle K^*\Big(p,\eta\big(m(\rho)\big)\Big)|\bar{s}\Gamma_X^\mu b|\bar{B}(p_B)\rangle\,, \qquad m(t)=m(0)=0\,, \quad m(\pm)=\pm \tag{D.1}$$

where $\rho = 0,\pm,t$ is the polarisation index which is not summed over and $\Gamma_T^\mu = iq_\nu\sigma^{\mu\nu}(1\pm\gamma_5)$, $\Gamma_{\mathcal{V}}^\mu = \gamma^\mu(1\mp\gamma_5)$ and $\Gamma_{\mathcal{D}}^\mu = (2i\overleftarrow{D})^\mu(1\pm\gamma_5)$ correspond to tensor, vector and derivative FFs. We get

$$\begin{aligned}
X^{(\perp)} &= \frac{1}{\sqrt{2}}\big(X^{(+)} - X^{(-)}\big) = i\sqrt{2}\sqrt{\lambda(q^2)}X_1\,,\\
X^{(\parallel)} &= \frac{1}{\sqrt{2}}\big(X^{(+)} + X^{(-)}\big) = \pm i\sqrt{2}(m_B^2 - m_{K^*}^2)X_2\,,\\
X^{(0)} &= \mp i\frac{\sqrt{q^2}(m_B^2 + 3m_V^2 - q^2)}{2m_{K^*}}X_0\,,\\
X^{(t)} &= \mp i\frac{\sqrt{\lambda(q^2)}}{2}X_P\,,
\end{aligned} \tag{D.2}$$

where $X_0 \equiv X_2 - c_{23}(q^2)X_3$ with

$$\begin{aligned}
c_{23}(q^2) &\equiv \frac{\lambda(q^2)}{(m_B^2 - m_{K^*}^2)(m_B^2 + 3m_{K^*}^2 - q^2)} = 1 + \mathcal{O}(q^2/m_B^2, m_{K^*}^2/m_B^2)\,,\\
\lambda(q^2) &\equiv \big((m_B + m_{K^*})^2 - q^2\big)\big((m_B - m_{K^*})^2 - q^2\big)\,,
\end{aligned} \tag{D.3}$$

and λ being the Källén-function. We infer that at the kinematic endpoint where $\lambda = 0$, only the X_2 structure contributes in accordance with general findings on endpoint symmetries [76].

For $X = T, \mathcal{V}, \mathcal{D}$, X_i is given by T_i (with $T_P \equiv 0$) $\mathcal{V}_i$ and $\mathcal{D}_i$ in eq. (2.3) and (2.10) respectively. The relation of T_0 and $\mathcal{V}_0$ to T_{23} and A_{12} used in the literature (e.g. [10]) is as follows:

$$T_0 = \frac{8m_B m_{K^*}^2}{(m_B + m_{K^*})(m_B^2 + 3m_{K^*}^2 - q^2)}T_{23}\,, \qquad \mathcal{V}_0 = \frac{-16m_B m_{K^*}^2}{q^2(m_B^2 + 3m_{K^*}^2 - q^2)}A_{12} \tag{D.4}$$

where

$$\begin{aligned}
A_{12} &= \frac{(m_B + m_{K^*})^2(m_B^2 - m_{K^*}^2 - q^2)A_1 - \lambda(q^2)A_2}{16m_B m_{K^*}^2(m_B + m_{K^*})}\\
&= \frac{q^2/2(m_B^2 + 3m_{K^*}^2 - q^2)A_1 + \lambda(q^2)m_{K^*}/(m_B + m_{K^*})A_3}{8m_B m_{K^*}^2(m_B - m_{K^*})}\\
T_{23} &= \frac{(m_B^2 - m_{K^*}^2)(m_B^2 + 3m_{K^*}^2 - q^2)T_2 - \lambda(q^2)T_3}{8m_B m_{K^*}^2(m_B - m_{K^*})}\,.
\end{aligned} \tag{D.5}$$

[33] Cf. appendix A [76] where the polarisation tensors η and ϵ correspond to γ and β respectively.

JHEP08(2016)098

$\sigma_{\mu\nu}q^\nu$	γ_μ	$\gamma_\mu\gamma_5$	γ_5	type
$T_{1,2,3}$	V	$A_{1,3,0}$	A_0	traditional
$T_{1,2,3}$	$\mathcal{V}_1$	$\mathcal{V}_{2,3,P}$	$\mathcal{V}_P$	EOM (2.6)–(2.9)
$T_{\perp,\parallel} \sim T_{1,2}$, $T_0 \sim T_{23}$	$\mathcal{V}_\perp \sim \mathcal{V}_1$	$V_\parallel \sim \mathcal{V}_2$, $\mathcal{V}_0 \sim A_{12}$, $\mathcal{V}_P$	$\mathcal{V}_P$	helicity

Table 13. The conversion factors between the traditional and the EOM FFs is given in (2.3). The 0-helicity FF are given by $T[\mathcal{V}]_0(q^2) = T[\mathcal{V}]_2(q^2) - c_{23}(q^2)T[\mathcal{V}]_3(q^2)$ with the kinematic function given as in (D.3) and the q^2 dependence of the factor relating $T[\mathcal{V}]_{\perp,\parallel} \sim T[\mathcal{V}]_{1,2}$ can be read off from (D.2). The 0 helicity FFs T_{23} and A_{12} whose notation is inspired by (D.5) are related to T_0 and $\mathcal{V}_0$ as given in (D.4).

We further notice that

$$A_{12}(0) = \frac{m_B^2 - m_{K^*}^2}{8m_B m_{K^*}} A_3(0) = \frac{m_B^2 - m_{K^*}^2}{8m_B m_{K^*}} A_0(0)\,, \tag{D.6}$$

which we implement, besides $T_1(0) = T_2(0)$, into the fit as a constraint.

D.2 Overview of form factor notation

Not including the derivative FFs there are seven independent FFs of which all others are linear combinations. The basis $T_{1,2,3}$, V and $A_{1,3,0}$ is the traditional basis (e.g. [2]; note: A_2 is linearly dependent on $A_{0,3}$ cf. (2.3)). The basis $T_{1,2,3}$, and $\mathcal{V}_{1,2,3,P}$ is suited for the EOM and the conversion between the two is given in (2.3). The helicity basis $T[\mathcal{V}]_{\perp,\parallel,0}$ and $\mathcal{V}_P$ is suited for phenomenology with $T[\mathcal{V}]_{\perp,\parallel} \sim T[\mathcal{V}]_{1,2}$ and $T[\mathcal{V}]_0 = T[\mathcal{V}]_2(q^2) - c_{23}(q^2)T[\mathcal{V}]_3(q^2)$. The 0-helicity FFs A_{12} and T_{23} have been introduced in [11] and their relation to the traditional basis is given in (D.5). An overview is given in table 13.

E Plots of form factors as a function of z

The plots of the FFs in the z-variable can be found in figures 5, 6, and 7 for the modes $B \to K^*$, $B_s \to \phi$ and $B_s \to \bar{K}^*$, respectively.

F SSE coefficients

In this appendix we list the central values and uncertainties of the SSE expansion coefficients of the $B \to K^*$, $B \to \rho$, $B \to \omega$, $B_s \to \phi$ and $B_s \to \bar{K}^*$ FFs from LCSR (table 14) as well as the combined fits to LCSR and lattice data for the $B \to K^*$ and $B_s \to \phi$ FFs (table 15). Note that of the 21 parameters for each transition, two are in fact redundant due to the exact relations (2.17).[34]

In addition to these central values and uncertainties, we also provide the full correlation and covariance matrices as ancillary files downloadable from the arXiv preprint page. The data are contained in 5 JSON files named `[Process]_[Fit].json`, where `[Process]` is

[34]Due to this redundancy, the 21×21 covariance matrices do not have full rank. Invertible covariance matrices can be obtained by removing the two redundant rows and columns.

JHEP08(2016)098

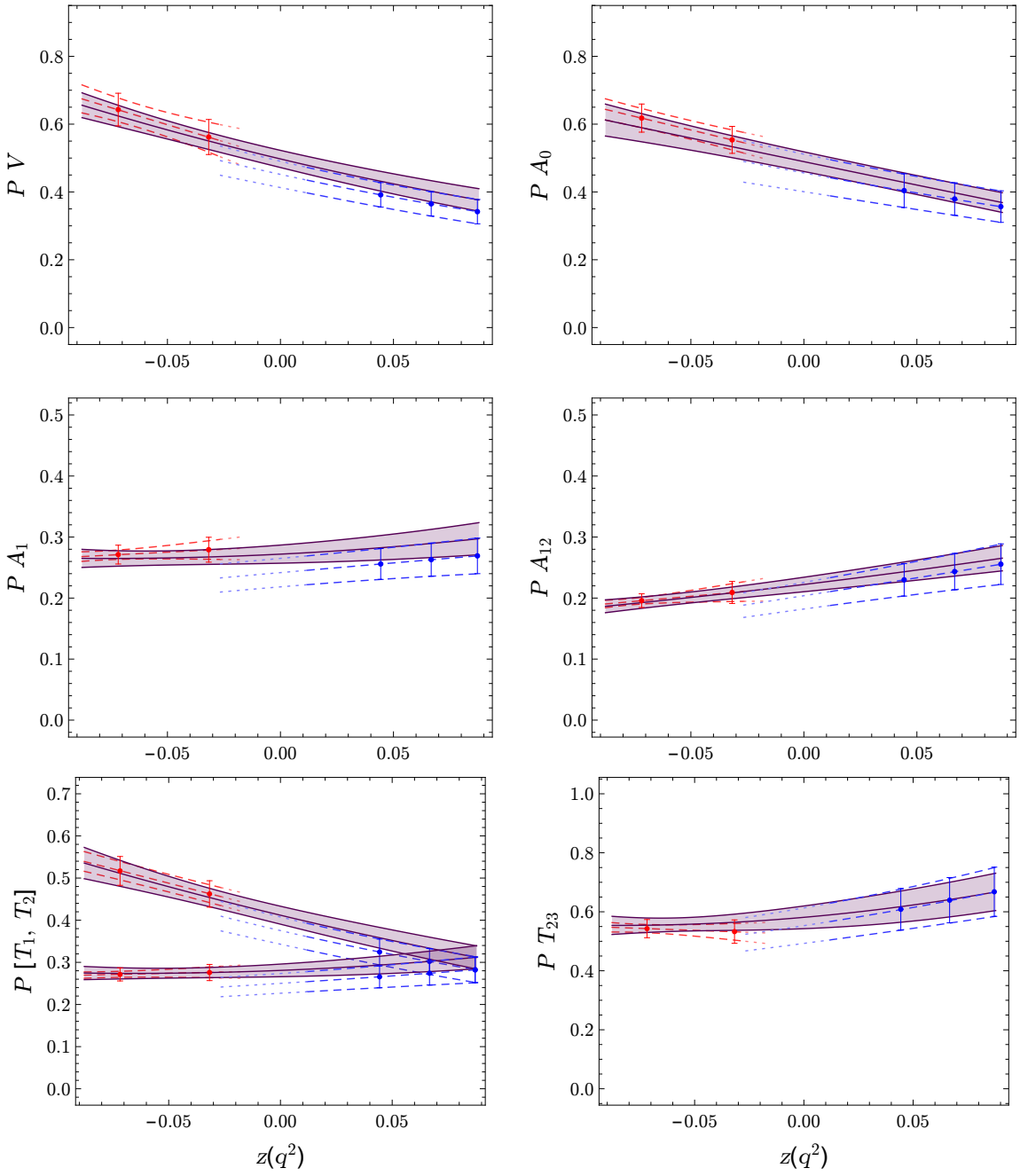

Figure 5. Combined LCSR and lattice fit to $B \to K^*$ FFs, where lattice data points are indicated in red, LCSR points in blue, the gray solid band shows the combined 3-parameter fit and the red dashed band the 2-parameter lattice fit from ref. [11].

JHEP08(2016)098

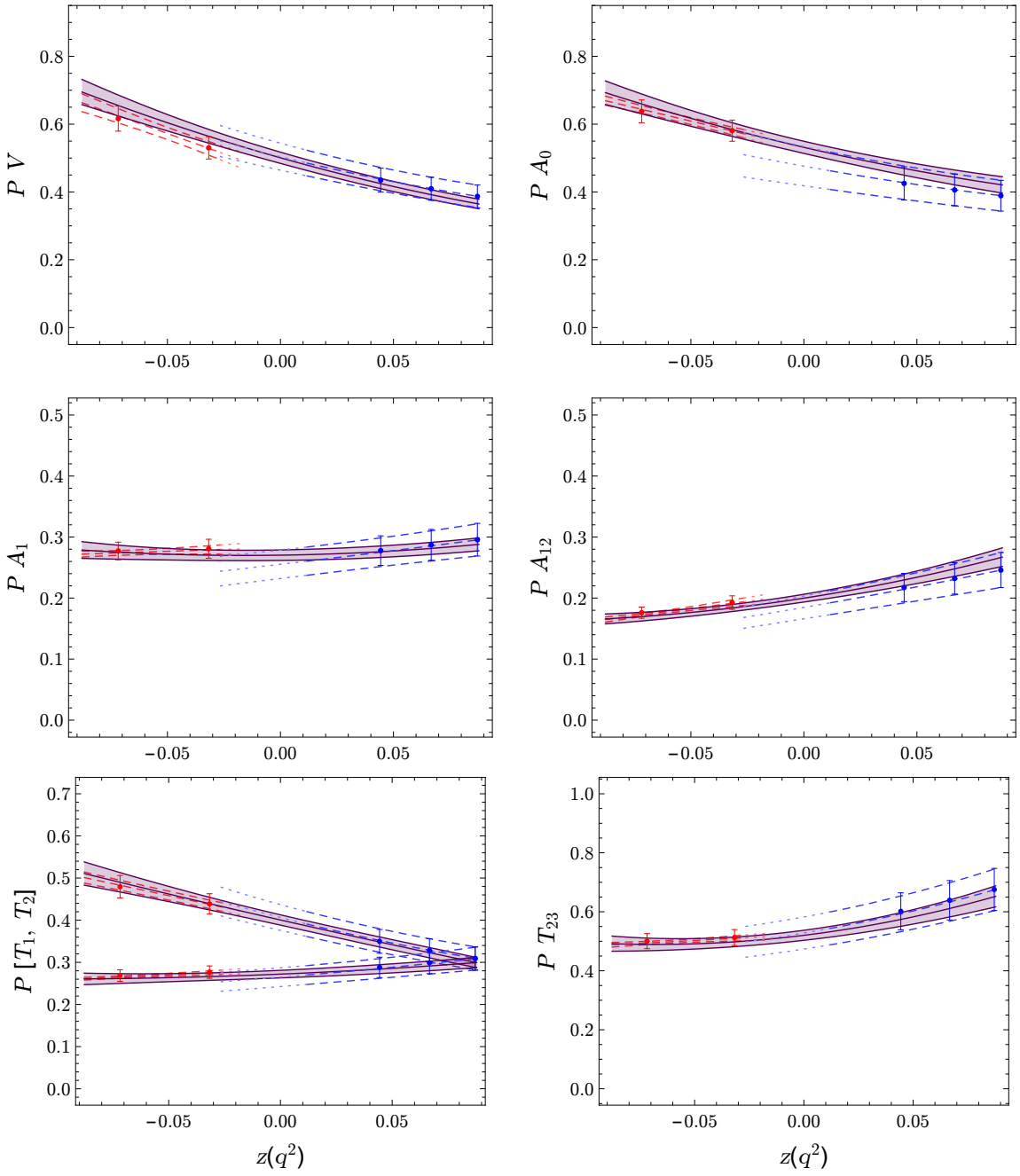

Figure 6. Combined LCSR and lattice fit to $B_s \to \phi$ FFs, where lattice data points are indicated in red, LCSR points in blue, the gray solid band shows the combined 3-parameter fit and the red dashed band the 2-parameter lattice fit from ref. [11].

JHEP08(2016)098

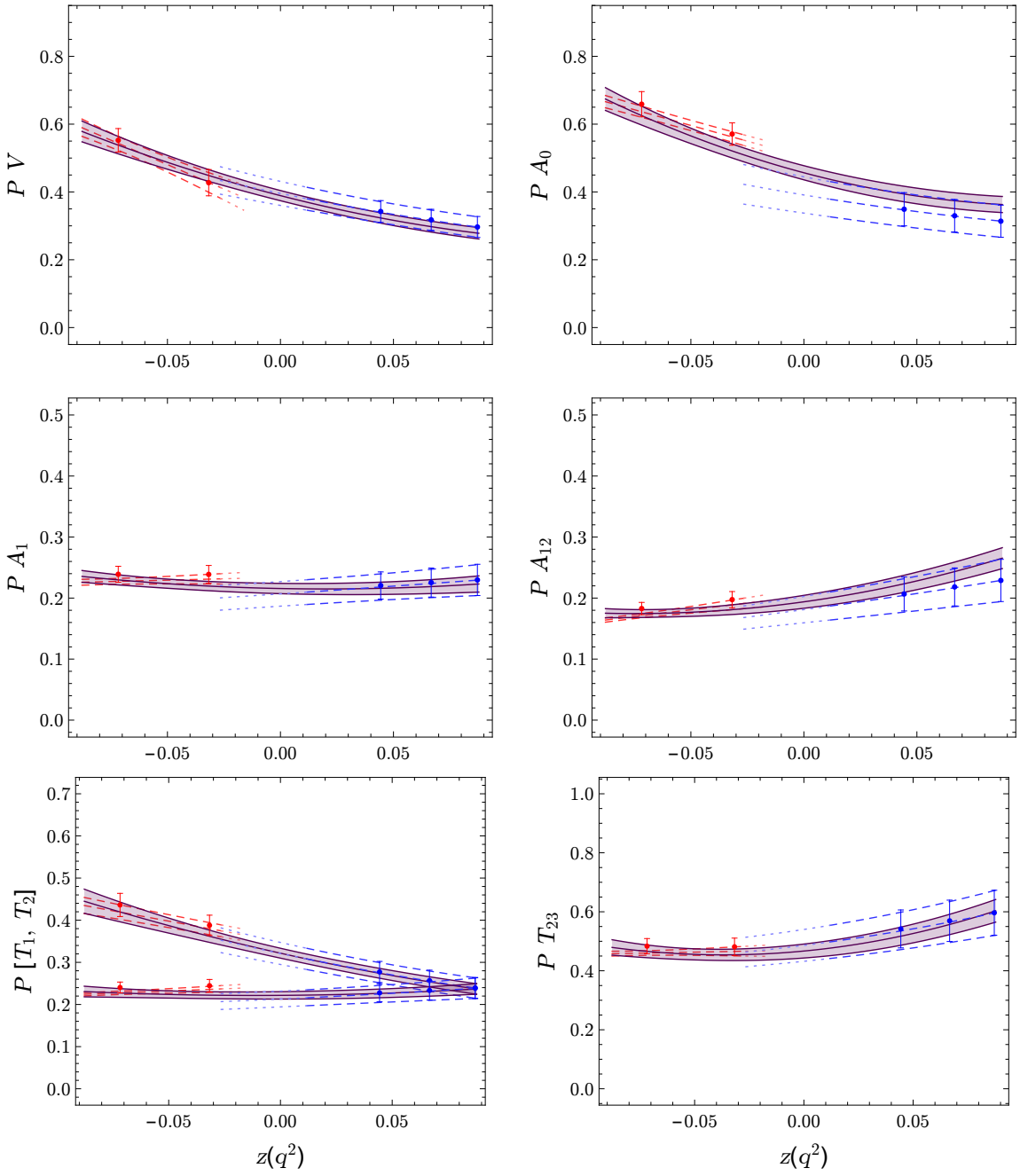

Figure 7. Combined LCSR and lattice fit to $B_s \to \bar{K}^*$ FFs, where lattice data points are indicated in red, LCSR points in blue, the gray solid band shows the combined 3-parameter fit and the red dashed band the 2-parameter lattice fit from ref. [11].

JHEP08(2016)098

	$B \to K^*$	$B \to \rho$	$B \to \omega$	$B_s \to \phi$	$B_s \to K^*$
$\alpha_0^{A_0}$	0.36 ± 0.05	0.36 ± 0.04	0.33 ± 0.05	0.39 ± 0.05	0.31 ± 0.05
$\alpha_1^{A_0}$	-1.04 ± 0.27	-0.83 ± 0.20	-0.83 ± 0.30	-0.78 ± 0.26	-0.66 ± 0.23
$\alpha_2^{A_0}$	1.12 ± 1.35	1.33 ± 1.05	1.42 ± 1.25	2.41 ± 1.48	2.57 ± 1.44
$\alpha_0^{A_1}$	0.27 ± 0.03	0.26 ± 0.03	0.24 ± 0.03	0.30 ± 0.03	0.23 ± 0.03
$\alpha_1^{A_1}$	0.30 ± 0.19	0.39 ± 0.14	0.34 ± 0.24	0.48 ± 0.19	0.27 ± 0.19
$\alpha_2^{A_1}$	-0.11 ± 0.48	0.16 ± 0.41	0.09 ± 0.57	0.29 ± 0.65	0.13 ± 0.56
$\alpha_0^{A_{12}}$	0.26 ± 0.03	0.30 ± 0.03	0.27 ± 0.04	0.25 ± 0.03	0.23 ± 0.03
$\alpha_1^{A_{12}}$	0.60 ± 0.20	0.76 ± 0.20	0.66 ± 0.26	0.76 ± 0.20	0.60 ± 0.21
$\alpha_2^{A_{12}}$	0.12 ± 0.84	0.46 ± 0.76	0.28 ± 0.98	0.71 ± 0.96	0.54 ± 1.12
α_0^{V}	0.34 ± 0.04	0.33 ± 0.03	0.30 ± 0.04	0.39 ± 0.03	0.30 ± 0.03
α_1^{V}	-1.05 ± 0.24	-0.86 ± 0.18	-0.83 ± 0.29	-1.03 ± 0.25	-0.90 ± 0.27
α_2^{V}	2.37 ± 1.39	1.80 ± 0.97	1.72 ± 1.24	3.50 ± 1.55	2.65 ± 1.33
$\alpha_0^{T_1}$	0.28 ± 0.03	0.27 ± 0.03	0.25 ± 0.03	0.31 ± 0.03	0.24 ± 0.02
$\alpha_1^{T_1}$	-0.89 ± 0.19	-0.74 ± 0.14	-0.72 ± 0.22	-0.87 ± 0.19	-0.76 ± 0.20
$\alpha_2^{T_1}$	1.95 ± 1.10	1.45 ± 0.77	1.41 ± 1.01	2.75 ± 1.19	2.08 ± 1.00
$\alpha_0^{T_2}$	0.28 ± 0.03	0.27 ± 0.03	0.25 ± 0.03	0.31 ± 0.03	0.24 ± 0.02
$\alpha_1^{T_2}$	0.40 ± 0.18	0.47 ± 0.13	0.41 ± 0.23	0.58 ± 0.19	0.34 ± 0.19
$\alpha_2^{T_2}$	0.36 ± 0.51	0.58 ± 0.46	0.46 ± 0.57	0.89 ± 0.71	0.52 ± 0.61
$\alpha_0^{T_{23}}$	0.67 ± 0.08	0.75 ± 0.08	0.68 ± 0.09	0.68 ± 0.07	0.60 ± 0.08
$\alpha_1^{T_{23}}$	1.48 ± 0.49	1.90 ± 0.43	1.65 ± 0.62	2.11 ± 0.46	1.58 ± 0.56
$\alpha_2^{T_{23}}$	1.92 ± 1.96	2.93 ± 1.81	2.47 ± 2.19	4.94 ± 2.25	3.65 ± 3.27

Table 14. Fit results for the SSE expansion coefficients in the fit to the LCSR computation only. These numbers are provided (to higher accuracy) in electronic form along with the full correlation matrices as arXiv ancillary files. The LCSR FFs are usually taken to be valid in the range from 0 to $14\,\mathrm{GeV}^2$.

`BKstar` for $B \to K^*$, `Brho` for $B \to \rho$, `Bomega` for $B \to \omega$, `Bsphi` for $B_s \to \phi$ and `BsKstar` for $B_s \to \bar{K}^*$ FFs; `[Fit]` is `LCSR` for the fit to LCSR only (valid at low q^2) and `LCSR-Lattice` for the combined fit valid in the full q^2 range.

The JSON format can be easily used in `Mathematica`. For example, reading in the file for the $B \to K^*$ LCSR FFs,

```
data = Import["BKstar_LCSR.json"]
```

the central value of $\alpha_0^{T_1}$ can be accessed simply via

```
OptionValue[data, "central" -> "T1" -> "a0"]
```

and the correlation between $\alpha_1^{A_0}$ and α_2^{V} as

```
OptionValue[data, "correlation" -> "A0V" -> "a1a2"]
```

and similarly for the objects `"uncertainty"` and `"covariance"`. In Python, the corresponding commands would read

JHEP08(2016)098

	$B \to K^*$	$B_s \to \phi$	$B_s \to K^*$
$a_0^{A_0}$	0.37 ± 0.03	0.42 ± 0.02	0.36 ± 0.02
$a_1^{A_0}$	-1.37 ± 0.26	-0.98 ± 0.24	-0.36 ± 0.20
$a_2^{A_0}$	0.13 ± 1.63	3.27 ± 1.36	8.03 ± 2.07
$a_0^{A_1}$	0.30 ± 0.03	0.29 ± 0.01	0.22 ± 0.01
$a_1^{A_1}$	0.39 ± 0.19	0.35 ± 0.10	0.24 ± 0.16
$a_2^{A_1}$	1.19 ± 1.03	1.70 ± 0.79	1.77 ± 0.85
$a_0^{A_{12}}$	0.27 ± 0.02	0.27 ± 0.02	0.27 ± 0.02
$a_1^{A_{12}}$	0.53 ± 0.13	0.95 ± 0.13	1.12 ± 0.11
$a_2^{A_{12}}$	0.48 ± 0.66	2.15 ± 0.48	3.43 ± 0.78
a_0^{V}	0.38 ± 0.03	0.36 ± 0.01	0.28 ± 0.02
a_1^{V}	-1.17 ± 0.26	-1.22 ± 0.16	-0.82 ± 0.19
a_2^{V}	2.42 ± 1.53	3.74 ± 1.73	5.08 ± 1.42
$a_0^{T_1}$	0.31 ± 0.03	0.30 ± 0.01	0.24 ± 0.01
$a_1^{T_1}$	-1.01 ± 0.19	-1.10 ± 0.08	-0.75 ± 0.15
$a_2^{T_1}$	1.53 ± 1.64	0.58 ± 1.00	2.49 ± 1.37
$a_0^{T_2}$	0.31 ± 0.03	0.30 ± 0.01	0.24 ± 0.01
$a_1^{T_2}$	0.50 ± 0.17	0.40 ± 0.08	0.31 ± 0.15
$a_2^{T_2}$	1.61 ± 0.80	1.04 ± 0.61	1.58 ± 0.93
$a_0^{T_{23}}$	0.67 ± 0.06	0.65 ± 0.04	0.60 ± 0.04
$a_1^{T_{23}}$	1.32 ± 0.22	2.10 ± 0.33	2.40 ± 0.27
$a_2^{T_{23}}$	3.82 ± 2.20	6.74 ± 1.80	9.64 ± 2.03

Table 15. Fit results for the SSE expansion coefficients in the combined LCSR + lattice fit. These numbers are provided (to higher accuracy) in electronic form along with the full correlation matrices as arXiv ancillary files.

```
import json
with open('BKstar_LCSR.json') as file:
  data = json.load(file)
```

and the parameters can be accessed via

```
data['central']['T1']['a0']
data['correlation']['A0V']['a1a2']
```

etc.

G Lifetime effect in $B_s \to \phi\mu^+\mu^-$

To compare the experimental measurement of the $B_s \to \phi\mu\mu$ branching ratio and angular observables from an untagged data sample to the theoretical predictions, the difference in finite width $\Delta\Gamma_s$ between the B_s mass eigenstates of widths Γ_L and Γ_H has to be taken

JHEP08(2016)098

into account [83, 106]. This leads to a difference between experimentally accessible time-integrated CP-averaged observables $\mathcal{O}_{\rm exp}$ and the theoretical definition of CP-averaged observables $\mathcal{O}_{\rm theo}$ in the flavour eigenstate basis. The former and the latter are defined as

$$\mathcal{O}_{\rm exp} = \int_0^\infty \frac{dt}{\tau_{B_s}} \mathcal{O}(t)\,, \qquad \mathcal{O}_{\rm theo} = \mathcal{O}(t=0)\,, \tag{G.1}$$

where τ_{B_s} is the lifetime of the B_s

$$\mathcal{O}(t)(B_s \to \phi\mu^+\mu^-) = \frac{1}{2}\big[\mathcal{O}\big(B_s(t) \to \phi\mu^+\mu^-\big) + \mathcal{O}\big(\bar{B}_s(t) \to \phi\mu^+\mu^-\big)\big]\,. \tag{G.2}$$

In the case where only vector operators are present (i.e. $H_{\rm eff} \sim \bar{b}\gamma_\mu(\gamma_5)s\bar{\ell}\gamma^\mu(\gamma_5)\ell$), the time-dependent CP-averaged observables $\mathcal{O}(t)$ can be written as functions $F_{\mathcal{O}}$ of bilinears of time-dependent transversity amplitudes $\mathcal{J}_{bX,aY}(t)$

$$\mathcal{O}(t) = F_{\mathcal{O}}\big(\mathcal{J}_{bX,aY}(t)\big)\,, \tag{G.3}$$

$$\mathcal{J}_{bX,aY}(t) = A_b^X(t)A_a^Y(t)^* + \bar{A}_b^X(t)\bar{A}_a^Y(t)^*, \tag{G.4}$$

where $a, b = 0, \|, \perp$ are the vector meson polarisation indices and $X, Y = L, R$ denote the chirality structure of the lepton production. The CP-conjugated amplitude is

$$\bar{A}_a^{L,R} = \eta_a A_a^{L,R}(\phi_w \to -\phi_w)\,, \tag{G.5}$$

where $\eta_{\|,0} = +1$ and $\eta_\perp = -1$ are the CP-eigenvalues of the amplitudes and $(\phi_w \to -\phi_w)$ refers to the conjugation of all weak (CP-odd) phases. Defining the quantity

$$\xi_a^\lambda = -e^{-i\phi_s}\frac{A_a^\lambda}{\bar{A}_a^\lambda}\,, \tag{G.6}$$

where ϕ_s is the B_s mixing phase, one can write

$$\mathcal{J}_{bX,aY}(t) = \mathcal{J}_{bX,aY}(0)\frac{1}{2}\big[(e^{-\Gamma_L t} + e^{-\Gamma_H t}) - \mathcal{A}_{\Delta\Gamma}^{bX,aY}(e^{-\Gamma_L t} - e^{-\Gamma_H t})\big]\,, \tag{G.7}$$

with

$$\mathcal{A}_{\Delta\Gamma}^{bX,aY} \equiv -\frac{\xi_b^{X*} + \xi_a^Y}{1 + \xi_b^{X*}\xi_a^Y}\,. \tag{G.8}$$

In summary for the experimental and theoretical expression in (G.1), we obtain

$$\begin{aligned} J_{bX,aY}|_{\rm exp} &= \int_0^\infty \frac{dt}{\tau_{B_s}}\,\mathcal{J}_{bX,aY}(t) = \frac{1 + y_s\mathcal{A}_{\Delta\Gamma}^{bX,aY}}{1 - y_s^2}\mathcal{J}_{bX,aY}(0)\,, \\ J_{bX,aY}|_{\rm theo} &= \mathcal{J}_{bX,aY}(0)\,, \end{aligned} \tag{G.9}$$

where

$$y_s \equiv \frac{\Gamma_L - \Gamma_H}{\Gamma_L + \Gamma_H} = \frac{\Delta\Gamma_s}{2\Gamma_s}\,, \qquad \Gamma_s = \frac{1}{\tau_{B_s}} = \frac{1}{2}(\Gamma_L + \Gamma_H)\,. \tag{G.10}$$

JHEP08(2016)098

As a simple example, we consider the differential branching ratio at low q^2 in the SM, within naive factorisation and the heavy quark and massless lepton limit, where the transversity amplitudes read

$$\begin{aligned} A_\perp^{L,R} &= \sqrt{2} N m_{B_s} (1-\hat{s}) \left(C_9^{\rm eff} \mp C_{10} + \frac{2 m_b m_B}{q^2} C_7^{\rm eff} \right) \xi_\perp \,, \\ A_\parallel^{L,R} &= -A_\perp^{L,R} \,, \\ A_0^{L,R} &= -\frac{N m_{B_s}^2 (1-\hat{s})^2}{2 m_\phi \sqrt{\hat{s}}} \left(C_9^{\rm eff} \mp C_{10} + \frac{2 m_b}{m_B} C_7^{\rm eff} \right) \xi_\parallel \,, \end{aligned} \tag{G.11}$$

with $\hat{s} = q^2/m_{B_s}^2$ and N being a normalisation factor including the CKM elements $V_{tb} V_{ts}^*$. Note that the soft FFs $\xi_{\parallel,\perp}$ are not to be confused with the ratio of amplitudes in (G.6). One finds

$$\xi_\perp^{L,R} = -1 \,, \qquad \xi_\parallel^{L,R} = +1 \,, \qquad \xi_0^{L,R} = +1 \,. \tag{G.12}$$

The theoretical and experimental CP-averaged differential branching ratios in the assumed limit read

$$\begin{aligned} \left. \frac{d\overline{\rm BR}}{dq^2} \right|_{\rm theo} &= \tau_{B_s} \left(|A_\perp^L|^2 + |A_\perp^R|^2 + |A_\parallel^L|^2 + |A_\parallel^R|^2 + |A_0^L|^2 + |A_0^R|^2 \right) \\ &= \tau_{B_s} \left[2 \left(|A_\perp^L|^2 + |A_\perp^R|^2 \right) + |A_0^L|^2 + |A_0^R|^2 \right] \end{aligned} \tag{G.13}$$

and

$$\begin{aligned} \left. \frac{d\overline{\rm BR}}{dq^2} \right|_{\rm exp} &= \tau_{B_s} \sum_{a=\perp,\parallel,0} \left(\frac{1 + y_s \mathcal{A}_{\Delta\Gamma}^a}{1 - y_s^2} \right) \left(|A_a^L|^2 + |A_a^R|^2 \right) \\ &= \tau_{B_s} \left[\frac{2}{1-y_s^2} \left(|A_\perp^L|^2 + |A_\perp^R|^2 \right) + \frac{1}{1+y_s} \left(|A_0^L|^2 + |A_0^R|^2 \right) \right] , \end{aligned} \tag{G.14}$$

where

$$\mathcal{A}_{\Delta\Gamma}^a = \mathcal{A}_{\Delta\Gamma}^{aL,aL} = \mathcal{A}_{\Delta\Gamma}^{aR,aR} = -\eta_a \,.$$

At low q^2, the sizeable longitudinal polarization fraction of the ϕ-meson signals that the last term in (G.14) dominates, so the time-integrated branching ratio at low q^2 is *suppressed* by $\mathcal{O}(y_s)$, where $y_s = 0.62(5)$ [80], with respect to the prompt one. This is in agreement with the findings in [83].

References

[1] T. Blake, G. Lanfranchi and D.M. Straub, *Rare B decays as tests of the standard model*, arXiv:1606.00916 [INSPIRE].

[2] P. Ball and R. Zwicky, $B_{d,s} \to \rho, \omega, K^*, \phi$ *decay form-factors from light-cone sum rules revisited*, *Phys. Rev.* **D 71** (2005) 014029 [hep-ph/0412079] [INSPIRE].

JHEP08(2016)098

[3] I. Sentitemsu Imsong, A. Khodjamirian, T. Mannel and D. van Dyk, *Extrapolation and unitarity bounds for the $B \to \pi$ form factor*, *JHEP* **02** (2015) 126 [arXiv:1409.7816] [INSPIRE].

[4] C. Hambrock, G. Hiller, S. Schacht and R. Zwicky, *$B \to K^*$ form factors from flavor data to QCD and back*, *Phys. Rev.* **D 89** (2014) 074014 [arXiv:1308.4379] [INSPIRE].

[5] J. Charles, A. Le Yaouanc, L. Oliver, O. Pène and J.-C. Raynal, *Heavy to light form-factors in the heavy mass to large energy limit of QCD*, *Phys. Rev.* **D 60** (1999) 014001 [hep-ph/9812358] [INSPIRE].

[6] M. Beneke and T. Feldmann, *Symmetry breaking corrections to heavy to light B meson form-factors at large recoil*, *Nucl. Phys.* **B 592** (2001) 3 [hep-ph/0008255] [INSPIRE].

[7] S. Descotes-Genon, L. Hofer, J. Matias and J. Virto, *On the impact of power corrections in the prediction of $B \to K^* \mu^+ \mu^-$ observables*, *JHEP* **12** (2014) 125 [arXiv:1407.8526] [INSPIRE].

[8] S. Jäger and J. Martin Camalich, *Reassessing the discovery potential of the $B \to K^* \ell^+ \ell^-$ decays in the large-recoil region: SM challenges and BSM opportunities*, *Phys. Rev.* **D 93** (2016) 014028 [arXiv:1412.3183] [INSPIRE].

[9] S. Descotes-Genon, T. Hurth, J. Matias and J. Virto, *Optimizing the basis of $B \to K^* \ell^+ \ell^-$ observables in the full kinematic range*, *JHEP* **05** (2013) 137 [arXiv:1303.5794] [INSPIRE].

[10] R.R. Horgan, Z. Liu, S. Meinel and M. Wingate, *Lattice QCD calculation of form factors describing the rare decays $B \to K^* \ell^+ \ell^-$ and $B_s \to \phi \ell^+ \ell^-$*, *Phys. Rev.* **D 89** (2014) 094501 [arXiv:1310.3722] [INSPIRE].

[11] R.R. Horgan, Z. Liu, S. Meinel and M. Wingate, *Rare B decays using lattice QCD form factors*, PoS(LATTICE2014)372 [arXiv:1501.00367] [INSPIRE].

[12] J. Lyon and R. Zwicky, *Isospin asymmetries in $B \to (K^*, \rho)\gamma / l^+ l^-$ and $B \to K l^+ l^-$ in and beyond the standard model*, *Phys. Rev.* **D 88** (2013) 094004 [arXiv:1305.4797] [INSPIRE].

[13] M.A. Shifman, A.I. Vainshtein and V.I. Zakharov, *QCD and resonance physics. Theoretical foundations*, *Nucl. Phys.* **B 147** (1979) 385 [INSPIRE].

[14] M.A. Shifman, A.I. Vainshtein and V.I. Zakharov, *QCD and resonance physics. Applications*, *Nucl. Phys.* **B 147** (1979) 448 [INSPIRE].

[15] I.I. Balitsky, V.M. Braun and A.V. Kolesnichenko, *Radiative decay $\sigma^+ \to p\gamma$ in quantum chromodynamics*, *Nucl. Phys.* **B 312** (1989) 509 [INSPIRE].

[16] V.L. Chernyak and I.R. Zhitnitsky, *B meson exclusive decays into baryons*, *Nucl. Phys.* **B 345** (1990) 137 [INSPIRE].

[17] M.A. Shifman, A.I. Vainshtein and V.I. Zakharov, *QCD and resonance physics. The ρ-ω mixing*, *Nucl. Phys.* **B 147** (1979) 519 [INSPIRE].

[18] P. Ball and R. Zwicky, *Improved analysis of $B \to \pi e \nu$ from QCD sum rules on the light cone*, *JHEP* **10** (2001) 019 [hep-ph/0110115] [INSPIRE].

[19] P. Ball and R. Zwicky, *New results on $B \to \pi, K, \eta$ decay form factors from light-cone sum rules*, *Phys. Rev.* **D 71** (2005) 014015 [hep-ph/0406232] [INSPIRE].

[20] G. Duplancić, A. Khodjamirian, T. Mannel, B. Melić and N. Offen, *Light-cone sum rules for $B \to \pi$ form factors revisited*, *JHEP* **04** (2008) 014 [arXiv:0801.1796] [INSPIRE].

JHEP08(2016)098

[21] P. Ball and V.M. Braun, *Exclusive semileptonic and rare B meson decays in QCD*, *Phys. Rev.* **D 58** (1998) 094016 [hep-ph/9805422] [INSPIRE].

[22] A. Khodjamirian, T. Mannel and N. Offen, *Form-factors from light-cone sum rules with B-meson distribution amplitudes*, *Phys. Rev.* **D 75** (2007) 054013 [hep-ph/0611193] [INSPIRE].

[23] F. De Fazio, T. Feldmann and T. Hurth, *SCET sum rules for $B \to P$ and $B \to V$ transition form factors*, *JHEP* **02** (2008) 031 [arXiv:0711.3999] [INSPIRE].

[24] B. Grinstein and D. Pirjol, *Exclusive rare $B \to K^* \ell^+ \ell^-$ decays at low recoil: controlling the long-distance effects*, *Phys. Rev.* **D 70** (2004) 114005 [hep-ph/0404250] [INSPIRE].

[25] N. Isgur and M.B. Wise, *Relationship between form-factors in semileptonic $\bar{B}$ and D decays and exclusive rare $\bar{B}$ meson decays*, *Phys. Rev.* **D 42** (1990) 2388 [INSPIRE].

[26] W. Altmannshofer et al., *Symmetries and asymmetries of $B \to K^* \mu^+ \mu^-$ decays in the standard model and beyond*, *JHEP* **01** (2009) 019 [arXiv:0811.1214] [INSPIRE].

[27] C.W. Bauer, S. Fleming, D. Pirjol and I.W. Stewart, *An effective field theory for collinear and soft gluons: heavy to light decays*, *Phys. Rev.* **D 63** (2001) 114020 [hep-ph/0011336] [INSPIRE].

[28] M. Beneke and D. Yang, *Heavy-to-light B meson form-factors at large recoil energy: spectator-scattering corrections*, *Nucl. Phys.* **B 736** (2006) 34 [hep-ph/0508250] [INSPIRE].

[29] G. Bell, M. Beneke, T. Huber and X.-Q. Li, *Heavy-to-light currents at NNLO in SCET and semi-inclusive $\bar{B} \to X_s \ell^+ \ell^-$ decay*, *Nucl. Phys.* **B 843** (2011) 143 [arXiv:1007.3758] [INSPIRE].

[30] A. Ali, V.M. Braun and H. Simma, *Exclusive radiative B decays in the light cone QCD sum rule approach*, *Z. Phys.* **C 63** (1994) 437 [hep-ph/9401277] [INSPIRE].

[31] M. Diehl, T. Gousset, B. Pire and O. Teryaev, *Probing partonic structure in $\gamma^* \gamma \to \pi\pi$ near threshold*, *Phys. Rev. Lett.* **81** (1998) 1782 [hep-ph/9805380] [INSPIRE].

[32] M.V. Polyakov, *Hard exclusive electroproduction of two pions and their resonances*, *Nucl. Phys.* **B 555** (1999) 231 [hep-ph/9809483] [INSPIRE].

[33] N. Kivel, L. Mankiewicz and M.V. Polyakov, *NLO corrections and contribution of a tensor gluon operator to the process $\gamma^* \gamma \to \pi\pi$*, *Phys. Lett.* **B 467** (1999) 263 [hep-ph/9908334] [INSPIRE].

[34] M. Diehl, *Generalized parton distributions*, *Phys. Rept.* **388** (2003) 41 [hep-ph/0307382] [INSPIRE].

[35] R.A. Briceño, M.T. Hansen and A. Walker-Loud, *Multichannel $1 \to 2$ transition amplitudes in a finite volume*, *Phys. Rev.* **D 91** (2015) 034501 [arXiv:1406.5965] [INSPIRE].

[36] D. Bečirević and A. Tayduganov, *Impact of $B \to K_0^* \ell^+ \ell^-$ on the new physics search in $B \to K^* \ell^+ \ell^-$ decay*, *Nucl. Phys.* **B 868** (2013) 368 [arXiv:1207.4004] [INSPIRE].

[37] U.-G. Meißner and W. Wang, *Generalized heavy-to-light form factors in light-cone sum rules*, *Phys. Lett.* **B 730** (2014) 336 [arXiv:1312.3087] [INSPIRE].

[38] LHCb collaboration, *Measurement of the resonant and CP components in $\bar{B}^0 \to J/\psi \pi^+ \pi^-$ decays*, *Phys. Rev.* **D 90** (2014) 012003 [arXiv:1404.5673] [INSPIRE].

[39] CLEO collaboration, B.H. Behrens et al., *Measurement of $B \to \rho l \nu$ decay and $|V_{ub}|$*, *Phys. Rev.* **D 61** (2000) 052001 [hep-ex/9905056] [INSPIRE].

JHEP08(2016)098

[40] CLEO collaboration, N.E. Adam et al., *A study of exclusive charmless semileptonic B decay and $|V_{ub}|$*, *Phys. Rev. Lett.* **99** (2007) 041802 [hep-ex/0703041] [INSPIRE].

[41] F. Jegerlehner and R. Szafron, *ρ^0-γ mixing in the neutral channel pion form factor $F_\pi^{(e)}(s)$ and its role in comparing e^+e^- with τ spectral functions*, *Eur. Phys. J.* **C 71** (2011) 1632 [arXiv:1101.2872] [INSPIRE].

[42] U.-G. Meißner and W. Wang, *$B_s \to K^{(*)}\ell\bar{\nu}$, angular analysis, S-wave contributions and $|V_{ub}|$*, *JHEP* **01** (2014) 107 [arXiv:1311.5420] [INSPIRE].

[43] S. Faller, T. Feldmann, A. Khodjamirian, T. Mannel and D. van Dyk, *Disentangling the decay observables in $B^- \to \pi^+\pi^-\ell^-\bar{\nu}_\ell$*, *Phys. Rev.* **D 89** (2014) 014015 [arXiv:1310.6660] [INSPIRE].

[44] X.-W. Kang, B. Kubis, C. Hanhart and U.-G. Meißner, *B_{l4} decays and the extraction of $|V_{ub}|$*, *Phys. Rev.* **D 89** (2014) 053015 [arXiv:1312.1193] [INSPIRE].

[45] G. Colangelo, E. Passemar and P. Stoffer, *A dispersive treatment of $K_{\ell 4}$ decays*, *Eur. Phys. J.* **C 75** (2015) 172 [arXiv:1501.05627] [INSPIRE].

[46] P. Ball and G.W. Jones, *Twist-3 distribution amplitudes of K^* and ϕ mesons*, *JHEP* **03** (2007) 069 [hep-ph/0702100] [INSPIRE].

[47] M. Dimou, J. Lyon and R. Zwicky, *Exclusive chromomagnetism in heavy-to-light FCNCs*, *Phys. Rev.* **D 87** (2013) 074008 [arXiv:1212.2242] [INSPIRE].

[48] R. Arthur et al., *Lattice results for low moments of light meson distribution amplitudes*, *Phys. Rev.* **D 83** (2011) 074505 [arXiv:1011.5906] [INSPIRE].

[49] P. Ball and R. Zwicky, SU(3) *breaking of leading-twist K and K^* distribution amplitudes — a reprise*, *Phys. Lett.* **B 633** (2006) 289 [hep-ph/0510338] [INSPIRE].

[50] P. Ball and V.M. Braun, *ρ meson light-cone distribution amplitudes of leading twist reexamined*, *Phys. Rev.* **D 54** (1996) 2182 [hep-ph/9602323] [INSPIRE].

[51] P. Ball and R. Zwicky, *$|V_{td}/V_{ts}|$ from $B \to V\gamma$*, *JHEP* **04** (2006) 046 [hep-ph/0603232] [INSPIRE].

[52] RBC-UKQCD collaboration, C. Allton et al., *Physical results from 2+1 flavor domain wall QCD and* SU(2) *chiral perturbation theory*, *Phys. Rev.* **D 78** (2008) 114509 [arXiv:0804.0473] [INSPIRE].

[53] A. Bharucha, *Two-loop corrections to the $B \to \pi$ form factor from QCD sum rules on the light-cone and $|V_{ub}|$*, *JHEP* **05** (2012) 092 [arXiv:1203.1359] [INSPIRE].

[54] T.M. Aliev and V.L. Eletsky, *On leptonic decay constants of pseudoscalar D and B mesons*, *Sov. J. Nucl. Phys.* **38** (1983) 936 [*Yad. Fiz.* **38** (1983) 1537] [INSPIRE].

[55] E. Bagan, P. Ball, V.M. Braun and H.G. Dosch, *QCD sum rules in the effective heavy quark theory*, *Phys. Lett.* **B 278** (1992) 457 [INSPIRE].

[56] LHCb collaboration, *Differential branching fraction and angular analysis of the decay $B^0 \to K^{*0}\mu^+\mu^-$*, *JHEP* **08** (2013) 131 [arXiv:1304.6325] [INSPIRE].

[57] LHCb collaboration, *Measurement of form-factor-independent observables in the decay $B^0 \to K^{*0}\mu^+\mu^-$*, *Phys. Rev. Lett.* **111** (2013) 191801 [arXiv:1308.1707] [INSPIRE].

[58] LHCb collaboration, *Differential branching fractions and isospin asymmetries of $B \to K^{(*)}\mu^+\mu^-$ decays*, *JHEP* **06** (2014) 133 [arXiv:1403.8044] [INSPIRE].

JHEP08(2016)098

[59] LHCb collaboration, *Angular analysis of the $B^0 \to K^{*0}\mu^+\mu^-$ decay using 3 fb^{-1} of integrated luminosity*, *JHEP* **02** (2016) 104 [arXiv:1512.04442] [INSPIRE].

[60] CMS collaboration, *Angular analysis and branching fraction measurement of the decay $B^0 \to K^{*0}\mu^+\mu^-$*, *Phys. Lett.* **B 727** (2013) 77 [arXiv:1308.3409] [INSPIRE].

[61] ATLAS collaboration, *Angular analysis of $B_d \to K^{*0}\mu^+\mu^-$ with the ATLAS experiment*, ATLAS-CONF-2013-038 (2013).

[62] BELLE collaboration, A. Abdesselam et al., *Angular analysis of $B^0 \to K^*(892)^0\ell^+\ell^-$*, in *LHC Ski 2016: a first discussion of 13 TeV results*, Obergurgl Austria, 10–15 Apr 2016 [arXiv:1604.04042] [INSPIRE].

[63] S. Descotes-Genon, J. Matias and J. Virto, *Understanding the $B \to K^*\mu^+\mu^-$ anomaly*, *Phys. Rev.* **D 88** (2013) 074002 [arXiv:1307.5683] [INSPIRE].

[64] W. Altmannshofer and D.M. Straub, *New physics in $B \to K^*\mu\mu$?*, *Eur. Phys. J.* **C 73** (2013) 2646 [arXiv:1308.1501] [INSPIRE].

[65] F. Beaujean, C. Bobeth and D. van Dyk, *Comprehensive Bayesian analysis of rare (semi)leptonic and radiative B decays*, *Eur. Phys. J.* **C 74** (2014) 2897 [*Erratum ibid.* **C 74** (2014) 3179] [arXiv:1310.2478] [INSPIRE].

[66] J. Lyon and R. Zwicky, *Resonances gone topsy turvy — the charm of QCD or new physics in $b \to s\ell^+\ell^-$?*, arXiv:1406.0566 [INSPIRE].

[67] W. Altmannshofer and D.M. Straub, *New physics in $b \to s$ transitions after LHC run 1*, *Eur. Phys. J.* **C 75** (2015) 382 [arXiv:1411.3161] [INSPIRE].

[68] H.H. Asatryan, H.M. Asatrian, C. Greub and M. Walker, *Calculation of two loop virtual corrections to $b \to sl^+l^-$ in the standard model*, *Phys. Rev.* **D 65** (2002) 074004 [hep-ph/0109140] [INSPIRE].

[69] M. Beneke, T. Feldmann and D. Seidel, *Systematic approach to exclusive $B \to V\ell^+\ell^-$, $V\gamma$ decays*, *Nucl. Phys.* **B 612** (2001) 25 [hep-ph/0106067] [INSPIRE].

[70] M. Beneke, T. Feldmann and D. Seidel, *Exclusive radiative and electroweak $b \to d$ and $b \to s$ penguin decays at NLO*, *Eur. Phys. J.* **C 41** (2005) 173 [hep-ph/0412400] [INSPIRE].

[71] LHCb collaboration, *Observation of a resonance in $B^+ \to K^+\mu^+\mu^-$ decays at low recoil*, *Phys. Rev. Lett.* **111** (2013) 112003 [arXiv:1307.7595] [INSPIRE].

[72] A. Khodjamirian, T. Mannel, A.A. Pivovarov and Y.M. Wang, *Charm-loop effect in $B \to K^{(*)}\ell^+\ell^-$ and $B \to K^*\gamma$*, *JHEP* **09** (2010) 089 [arXiv:1006.4945] [INSPIRE].

[73] P. Ball, G.W. Jones and R. Zwicky, *$B \to V\gamma$ beyond QCD factorisation*, *Phys. Rev.* **D 75** (2007) 054004 [hep-ph/0612081] [INSPIRE].

[74] F. Muheim, Y. Xie and R. Zwicky, *Exploiting the width difference in $B_s \to \phi\gamma$*, *Phys. Lett.* **B 664** (2008) 174 [arXiv:0802.0876] [INSPIRE].

[75] S. Jäger and J. Martin Camalich, *On $B \to V\ell\ell$ at small dilepton invariant mass, power corrections and new physics*, *JHEP* **05** (2013) 043 [arXiv:1212.2263] [INSPIRE].

[76] G. Hiller and R. Zwicky, *(A)symmetries of weak decays at and near the kinematic endpoint*, *JHEP* **03** (2014) 042 [arXiv:1312.1923] [INSPIRE].

[77] S. Descotes-Genon, J. Matias, M. Ramon and J. Virto, *Implications from clean observables for the binned analysis of $B \to K^*\mu^+\mu^-$ at large recoil*, *JHEP* **01** (2013) 048 [arXiv:1207.2753] [INSPIRE].

JHEP08(2016)098

[78] J. Gratrex, M. Hopfer and R. Zwicky, *Generalised helicity formalism, higher moments and the $B \to K_{J_K}(\to K\pi)\bar{\ell}_1\ell_2$ angular distributions*, *Phys. Rev.* **D 93** (2016) 054008 [arXiv:1506.03970] [INSPIRE].

[79] PARTICLE DATA GROUP collaboration, K.A. Olive et al., *Review of particle physics*, *Chin. Phys.* **C 38** (2014) 090001 [INSPIRE].

[80] HEAVY FLAVOR AVERAGING GROUP (HFAG) collaboration, Y. Amhis et al., *Averages of b-hadron, c-hadron and τ-lepton properties as of summer 2014*, arXiv:1412.7515 [INSPIRE].

[81] LHCb collaboration, *Measurement of the $B^0 \to K^{*0}e^+e^-$ branching fraction at low dilepton mass*, *JHEP* **05** (2013) 159 [arXiv:1304.3035] [INSPIRE].

[82] LHCb collaboration, *Angular analysis of the $B^0 \to K^{*0}e^+e^-$ decay in the low-q^2 region*, *JHEP* **04** (2015) 064 [arXiv:1501.03038] [INSPIRE].

[83] S. Descotes-Genon and J. Virto, *Time dependence in $B \to V\ell\ell$ decays*, *JHEP* **04** (2015) 045 [*Erratum ibid.* **07** (2015) 049] [arXiv:1502.05509] [INSPIRE].

[84] LHCb collaboration, *Measurement of the ratio of branching fractions $\mathcal{B}(B^0 \to K^{*0}\gamma)/\mathcal{B}(B_s^0 \to \phi\gamma)$*, *Phys. Rev.* **D 85** (2012) 112013 [arXiv:1202.6267] [INSPIRE].

[85] LHCb collaboration, *Differential branching fraction and angular analysis of the decay $B_s^0 \to \phi\mu^+\mu^-$*, *JHEP* **07** (2013) 084 [arXiv:1305.2168] [INSPIRE].

[86] CDF collaboration, *Precise measurements of exclusive $b \to s\mu^+\mu^-$ decay amplitudes using the full CDF data set*, CDF Public Note 10894 (2012).

[87] BABAR collaboration, P. del Amo Sanchez et al., *Study of $B \to \pi\ell\nu$ and $B \to \rho\ell\nu$ decays and determination of $|V_{ub}|$*, *Phys. Rev.* **D 83** (2011) 032007 [arXiv:1005.3288] [INSPIRE].

[88] BELLE collaboration, A. Sibidanov et al., *Study of exclusive $B \to X_u\ell\nu$ decays and extraction of $|V_{ub}|$ using full reconstruction tagging at the Belle experiment*, *Phys. Rev.* **D 88** (2013) 032005 [arXiv:1306.2781] [INSPIRE].

[89] BABAR collaboration, J.P. Lees et al., *Branching fraction measurement of $B^+ \to \omega\ell^+\nu$ decays*, *Phys. Rev.* **D 87** (2013) 032004 [*Erratum ibid.* **D 87** (2013) 099904] [arXiv:1205.6245] [INSPIRE].

[90] BABAR collaboration, J.P. Lees et al., *Branching fraction and form-factor shape measurements of exclusive charmless semileptonic B decays and determination of $|V_{ub}|$*, *Phys. Rev.* **D 86** (2012) 092004 [arXiv:1208.1253] [INSPIRE].

[91] F.U. Bernlochner, Z. Ligeti and S. Turczyk, *New ways to search for right-handed current in $B \to \rho\ell\bar{\nu}$ decay*, *Phys. Rev.* **D 90** (2014) 094003 [arXiv:1408.2516] [INSPIRE].

[92] CKMFITTER GROUP collaboration, J. Charles et al., *CP violation and the CKM matrix: assessing the impact of the asymmetric B factories*, *Eur. Phys. J.* **C 41** (2005) 1 [hep-ph/0406184] [INSPIRE].

[93] UTFIT collaboration, M. Bona et al., *The unitarity triangle fit in the standard model and hadronic parameters from lattice QCD: a reappraisal after the measurements of Δm_s and $\mathrm{BR}(B \to \tau\nu_\tau)$*, *JHEP* **10** (2006) 081 [hep-ph/0606167] [INSPIRE].

[94] V.L. Chernyak and A.R. Zhitnitsky, *Asymptotic behavior of exclusive processes in QCD*, *Phys. Rept.* **112** (1984) 173 [INSPIRE].

JHEP08(2016)098

[95] P. Ball, V.M. Braun, Y. Koike and K. Tanaka, *Higher twist distribution amplitudes of vector mesons in QCD: formalism and twist-three distributions*, *Nucl. Phys.* **B 529** (1998) 323 [hep-ph/9802299] [INSPIRE].

[96] P. Ball, V.M. Braun and A. Lenz, *Twist-4 distribution amplitudes of the K^* and ϕ mesons in QCD*, *JHEP* **08** (2007) 090 [arXiv:0707.1201] [INSPIRE].

[97] P. Ball and V.M. Braun, *Higher twist distribution amplitudes of vector mesons in QCD: twist-4 distributions and meson mass corrections*, *Nucl. Phys.* **B 543** (1999) 201 [hep-ph/9810475] [INSPIRE].

[98] K. Maltman and C.E. Wolfe, *Isospin breaking vector meson decay constants from continuous families of finite energy sum rules*, *Phys. Rev.* **D 59** (1999) 096003 [hep-ph/9810441] [INSPIRE].

[99] K. Maltman, private communication.

[100] C.E. Wolfe and K. Maltman, *Consequences of the BaBar and KLOE $e^+e^- \to \pi^+\pi^-$ data for the determination of model-dependent ρ-ω mixing effects in $\Pi_{\rho\omega}(m_\rho^2)$ and $(g-2)_\mu$*, *Phys. Rev.* **D 83** (2011) 077301 [arXiv:1011.4511] [INSPIRE].

[101] BaBar collaboration, B. Aubert et al., *Precise measurement of the $e^+e^- \to \pi^+\pi^-(\gamma)$ cross section with the initial state radiation method at BABAR*, *Phys. Rev. Lett.* **103** (2009) 231801 [arXiv:0908.3589] [INSPIRE].

[102] E. Braaten and C.-S. Li, *Electroweak radiative corrections to the semihadronic decay rate of the τ lepton*, *Phys. Rev.* **D 42** (1990) 3888 [INSPIRE].

[103] Y. Grossman, M. König and M. Neubert, *Exclusive radiative decays of W and Z bosons in QCD factorization*, *JHEP* **04** (2015) 101 [arXiv:1501.06569] [INSPIRE].

[104] M. König and M. Neubert, *Exclusive radiative Higgs decays as probes of light-quark Yukawa couplings*, *JHEP* **08** (2015) 012 [arXiv:1505.03870] [INSPIRE].

[105] P. Golonka and Z. Was, *PHOTOS Monte Carlo: a precision tool for QED corrections in Z and W decays*, *Eur. Phys. J.* **C 45** (2006) 97 [hep-ph/0506026] [INSPIRE].

[106] K. De Bruyn et al., *Branching ratio measurements of B_s decays*, *Phys. Rev.* **D 86** (2012) 014027 [arXiv:1204.1735] [INSPIRE].

JHEP08(2016)098